

**EFFECT OF SEAL AND BACKFILL COMPOSITIONS
ON PILLAR DEFORMATION IN SALT AND POTASH
MINES**



**A Thesis Submitted in Partial Fulfillment of the Requirements for the
Degree of Master of Engineering in Geotechnology
Suranaree University of Technology
Academic Year 2017**

ผลกระทบของส่วนผสมวัสดุอุดและวัสดุอมกลับต่อการเปลี่ยนรูปร่างของเสา
ค้ำยันในเหมืองเกลือและเหมืองโพแทช



นางสาวฉัตรชิตา ธีระพันธ์

วิทยานิพนธ์นี้เป็นส่วนหนึ่งของการศึกษาตามหลักสูตรปริญญาวิศวกรรมศาสตรมหาบัณฑิต
สาขาวิชาเทคโนโลยีธรณี
มหาวิทยาลัยเทคโนโลยีสุรนารี
ปีการศึกษา 2560

**EFFECT OF SEAL AND BACKFILL COMPOSITIONS ON
PILLAR DEFORMATION IN SALT AND POTASH MINES**

Suranaree University of Technology has approved this thesis submitted in partial fulfillment of the requirements for a Master's Degree.

Thesis Examining Committee



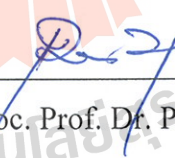
(Prof. Dr. Kittitep Fuenkajorn)

Chairperson



(Asst. Prof. Dr. Decho Phueakphum)

Member (Thesis Advisor)



(Assoc. Prof. Dr. Pornkasem Jongpradist)

Member



(Prof. Dr. Santi Maensiri)

Vice Rector for Academic Affairs
and Internationalization



(Assoc. Prof. Flt. Lt. Dr. Kontorn Chamniprasart)

Dean of Institute of Engineering

ฉัตรชิตา ถิระพันธ์ : ผลกระทบของส่วนผสมวัสดุอุดและวัสดุถมกลับต่อการเปลี่ยนรูปร่าง
ของเสาค้ำยันในเหมืองเกลือและเหมืองโพแทช (EFFECT OF SEAL AND BACKFILL
COMPOSITIONS ON PILLAR DEFORMATION IN SALT AND POTASH MINES)
อาจารย์ที่ปรึกษา : ผู้ช่วยศาสตราจารย์ ดร. เคโซ เผือกภูมิ, 87 หน้า

เหมืองเกลือและเหมืองโพแทชโดยทั่วไปจะใช้เสาหางแร่เป็นวัสดุถมกลับเพื่อลดปริมาณ
ของเสียที่เกิดขึ้นและควบคุมการทรุดตัวของผิวดิน วัตถุประสงค์ของงานวิจัยนี้จึงได้ทดสอบใน
ห้องปฏิบัติการเพื่อศึกษาผลกระทบของส่วนผสมของวัสดุถมกลับต่อการเปลี่ยนแปลงรูปร่างของ
เสาค้ำยันในเหมืองเกลือและเหมืองโพแทช การทดสอบการคืบในแกนเดียวได้ดำเนินการบน
ตัวอย่างเกลือหินและโพแทชเป็นระยะเวลา 21 วัน ภายใต้การผันแปรความเค้นกดตั้งฉากตั้งแต่ 2 ถึง
12 เมกะปาสกาล โดยหลังจากแท่งตัวอย่างเกลือหินอยู่ภายใต้การคืบในแกนเดียวเป็นระยะเวลา 7
วัน แท่งตัวอย่างทั้งหมดจะถูกแบ่งแฉ่ภายใต้สารละลาย 3 ชนิด ที่ถูกเตรียมจากน้ำเกลือเฮไลต์
น้ำเกลือคาร์บอเนตไลต์ และน้ำแมกนีเซียมคลอไรด์ โดยสารละลายเหล่านี้จะถูกนำออกหลังจากครบ
ระยะเวลาอีก 7 วัน ค่าตัวแปรสัมประสิทธิ์ความหนืดแบบพลาสติกของ Burgers ได้ถูกคำนวณใน
แต่ละช่วงของการแช่ในสารละลาย ผลการทดสอบระบุว่าตัวอย่างที่ประกอบด้วยแร่เฮไลต์บริสุทธิ์
จะไม่อ่อนไหวต่อสารละลายทั้ง 3 ชนิด ซึ่งสามารถสังเกตได้จากค่าอัตราความเครียดในการคืบที่วัด
ได้ก่อน ระหว่าง และหลังแช่ในน้ำเกลือไม่มีการเปลี่ยนแปลง ตัวอย่างโพแทชที่มีแร่คาร์บอเนตไลต์เจือ
ปนระหว่าง 30 ถึง 90 เปอร์เซ็นต์โดยมวล มีความอ่อนไหวต่อน้ำเกลือเฮไลต์และน้ำเกลือคาร์
บอเนตไลต์ แต่ไม่มีความอ่อนไหวต่อน้ำแมกนีเซียมคลอไรด์ ค่าสัมประสิทธิ์ความหนืดแบบพลาสติก
ของตัวอย่างเกลือหินภายใต้ความเค้นกดตั้งฉากสูงมีค่าลดลงเมื่อใส่น้ำเกลือเฮไลต์ อาจเนื่องมาจากการ
เกิดขึ้นของรอยแตกเล็กๆ จึงส่งผลให้พื้นที่ผิวสัมผัสบริเวณรอบๆ ตัวอย่างเพิ่มขึ้น สำหรับค่า
สัมประสิทธิ์ความหนืดแบบพลาสติกของตัวอย่างโพแทชค่อนข้างคงที่ทั้งก่อน ระหว่าง และหลังแช่
ในสารละลายแมกนีเซียมคลอไรด์ ผลกระทบของน้ำเกลือที่ใช้ผสมกับวัสดุถมกลับต่อการ
เปลี่ยนแปลงรูปร่างของช่องเหมืองและการทรุดตัวของผิวดินสามารถประเมินด้วยการสร้าง
แบบจำลองทางคอมพิวเตอร์ สารละลายทั้ง 3 ชนิด สามารถใช้เป็นส่วนผสมในวัสดุถมกลับหรือกัก
เก็บในเหมืองเกลือ สำหรับเหมืองโพแทช น้ำแมกนีเซียมคลอไรด์มีความเหมาะสมมากกว่า
สารละลายชนิดอื่นเนื่องจากเสาค้ำยันและหลังคาของแร่คาร์บอเนตไลต์โดยรอบจะไม่อ่อนไหวต่อ
สารละลายแมกนีเซียมคลอไรด์

สาขาวิชา เทคโนโลยีธรณี
ปีการศึกษา 2560

ลายมือชื่อนักศึกษา ฉัตรชิตา ถิระพันธ์
ลายมือชื่ออาจารย์ที่ปรึกษา Dr. Theeraphum

CHATCHITA THEERAPUN : EFFECT OF SEAL AND BACKFILL
COMPOSITIONS ON PILLAR DEFORMATION IN SALT AND POTASH
MINES. THESIS ADVISOR : ASST. PROF. DECHO PHUEKPHUM, Ph.D.,
87 PP.

PILLAR/ SEAL/ CARNALLITE/ CREEP/ ROCK SALT

Potash and salt mines have commonly used salt tailing as backfill to reduce the mine waste and to control the surface subsidence. The objective of this study is to laboratory investigate the effects of various backfill compositions on the deformation of pillars in salt and potash mines. Uniaxial creep tests have been performed on halite and carnallite specimens for up to 21 days under constant axial stresses from 2 to 12 MPa. After the specimens are under loading for 7 days, they are separately submerged in three types of solution prepared from halite (NaCl), carnallite ($\text{KMgCl}_3 \cdot 6\text{H}_2\text{O}$) and magnesium brine (MgCl_2). The solution is removed after 7 days interval. The visco-plastic coefficient from the Burgers parameter are calculated for each phase of solution submersion. The results indicate that the specimens that are composed of pure halite is insensitive to the three solutions, as evidenced by that the creep strain rates measured before, during and after brine submersion remain unchanged. The potash specimens containing carnallite of 30% to 90% by weight are notably sensitive to halite and carnallite brines, but insensitive to magnesium brine. The visco-plastic coefficient of the salt specimens under high stress decreases when the halite brine is added. This is probably because the induced micro-cracks increase the surface contact area around the specimens. The visco-plastic coefficient of the potash specimens seems consistent

before, during, and after submersion in $MgCl_2$ solution. The effects of brine backfill on the mine deformation and surface subsidence are assessed by performing computer simulations. All the three solutions can be used as a mixing component for the backfill material or storage in the salt mine openings. For potash mine openings, the magnesium brine is more suitable because the surrounding carnallite pillars and roof are insensitive to the $MgCl_2$ solution.



School of Geotechnology

Academic Year 2017

Student's Signature นิพนธ์ คุ้มพันธ์

Advisor's Signature D. Phueakphim

ACKNOWLEDGMENTS

I wish to acknowledge the funding support from Suranaree University of Technology (SUT).

I would like to express my sincere thanks to Prof. Dr. Kittitep Fuenkajorn for his valuable guidance and efficient supervision. I appreciate his strong support, encouragement, suggestions and comments during the research period. I also would like to express my gratitude to Asst. Prof. Dr. Decho Phueakphum and Asst. Prof. Dr. Prachya Tepnarong for their constructive advice, valuable suggestions and comments on my research works as thesis committee members. Grateful thanks are given to all staffs of Geomechanics Research Unit, Institute of Engineering who supported my work.

Finally, I would like to thank beloved parents for their love, support and encouragement.

มหาวิทยาลัยเทคโนโลยีสุรนารี

Chatchita Theerapun

TABLE OF CONTENTS

	Page
ABSTRACT (THAI)	I
ABSTRACT (ENGLISH).....	II
ACKNOWLEDGEMENTS.....	IV
TABLE OF CONTENTS.....	V
LIST OF TABLES.....	IX
LIST OF FIGURES	XI
SYMBOLS AND ABBREVIATIONS.....	XVII
CHAPTER	
I INTRODUCTION	1
1.1 Background and rationale	1
1.2 Research objectives.....	1
1.3 Research methodology.....	2
1.3.1 Literature review.....	2
1.3.2 Sample collection and preparation	4
1.3.2.1 Specimens preparation.....	4
1.3.2.2 Cement grout preparation	4
1.3.3 Laboratory testing methods and results	5
1.3.4 Calibration of Burgers parameters.....	5

TABLE OF CONTENTS (Continued)

	Page
1.3.5 Modelling of brine storage in mine openings	5
1.3.6 Discussions and conclusion	6
1.3.7 Thesis writing	6
1.4 Scope and limitations	6
1.5 Thesis contents	6
II LITERATURE REVIEW	8
2.1 Introduction	8
2.2 Environmental effect on salt	8
2.3 Environmental effect on potash	9
2.4 Effect of brine in salt and potash mine	10
2.5 Effect of cement seal in salt and potash mine	12
2.6 Environmental influence of creep test	14
2.7 Backfill technologies	19
III SAMPLE PREPARATION	23
3.1 Introduction	23
3.2 Sample preparation	23
IV LABORATORY TESTING METHODS AND RESULTS	29
4.1 Introduction	29
4.2 Uniaxial creep test	29

TABLE OF CONTENTS (Continued)

	Page
4.3 Humidity Testing	34
4.4 Weight Loss Testing	35
4.5 Test results	36
4.5.1 Uniaxial creep test.....	36
4.5.2 Humidity test.....	44
4.5.3 Weight loss testing.....	45
V CALIBRATION OF BURGERS PARAMETERS	52
5.1 Introduction.....	52
5.2 Burgers Model	52
5.3 Discussions	60
VI MODELLING OF BRINE STORAGE IN MINE	
OPENINGS.....	62
6.1 Introduction.....	62
6.2 Numerical simulations	62
6.3 Property parameters used in numerical modelling.....	63
6.4 Numerical results	68
6.4.1 Pillar and roof deformations	68
6.4.2 Surface subsidence.....	76
VII DISCUSSIONS AND CONCLUSIONS	82
7.1 Discussions	82

TABLE OF CONTENTS (Continued)

	Page
7.2 Conclusions.....	84
7.3 Recommendations for future studies	86
REFERENCES	88
APPENDIX A RESULTS OF COMPUTER SIMULATION	97
APPENDIX B TECHNICAL PUBLICATION	107
BIOGRAPHY	109

LIST OF TABLES

Table	Page
3.1	Nominal dimension of specimens for difference tests24
3.2	Salt specimens prepared for uniaxial creep tests24
3.3	Potash specimens prepared for uniaxial creep tests.....26
3.4	Specimens prepared for humidity tests.....26
4.1	Weight compositions of cement.....31
4.2	Comparison of some specimen configurations during submersion in halite brine each day46
4.3	Comparison of some specimen configurations during submersion in carnallite brine each day47
4.4	Comparison of some specimen configurations during submersion in magnesium brine each day.....48
5.1	Calibration of the Burgers parameters for salt specimens before submersion53
5.2	Calibration of the Burgers parameters for potash specimens before submersion.....54
5.3	Strain rate and visco-plastic coefficients measured before, during and after submersion in halite brine56
5.4	Strain rate and visco-plastic coefficients measured before, during and after submersion in carnallite brine57

LIST OF TABLES (Continued)

Table		Page
5.5	Strain rate and visco-plastic coefficients measured before, during and after submersion in magnesium brine.....	58
5.6	Visco-plastic coefficients measured before, during and after submersion in different solutions.....	59
5.7	Strain rate and visco-plastic coefficients measured before and during casted in cement	59
6.1	Overburden parameters used in numerical simulations	67
6.2	Material property parameters of Lower Salt used in the FLAC.....	67
6.3	Burgers parameters of Lower Salt used in the FLAC	68

LIST OF FIGURES

Figure	Page
1.1 Research Methodology.....	3
2.1 The typical deformation as a function of time of creep materials.....	16
3.1 Some salt specimens prepared for uniaxial creep tests with $L/D = 2.0$	27
3.2 Some potash specimens prepared for uniaxial creep tests with $L/D = 2.0$	27
3.3 Some rock salt specimens prepared for humidity tests	28
4.1 Consolidation load frame used for creep testing of salt and potash specimens.....	32
4.2 The solution is removed by syringe and rubber tube.....	33
4.3 The specimens under three conditions before, during and after solution or cement submersion	34
4.4 Humidity testing instrument.....	35
4.5 Strain-time curves obtained for creep testing of pure halite submerged in halite brine	37
4.6 Strain-time curves obtained for creep testing of pure halite submerged in carnallite brine	38
4.7 Strain-time curves obtained for creep testing of pure halite submerged in magnesium brine.....	39
4.8 Strain-time curves obtained for creep testing of potash specimen submerged in halite brine.....	40

LIST OF FIGURES (Continued)

Figure	Page
4.9	Strain-time curves obtained for creep testing of potash specimen submerged in carnallite brine.....41
4.10	Strain-time curves obtained for creep testing of potash specimen submerged in magnesium brine42
4.11	Strain-time curves obtained for creep testing of pure halite submerged in cement slurry43
4.12	Cross-section of some tested specimens after cement setting43
4.13	Weight loss (%) of the carnallite specimen as a function of time44
4.14	Weight loss (%) of the carnallite specimens as a function of time under halite brine49
4.15	Weight loss (%) of the carnallite specimens as a function of time under carnallite brine49
4.16	Weight loss (%) of the carnallite specimens as a function of time under magnesium brine.....50
4.17	Rate of dissolution of the carnallite specimens as a function of time under halite brine50
4.18	Rate of dissolution of the carnallite specimens as a function of time under carnallite brine51
4.19	Rate of dissolution of the carnallite specimens as a function of time under magnesium brine.....51

LIST OF FIGURES (Continued)

Figure	Page
5.1	Modular components of Burgers model53
5.2	Visco-plastic coefficients of pure halite specimens measured before, during and after submersion in halite brine56
5.3	Visco-plastic coefficients of pure halite specimens measured before, during and after submersion in carnallite brine57
5.4	Visco-plastic coefficients of pure halite specimens measured before, during and after submersion in magnesium brine58
5.5	Visco-plastic coefficients of pure halite specimens measured before and during casted in cement60
6.1	Finite difference mesh developed for FLAC simulation, mining depths are 175, 250 and 300 m and pillar height is 5 m64
6.2	Finite difference mesh developed for FLAC simulation, mining depths are 175, 250 and 300 m and pillar height is 10 m65
6.3	Finite difference mesh developed for FLAC simulation, mining depths are 175, 250 and 300 m and pillar height is 15 m66
6.4	Pillar deformations after 20 years in salt openings storing with halite brine (a, b, c), carnallite brine (d, e, f) and magnesium brine (g, h, i) with different pillar heights and depths (D)69
6.5	Pillar deformations after 20 years in potash openings storing with magnesium brine with different pillar heights and depths70

LIST OF FIGURES (Continued)

Figure	Page
6.6	Roof deformations after 20 years in salt openings storing with halite brine (a, b, c), carnallite brine (d, e, f) and magnesium brine (g, h, i) with different pillar heights and depths71
6.7	Roof deformations after 20 years in potash openings storing with magnesium brine with different pillar heights and depths72
6.8	Floor deformations after 20 years in salt openings storing with halite brine (a, b, c), carnallite brine (d, e, f) and magnesium brine (g, h, i) with different pillar heights and depths73
6.9	Floor deformations after 20 years in potash openings storing with magnesium brine with different pillar heights and depths74
6.10	Room vertical closure after 20 years in salt openings storing with halite brine (a, b, c), carnallite brine (d, e, f) and magnesium brine (g, h, i) with different pillar heights and depths75
6.11	Room vertical closure after 20 years in potash openings storing with magnesium brine with different pillar heights and depths76
6.12	Surface subsidence as a function of time after 20 years in salt openings storing with halite brine (a, b, c), carnallite brine (d, e, f) and magnesium brine (g, h, i) with different pillar heights and depths77
6.13	Surface subsidence as a function of time after 20 years in potash openings storing with magnesium brine with different pillar heights and depths78

LIST OF FIGURES (Continued)

Figure	Page
6.14	Rate of surface subsidence after 20 years in salt openings storing with halite brine (a, b, c), carnallite brine (d, e, f) and magnesium brine (g, h, i) with different pillar heights and depths80
6.15	Rate of surface subsidence after 20 years in potash openings storing with magnesium brine with different pillar heights and depths81
A.1	Stress distribution in salt mine opening for depth 175 m with 5 pillar height after halite (a), carnallite (b) and magnesium brine (c) storage98
A.2	Stress distribution in salt mine opening for depth 175 m with 10 pillar height after halite (a), carnallite (b) and magnesium brine (c) storage98
A.3	Stress distribution in salt mine opening for depth 175 m with 15 pillar height after halite (a), carnallite (b) and magnesium brine (c) storage99
A.4	Stress distribution in salt mine opening for depth 250 m with 5 pillar height after halite (a), carnallite (b) and magnesium brine (c) storage99
A.5	Stress distribution in salt mine opening for depth 250 m with 10 pillar height after halite (a), carnallite (b) and magnesium brine (c) storage100
A.6	Stress distribution in salt mine opening for depth 250 m with 15 pillar height after halite (a), carnallite (b) and magnesium brine (c) storage100
A.7	Stress distribution in salt mine opening for depth 300 m with 5 pillar height after halite (a), carnallite (b) and magnesium brine (c) storage101
A.8	Stress distribution in salt mine opening for depth 300 m with 10 pillar height after halite (a), carnallite (b) and magnesium brine (c) storage101

LIST OF FIGURES (Continued)

Figure	Page
A.9	Stress distribution in salt mine opening for depth 300 m with 15 pillar height after halite (a), carnallite (b) and magnesium brine (c) storage102
A.10	Stress distribution in potash mine opening for depth 175 m with 5 pillar height after magnesium brine storage102
A.11	Stress distribution in potash mine opening for depth 175 m with 10 pillar height after magnesium brine storage103
A.12	Stress distribution in potash mine opening for depth 175 m with 15 pillar height after magnesium brine storage103
A.13	Stress distribution in potash mine opening for depth 250 m with 5 pillar height after magnesium brine storage104
A.14	Stress distribution in potash mine opening for depth 250 m with 10 pillar height after magnesium brine storage104
A.15	Stress distribution in potash mine opening for depth 250 m with 15 pillar height after magnesium brine storage105
A.16	Stress distribution in potash mine opening for depth 300 m with 5 pillar height after magnesium brine storage105
A.17	Stress distribution in potash mine opening for depth 300 m with 10 pillar height after magnesium brine storage106
A.18	Stress distribution in potash mine opening for depth 300 m with 15 pillar height after magnesium brine storage106

SYMBOLS AND ABBREVIATIONS

$\dot{\varepsilon}$	=	Strain rate
$\varepsilon(t)$	=	Transient creep strain
η_1	=	Visco-plastic viscosity
η_2	=	Visco-elastic viscosity
ν	=	The Poisson's ratio
ρ	=	Density of the specimen
ρ_c	=	Density of carnallite (1.60 g/cc)
ρ_s	=	Density of halite (2.16 g/cc)
σ_0	=	Stress
C	=	Carnallite brine
D	=	Depth
E	=	The elastic modulus
E_1	=	The elastic modulus
E_2	=	The spring constant in visco-elastic phase
G	=	The shear modulus
H	=	Halite brine
K	=	The bulk modulus
M	=	Magnesium brine
T	=	Tensile strength
t	=	Time

CHAPTER I

INTRODUCTION

1.1 Background and rationale

Pillars in salt and potash mines get the overburden loads throughout mining period. Later, the pressures from overburden cause pillars swelling affect deflection of the roof and induce the ground surface subsidence in the mining area at a later time. Recycling the mine waste (tailings) into cemented backfilling material has economical and environmental advantages for the mining industry. Backfilling material as a slurry may affect the stability or solvency of salt and potash pillars in the mines because the process has to use water as a composition in backfilling material. Humidity and moisture may also affect salt creep deformation and strength. Moisture and brine around the pillars may change they axial, radial, and volumetric strain rates, and hence affects the salt creep deformation and strength (Brodsky and Munson, 1991). Creep of halite is affected by humidity of the atmosphere, especially above 75% R.H. Higher humidity induces a higher rate of deformation (Varo and Passaris, 1977). The quantitative effect of cement and brine on pillar deformation, however, has not been quantitatively determined due to insufficient data.

1.2 Research objectives

The objective of this study is to laboratory investigate the effects of backfill compositions on the mechanical stability of supported pillars in salt and potash mines.

Uniaxial creep tests are performed on halite and carnallite specimens for up to 21 days. The test procedure and calculation follow the ASTM (D7070-08) standard practice. A total of 20 specimens have been tested. A saturated brine prepared from halite, carnallite and magnesium chloride have been used to submerge the specimens. The results can be used to determine the deformation of pillars in salt and potash mines. This may lead to selection criteria for the suitable seal and backfill compositions.

1.3 Research methodology

The research methodology shown in Figure 1.1 comprises 7 steps; including literature review, sample preparation, laboratory testing methods and results, calibration of Burgers parameters, modelling of brine storage in mine openings, discussions and conclusions, and thesis writing.

1.3.1 Literature review

Literature review is carried out to study researches about environmental effect on salt and potash, cement sealing material, environmental influence of creep test and backfill technologies. The sources of information are from journals, technical reports and conference papers. A summary of the literature review is given in the thesis.

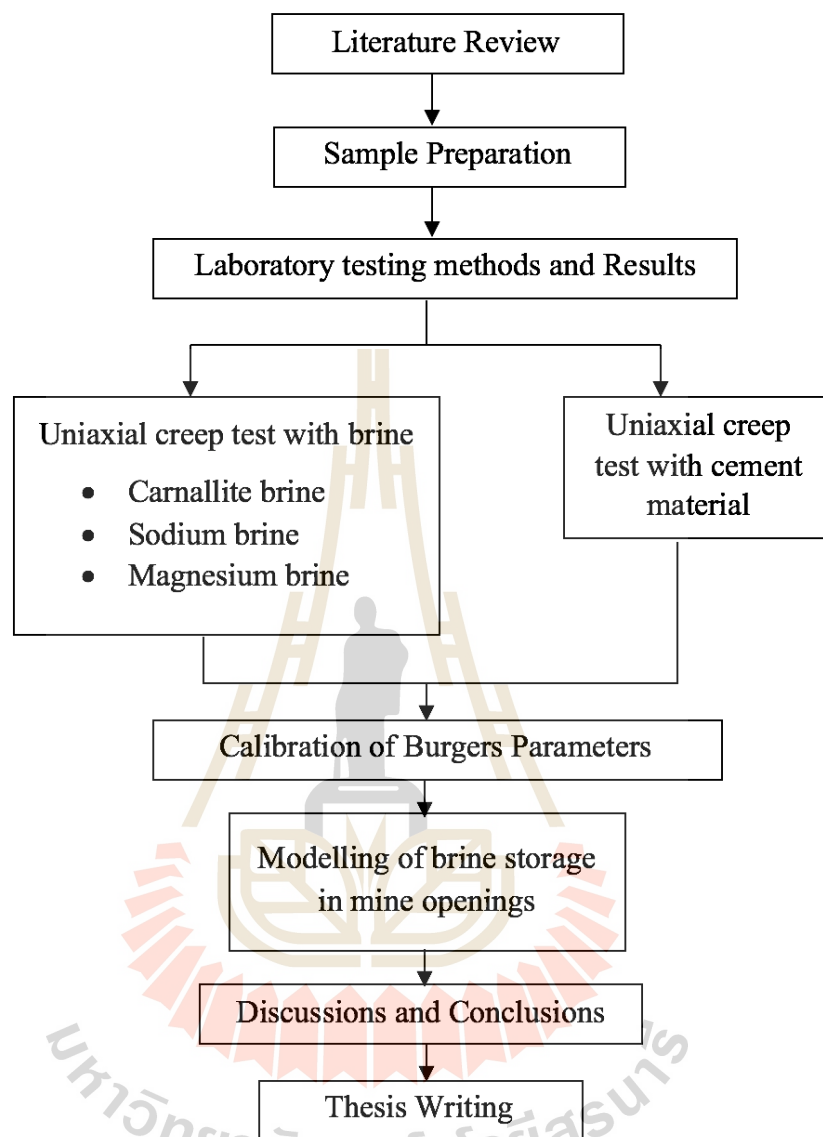


Figure 1.1 Research Methodology.

1.3.2 Sample preparation

1.3.2.1 Specimens preparation

Rock samples used here have been obtained from underground openings of ASEAN Potash Mining Co., Ltd. (APMC) from the Khorat basin, northeast of Thailand. They belong to the Lower Salt member of the Maha Sarakham formation. Sample preparation is carried out in the laboratory at Suranaree University of Technology. The specimens are prepared to obtain rectangular blocks with nominal dimensions of $54 \times 54 \times 108 \text{ mm}^3$ ($L/D=2$). Preparations of these samples will follow as much as practical the American Society for Testing and Materials (ASTM D7070-08). The total of 36 specimens are used for this study.

1.3.2.2 Cement grout preparation

The cement is mixed according to the API No. 10 (American Petroleum Institute, 1986; Akgün and Daemen, 1997) by mixing cement with salt (NaCl) saturated brine. The components of the slurry are commercial grade Portland cement mixed with chloride resistant agent, anti-form agent, saturated brine and a liquid additive. The brine is prepared either by dissolving clean rock salt (pure halite) in fresh water. Portland-pozzolan cement is chosen for its low brine demand, sulfate resistance and widely used in construction industry. A liquid additive contributes to expansiveness of mixture. An anti-forming agent is used to decrease the air content of the slurry and to ease the control of weight and volume. The saturated brine is poured into the mixing container at a low mixture speed, and all components will be added to the brine within 15 seconds. After all the cement is added, the slurry is mixed at high speed for additional 35 seconds.

1.3.3 Laboratory testing methods and results

The laboratory testing includes uniaxial creep tests following ASTM D7070-08. A dial gages are used to monitor the induced axial strains. A total of 20 specimens have been tested. The constant axial stresses are varied from 2 to 12 MPa. The test can be divided into 2 parts as follow:

1) The specimens are under loading for 7 days, they are submerged in saturated brine prepared from halite, carnallite and magnesium chloride. Then the solution is removed after 7 days.

2) The specimens are under loading for 7 days, they are submerged in cement sealing material.

The results can be used to determine the creep strain of pillars in salt and potash mines under brine and cement submerged.

1.3.4 Calibration of Burgers parameters

The results are used to calibrate the elastic, visco-elastic and visco-plastic parameters of the rock. It is assumed here that the salt behavior can be described by the Burgers model. The regression analysis on the linear visco-elastic equation has been made on the test data.

1.3.5 Modelling of brine storage in mine openings

The calibration of Burgers parameters can be applied for the pillars in salt and potash mines to determine the effect of brine in salt and potash openings. This is to study the deformation of rock salt has been affected by the stress and brine submersion.

1.3.6 Discussions and Conclusions

Discussions are made on the reliability and adequacies of the test data and the correctness of the interpretation and analysis. Future research needs are identified.

1.3.7 Thesis writing

All research activities, methods, and results are documented and complied in the thesis.

1.4 Scope and limitations

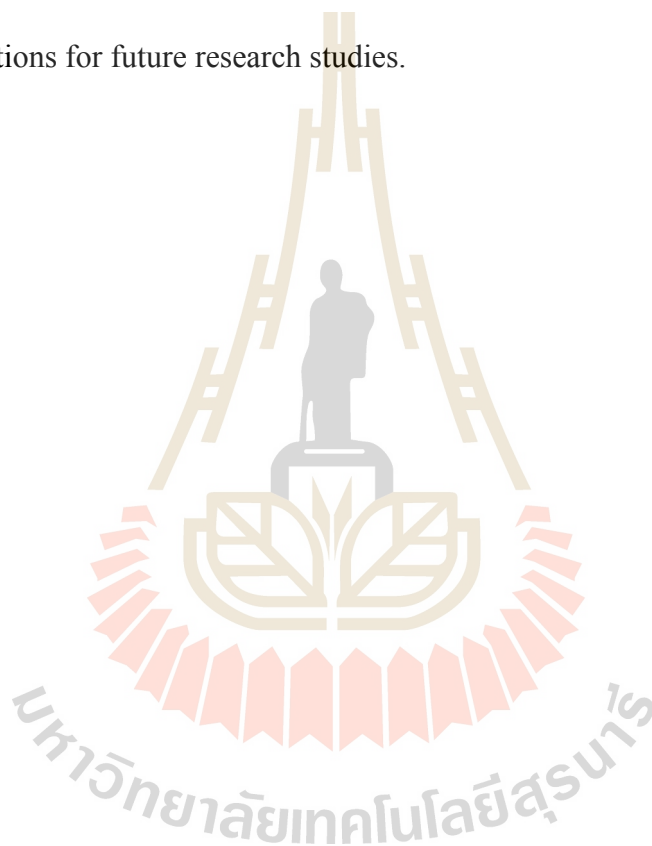
The scope and limitations of the research include as follows.

1. All specimens are conducted on rock salt specimens obtained from the Maha Sarakham formation (ASEAN Potash Mining Co., Ltd. (APMC)).
2. The nominal dimensions of rectangular blocks are $54 \times 54 \times 108 \text{ mm}^3$.
3. The applied constant axial stresses are varied from 2 to 12 MPa.
4. Saturated brine is prepared from halite, carnallite and magnesium chloride.
5. No field testing is conducted.
6. The testing procedure will follow the relevant ASTM standard practice, as much as, practical.
7. The research findings are published in conference paper or journal.

1.5 Thesis contents

This first chapter introduces the thesis by briefly describing the rationale and background and identifying the research objectives. The third section identifies the research methodology. The fourth section describes scope and limitations. The fifth

section gives a chapter by chapter overview of the contents of this thesis. The second chapter summarizes results of the literature review. Chapter three describes samples preparation. The methods and results of the laboratory testing methods and results are described in chapter four. The calibration of Burgers parameters is described in chapter five. The results from calibration are used in the modelling of brine storage in mine openings in chapter six. Chapter seven provides the discussion, conclusion and recommendations for future research studies.



CHAPTER II

LITERATURE REVIEW

2.1 Introduction

This chapter summarizes the results of literature review carried out to improve an understanding of rock salt behavior. The topics reviewed here include environmental effect on salt and potash, effect of brine in salt and potash mine, environmental influence of creep test and backfill technologies.

2.2 Environmental effect on salt

Temperature has influence on rock salt deformation and affects its creep and viscosity. The research about relation between temperature and depth were studied by several researchers (Franssen and Spiers, 1990; Raj and Pharr, 1992; Senseny et al., 1992) can inferred when depth of formation increases, the thermal increases and rock salt behave more plastic effecting to compressive strength decreases. Generally, the melting point of rock salt is 800°C but when heating at 600°C for 8 hours, rock salt can also decrease compressive strength.

Humidity and moisture reduce the strength of rock salt (Hunsche and Schulze, 1996). Hydrated reaction between salt and water occurs when salt contacts with environment humidity. The temperature effects can catalyze the hydration. They find that when subjecting to air humidity, the strength of salt can be decreased by up to 1 MPa (Billiotte et al., 1996; Bonte, 1996). The solid rock salt continues to absorb more

moisture from surroundings and generates more brine solution. Khalid (2010) studies air variable condition in mine and found the relative humidity in an enclosed chamber of hygroscopic salt fluctuate in low percentage than the absolute humidity.

Bachu et al. (2005) propose the salt characteristics and behavior of the Middle Devonian Elk Point Group in the Alberta basin in western Canada, these salt beds are found at depth that range from several hundred meters to more than 2000 meter. The salt beds range in thickness from several tens to a few hundred meters. The vertical stress (weight of the overburden) at the top of these salt beds ranges from 10 to 50 MPa, and temperatures vary between 20 and 70°C. Stresses are assumed to be isotropic and equal to the lithostatic (overburden) within the salt beds, because salt visco-plastic properties and slow creep tend to dissipate shear stresses. Vertical stress gradients at the top and bottom of the salt beds are in the 24-25 kPa/m range, and differ by only 0.1-0.3 kPa/m between the two, indicating that they are basically constant across the entire rock package containing the salt beds. If a salt cavern is filled with a fluid at an initial pressure, in the long term the pressure inside the cavern will change as a result of any of: (1) salt creep, (2) leakage along the well bore, (3) thermal expansion of the cavern fluid, (4) flow of the fluid out of the cavern into the adjacent strata, or (5) additional salt solution or precipitation in the cavern (Berest et al., 2000).

2.3 Environmental effect on potash

Potash-bearing salt is highly soluble and susceptible to alteration, recrystallization, and dissolution by surface water, less saline brine, and groundwater (Warren, 2010). Fluid and solid inclusions in potash have been purged to grain boundaries so that the depositional textures are completely eradicated. These features

must almost certainly result from recrystallization and annealing due to increased temperatures and pressures related to burial (Stanton and Gorman, 1968; Spencer and Lowenstein, 1990; Warren, 1999).

2.4 Effect of brine in salt and potash mine

Urai et al. (1986) study creep test on dry and brine-bearing salt samples, showing wet samples to be much weaker, especially at very low strain rates ($< 10^{-7} \text{ s}^{-1}$). Low strain rates were considered comparable to those observed in natural environments, as opposed to rapid strain rates commonly used in laboratory triaxial tests. The weaker behavior is associated with solution - precipitation creep associated with recrystallization.

Brodsky and Munson (1991) study the creep on rock salt specimens under saturated brine introducing around each specimen. Brine around the specimen caused immediately changes in axial, radial, and volumetric strain rates. Strain rates returned to their pre-brine-introduction values for tests conducted with confining pressures more than 3.5 MPa. The results indicate that the effects of moisture do not occur when the confining pressure is sufficiently high to suppress specimen dilation.

Lee and Souza (1998) study the effects of brine contact on the dissolution and strength properties of evaporite ores evaluating operational problems in evaporite deposit utilization associated with brine, halite, sylvinite, and carnallitic ore were creep tested under unconfined conditions, both with and without added brine. Axial deformation and dissolution chemistry were observed throughout the tests. In both the sylvinite and carnallitic ore tests, selective dissolution of sylvite and carnallite minerals was associated with the precipitation of halite. The nature of this process was

dependent on temperature and initial brine and ore composition. Generally, the presence of brine caused a decrease in the resistance to creep deformation and increase more mechanism fracture. It is suggested that observed weakening in evaporites under dilatant conditions and in the presence of brine is due primarily to the enhancement of fracture mechanics processes through selective dissolution from stressed areas in the rock, such as fracture-process zones and asperities acting as barriers to slip.

Shende (2003) studies the effect of brine on the performance of mine supports with and without dissolution control measures (DCM) in uniaxial loading conditions. Acoustic emission (AE), as a nondestructive testing technique, was used to evaluate the dissolution chemistry processes and the time dependent behavior of potash rock. The uniaxial testing program consisted of loading potash specimens in a creep frame to reproduce pillar loading, and then to simulate the presence of brine using three different brine inflow scenarios, increasing, stagnant and continuously refreshing brine conditions. Brine temperature ranged between 20°C and 60°C, and pillar load conditions varied from unloaded to 50% of the unconfined compressive strength (UCS) of the rock. Potash specimens were fitted with AE transducers to monitor energy emission and brine sampling was used to assess dissolution reactions. The results of uniaxial testing without DCM indicated that dissolution rates and strength characteristics are highly dependent on the brine inflow pattern, brine temperature and load conditions. Loads approaching 50% UCS tend to generate very high rates of energy emission, often leading to the failure of the simulated pillars. It was demonstrated that AE could be effectively used for predicting the strength behavior and failure progression of pillars when exposed to brine inflow under uniaxial loading conditions.

Source and flow direction of brine flooding in salt and potash mine can use stable isotopes of oxygen and hydrogen to map the flow of water between formations and to identify accurately the source of mine water leaks in order to undertake proper preventative or remedial action (Wittrup et al., 2010). Flow direction of flooding in salt and potash mine can also use 3D numerical models. The impact of these different chemical and physical relations may have a relevant impact on the 3D numerical modeling result. The 3D numerical models provide many advantages for better way and work as a basis for decision making and sustainable remedy (Ruhaak et al., 2009).

2.5 Effect of cement seal in salt and potash mine

Cement can be used as sealing materials in salt and potash mine for reducing surface subsidence above mining area. Sealing actively used boreholes involved sealing of the annular zone between casing or pipe and the host rock and sealing of open boreholes that would be used in the future. The reasons for sealing of actively used boreholes were to protect the casing from corrosion, to prevent blowouts by quickly forming a seal, to protect the casing from shock loads in drilling deeper, and to seal off zones of circulation or thief zones (Econoides et al., 1998).

Eyermann et al. (1995) survey and collected data of sealing method and materials that used in salt and potash mining industries. At first given important to concrete and then expanded to include other materials. The case studies could provide useful design, construction, and performance information for design development. Tepnarong (2012) studies frictional shear strengths between cement grout and rock salt fracture by borehole push-out testing and direct shear testing. As a result, the push-out test show significantly higher values of the frictional resistance at the interface than

does the direct shear testing and high axial strength generally lead to high bond strength. In general, the tested cement grout has satisfied the mechanical performance requirement.

Fuenkajorn and Daemen (1987) study mechanical relationship between cement, bentonite and surrounding rock. The study dealt with the mechanical interaction between multiple plugs and surrounding rock and identification of potential failure. Two conceptual plug designs were studied. Pipe tests were performed to determine the swelling pressures of 60 mm diameter bentonite plugs and of 64 mm diameter cement plugs. The axial and radial swelling pressures of a bentonite plug specimen were 7.5 and 2.6 MPa after adsorbing water for 5 days. The maximum radial expansive stresses of the cement plugs cured for 25 days were 4.7 and 2.7 MPa for system 1 and system 3 cement. Results from the experiment indicated that in order to obtain sufficient mechanical stability of bentonite seal, the sealing should be done below groundwater level. If cement material was used to seal in hard rock, the mechanical stability would be higher than sealing in soft rock.

The result from cement mechanical testing that used sodium chloride as additive in plain concrete work varying between 2 and 6 percentages can increase the compressive strength of concrete (Oladapo and Ekanem, 2014) and when increasing more curing time, the uniaxial compressive strength, the elastic modulus and the Brazilian tensile strength of cement grout increases and the intrinsic permeability of cement grout decreases (Pattani and Tepnarong, 2015). Akgün and Daemen (1997) study the bond strength of cement grout plugs cast in boreholes in welded tuff cylinders and varying radius and length-to-radius ratio of boreholes. The results show that borehole plugs with smaller radius and greater lengths give higher axial strengths.

2.6 Environmental influence of creep test

Jeremic (1994) discusses the mechanical characteristics of the salt. They are divided into three characteristics: the elastic, the elastic-plastic, and the plastic behavior. The elastic behavior of rock salt is assumed to be linearly elastic with brittle failure. The rock salt is observed as linear elastic only for a low magnitude of loading. The range of linear elastic mainly depends on the content of elastic strain and can be used to formulate the modulus of elasticity. Normally, the modulus of elasticity of rock salt is relatively low. The elastic and plastic behavior of rock salt can be investigated from the rock salt specimen. The confined rock salt specimen at the beginning of incremental loading shows linear elastic deformation but with further load increases the plastic behavior is induced, which continues until yield failure. Elastic and plastic deformation are considered as separated modes of deformability in the majority of cases. The salt material simultaneously exhibits both elastic strain and plastic strain. The difference between elastic behavior and plastic behavior is that elastic deformation is temporary (recoverable) and plastic deformation is permanent (irrecoverable). The degree of permanent deformation depends on the ratio of plastic strain to total strain. The elastic and plastic deformation can also be observed by short-term loading, but at higher load magnitude. The plastic behavior of rock salt does not occur if the applied stress is less than the yield stress. The rock salt is deformed continually if the high stress rate is still applied and is more than the yield stress. Increasing the load to exceed the strain limit of the rock salt beyond its strength causes it to fail. The deformation of 16 rocks salt by the increase of temperature can also result in the transition of brittle-to-ductile behavior.

Specifications for standard test method for creep are given test by American Society for Testing and Materials, ASTM (D7070-08). The time-dependent deformation (or creep) is the process at which the rock can continue deformation without changing stress. Creep deformation occurs in three different phases, as shown in Figure 2.1, which relatively represents a model of salt properties undergoing creep deformation due to the sustained constant load. Upon application of a constant force on the rock salt, an instantaneous elastic strain (ϵ_e) is induced. The elastic strain is followed by a primary or transient strain, shown as Region I. Region II, characterized by an almost constant slope in the diagram, corresponds to secondary or steady state creep. Tertiary or accelerating creep leading to rather sudden failure is shown in Region III. Laboratory investigations show that removal of applied load in Region I at point L will cause the strain to fall rapidly to the M level and then asymptotically back to zero at N. The distance LM is equal to the instantaneous strain ϵ_e . No permanent strain is induced here. If the removal of stress takes place in the steady-state phase the permanent strain (ϵ_p) will occur. From the stability point of view, salt structure deformations after constant load removal have only academic significance, since the stresses imposed underground due to mining operations are irreversible. The behavior of the salts with time-dependent deformation under constant load is characterized as a visco-elastic and visco-plastic phenomenon. Under these conditions the strain criteria are superior to the strength criteria for design purposes, because failure of most salt pillars occurs during accelerated or tertiary phase of creep, due to the almost constant applied load. The dimensions of a pillar in visco-elastic and visco-plastic rock should be established on the basis of a prediction of its long-term strain, to guard against

adequate safety factor accelerating creep (Fuenkajorn and Daemen, 1988; Dusseault and Fordham, 1993; Jeremic, 1994; Knowles et al., 1998).

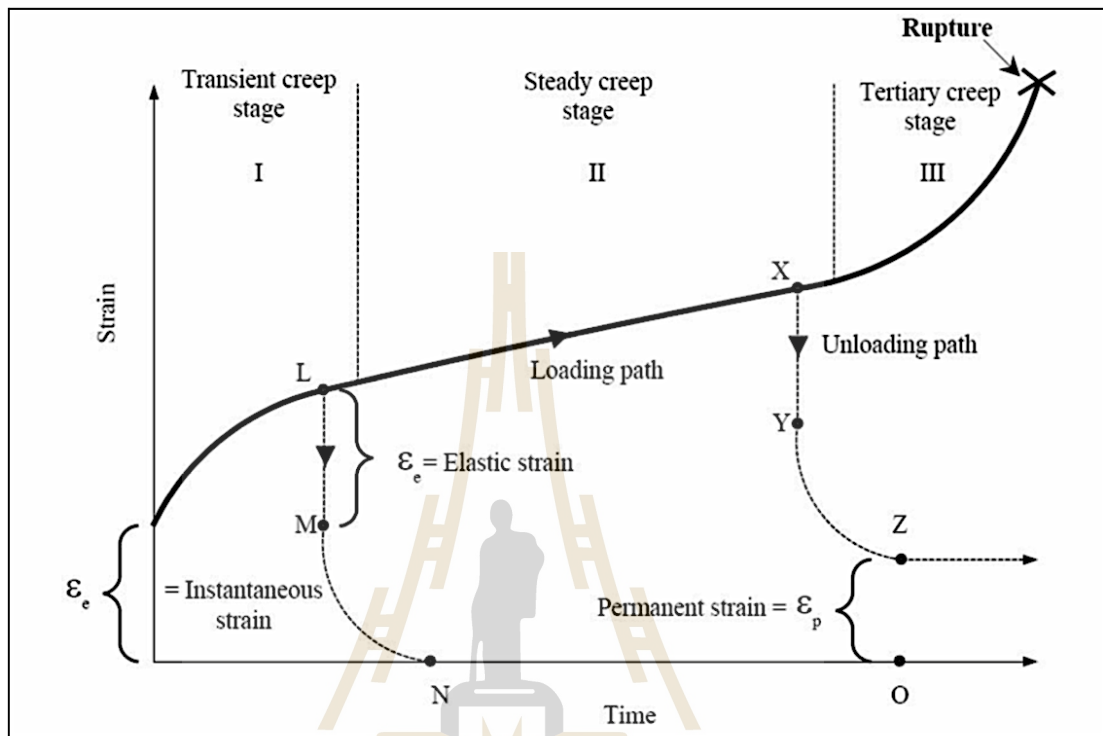


Figure 2.1 The typical deformation as a function of time of creep materials (Jeremic, 1994).

Environmental condition affects the behavior of salt and potash creep, such as temperature, pressure and moisture etc. The effects on rock salt characteristics by these factors are normally shown by the differences in deformation and creep properties.

Effect of temperature on creep increases the plastic property of salt and long-term deformation leading to creep strain increase with increasing temperature (Pudewills et al., 1995; Yang and Daemen, 1997). Jeremic (1994) postulated that rock salts lose their brittleness after extension tempering at approximately 600°C and exhibit a critical shear stress up to 1 MPa.

Hamami et al. (1996) study the triaxial creep testing on salt. The triaxial creep test with low deviatoric stress under an axial stress varying between 5.5 and 15 MPa with a step of 2.5 MPa each 3 months. The triaxial creep test with constant deviatoric stress (under an axial stress of 13 MPa) and decreasing (and increasing) the temperature from 20°C to 90°C (and 90°C to 20°C) with a step of 10°C each 1.5 months. The results concluded that the temperature increase, as for the deviatoric stress, results in an increase of the material deformation. A decrease in temperature reduces remarkably the sample deformation, which is subjected to an important deformation at higher temperatures in the beginning of test. This phenomenon is strain hardening. The strain rate depends on the stress, the temperature and the previous strain.

Cristescu and Hunsche (1996) study the temperature effect on the strain rate suitable for laboratory testing. They suggested that the appropriate strain rate for testing at 100°C and 200°C is 10^{-8} s^{-1} and 10^{-7} s^{-1} because the temperature can affect the creep deformation and strength of salt under high temperatures. In other words, compressive strength of rocks decrease with the increasing temperature (Inada et al., 1997).

Charpentier (1984) studies the time-dependent behavior of rock salt under temperature to develop specific creep equipment. At present, the experimental installation of three temperature levels between 20°C and 200°C for uniaxial creep. Two specimens tested at 20°C applies the uniaxial stresses of 15.3 MPa and 17.8 MPa correspond respectively to 65% and 75% of the uniaxial compressive strength. The creep was observed during two months. At this stage the strain rate is not stable yet and they are still in a transient phase for the two samples. This primary creep can be interpreted by means of a time - hardening law. Test at 100°C applied the uniaxial stresses of 11.3 MPa and 15.3 MPa correspond respectively to 65% and 75% of the

uniaxial compressive strength. During about 30 days the values of strain rates are $13 \times 10^{-6} \text{ hr}^{-1}$ and $18 \times 10^{-6} \text{ hr}^{-1}$. For the most severely loaded sample, the increase of the strain rate after two months denotes the existence of a tertiary state which can probably lead to failure. Three specimens obtained on test at 200°C . The uniaxial stresses of 3.4 MPa, 5 MPa and 7.5 MPa correspond respectively to 20%, 30% and 45% of the uniaxial compressive strength. For the two specimens with the highest levels of load the creep is very important, the strains are 15% and 25% after about two months. This fact shows the major effect of temperature on the time-dependent behavior of rock salt. For the specimens with the smallest load, they have measured only 2% of strain after two months.

Yang et al. (1999) study the confining pressure effects on the time-dependent stress strain behavior of salt rock. The steady-state creep strain rate increases as deviatoric stress increases but decreases as confining pressure increases. An exponential function is suggested to model the creep strain from transient to steady-state and found fitting well the creep strain. Calculated values using the proposed functions are compared with experimental results. The relationship between the steady-state creep strain rate and confining pressure can be approximated by an exponential function. The relationship between the steady-state creep strain rate and deviatoric stress can be approximated by a power function. The result indicated that the transient creep strain (initial creep) depends on confining pressure, especially at low confining pressures ($<3 \text{ MPa}$). The transient creep strain obviously decreases with increasing confining pressuring and steady-state strain rate appears not to be sensitive to confining pressure when confining pressure is high.

Creep of halite is affected by humidity of the atmosphere, especially above 75% R.H., when dissolution of the sample occurs. Below 75% R.H., no detectable dissolution occurs, but creep is still affected by the humidity. Higher humidity induces a higher rate of deformation. The creep of halite specimens submerged in saturated brine is as high as those tested at 75% R.H. The sample tested underwater fail rapidly due to dissolution (Varo and Passaris, 1977).

Wilalak (2016) proposes the effects of $C_{\%}$ on the creep rate tend to be largest for the specimens with $C_{\%}$ between 20% and 40%. Both amount and distribution of the carnallite have a significant impact on the strength and time-dependent deformation of the rock salt specimens. Larger strains and strain rates are obtained for the specimens with higher $C_{\%}$. The presence of carnallite layers notably reduces the strain rates in the steady-state creep phase. Under the same $C_{\%}$, increasing the number of carnallite layers further reduces the strain rates. This is because the additional carnallite layers increase the number of interfaces between the carnallite and halite, and hence increases the localized shear stress locations which enhances the lateral resistance within the specimens.

2.7 Backfill technologies

Backfill refers to any waste material that is placed into voids mined underground for the purpose of either disposal or to perform some engineering functions (Liu et al., 1999). According to Tony Grice from Australian Mining Consultants, there are three major traditional backfill methods: Rock backfill, hydraulic backfill and paste backfill (Grice, 1998). Rock backfill is a technology which transports backfill materials such as stone, gravel, soil, industrial solid waste through manpower,

gravity or mechanical equipment in order to form compressible backfill body. The raw material usually prepared by crushing, sieving and mixing by mechanical force according to the particle size distribution pattern. Hydraulic backfill is a technology which takes water as transports medium to carry the hydraulic backfill materials, such as mountain sand, river sand, crushing sand, tailings or water quenching slag. Paste backfill is transports cemented slurry that is prepared by mixing and stirring water with aggregate materials.

The use of cement backfill is an increasingly component of underground mining operations and is becoming a standard practice for use in many cut-and-fill mines (Landriault et al., 1997). Backfill materials were placed into previously mined stopes to provide a stable platform for the miners to work on and ground support for the walls of the adjacent adits as mining progresses by reducing the amount of open space which could potentially be fill by a collapse of the surrounding pillars (Barret et al., 1978). Thus, the cement backfill placement provides an extremely flexible system for coping with changes in geometry of the orebody, that result in changing stope width, dip, and length (Wayment, 1978). The method of the fill delivery depends upon the amount of energy required to deliver the backfill material underground which depends on its distribution cone (Arioglu, 1983). The cement backfill is usually transported underground through reticulated pipelines.

Mine waste backfill is an innovative tailings management method that returns much of this waste material to the underground mine cavities (Mostafa et al., 2004). At the same time, it can be used as a structural element participating in the ground support. This allows the mine operator to extract a greater amount of the underground ore. Cemented backfill is composed of mine tailings generated during mineral processing

which are mixed with additives such as Portland cement, lime, bentonite, fly ash, and slag. The purpose of the binding agents is to develop cohesion within cement material. Kaew-iod (2011) studies the properties of tailing potash, fly ash, FGD gypsum to replace the cement and find suitable properties backfill materials the underground potash mine. The experiments are divided into two series: Series 1, using tailing potash 50% by weight, fly ash 30% by weight, FGD gypsum 15%, 17% and 19% and cement 5%, 3% and 1% with water - binder ratios (w/b) of 0.5, 0.6 and 0.7, respectively; and Series 2, tailing potash 70% by weight, fly ash 20% by weight, FGD gypsum 5%, 7% and 9% and cement 5%, 3% and 1% with water - binder ratios (w/b) of 0.5, 0.6 and 0.7. Found, mixing ratio of fly ash can be used as backfill material ranging from 20% to 30% and mixing ratio of FGD gypsum can be used as backfill materials ranging from 5% to 15% mixture of backfill materials suitable for low compressive strength 2 - 8 MPa and experiment indicated that backfill can reduce collapse rate in the underground mines.

An abandoned potash mine in northern Germany was intentionally flooded with brine from a solution- mining operation. Prior to flooding, the mine was instrumented to measure the effects of flooding on the mine and salt. As part of the abandonment and test program, a bulkhead was constructed in a deadend drift. The bulkhead was instrumented to determine its mechanical response to loading by the brine as the mine was flooded and to determine if water leaked past the bulkhead. The 500-m-deep (1640-ft- deep) drift was about 20 years old at the time the bulkhead was constructed.

Fischle and Stover (1986) construct a bulkhead and measured under brine pressure. The bulkhead consisted of two salt-saturated concrete elements with a sand-asphalt seal between them. The sand-asphalt mixture was about one-third bitumen by

volume with the remainder being 80 percent sand and 20 percent powdered limestone. The concrete mix had a water:cement ratio of 0.5:1 with 3 percent salt (by weight). The uniaxial compressive strength of the concrete was 23.7 MPa (3,450 psi). The concrete permeability to brine was about 10^{-18} m². The outer face of the bulkhead was covered with a membrane composed of alternating layers of bitumen and stainless steel strips. The membrane was supported with a masonry block wall to prevent the strips from peeling away from the face.



CHAPTER III

SAMPLE PREPARATION

3.1 Introduction

This chapter describes the rock salt sample preparation procedure to be used in the uniaxial creep tests and humidity tests. The salt is obtained from underground openings of ASEAN Potash Mining Co., Ltd. (APMC).

3.2 Sample preparation

The tested samples belong to the Lower Salt Member of the Maha Sarakham formation, Khorat basin, northeast of Thailand. Warren (1999) describes the origin and geological structures of the Maha Sarakham salt. The samples contain mixture between halite and carnallite. An attempt to obtain cylindrical cores has been made in the laboratory. During drilling the cores with high carnallite content tended to break along the bedding planes, particularly at the interfaces between the carnallite and halite. The specimens used for uniaxial creep tests are therefore prepared as rectangular blocks with nominal dimensions of $54 \times 54 \times 108 \text{ mm}^3$. A high speed rock cutting device is used. Organic oil is used as cutting fluid. The nominal sizes of specimen that is shown in Table 3.1. Table 3.2 to Table 3.4 show the summary of salt specimen dimension prepared for each test type. Twenty nine salt specimens prepared for the uniaxial creep tests have 54 mm in diameter (Figure 3.1). The ratio of specimen length to specimen diameter (L/D) is 2.0. Seven potash specimens prepared for the uniaxial creep tests

have 54 mm in diameter (Figure 3.2). The ratio of specimen length to specimen diameter (L/D) is 2.0. Fifteen rock salt specimens prepared for the humidity tests have 45 mm in diameter (Figure 3.3). Due to the difference of densities between halite and carnallite, the carnallite content (C%) for each specimen can be determined by the following relation:

$$C_{\%} = \left(\frac{\rho - \rho_s}{\rho_c - \rho_s} \right) \times 100 \quad (1)$$

where ρ is density of the specimen, ρ_s is density of halite (2.16 g/cc) and ρ_c is density of carnallite (1.60 g/cc) (Klein et al., 1998).

Table 3.1 Nominal dimension of specimens for different tests.

Methods	L/D ratio	Nominal Diameter (mm)	Nominal Length (mm)	Number of Specimens
Salt specimens for uniaxial creep test	2.0	54	108	29
Potash specimens for uniaxial creep test	2.0	54	108	7
Carnallite specimens for humidity test	-	45	90	15

Table 3.2 Salt specimens prepared for uniaxial creep tests.

Specimen Number	Average Width (mm)	Average Length (mm)	Average Height (mm)	Weight (g)	Density (g/cc)
RS-Creep-01	53.30	54.23	107.88	668.1	2.13
RS-Creep-02	53.10	52.68	106.28	661.3	2.22
RS-Creep-03	53.15	54.50	107.89	670.6	2.15
RS-Creep-04	54.93	54.15	100.70	657.4	2.12
RS-Creep-05	53.56	53.05	106.83	652.7	2.14

Table 3.2 Salt specimens prepared for uniaxial creep tests (continued).

Specimen Number	Average Width (mm)	Average Length (mm)	Average Height (mm)	Weight (g)	Density (g/cc)
RS-Creep-06	54.30	54.30	108.23	693.8	2.24
RS-Creep-07	54.88	54.15	108.45	691.3	2.18
RS-Creep-08	55.05	53.93	107.73	691.6	2.17
RS-Creep-09	53.45	52.70	108.08	688.0	2.22
RS-Creep-10	53.78	53.73	108.16	670.5	2.13
RS-Creep-11	54.28	54.23	107.51	661.0	2.09
RS-Creep-12	54.43	54.45	107.28	662.5	2.09
RS-Creep-13	54.05	54.45	107.56	662.7	2.09
RS-Creep-14	52.59	54.75	108.24	660.0	2.13
RS-Creep-15	53.36	53.26	108.08	674.0	2.15
RS-Creep-16	53.01	54.36	108.06	662.5	2.14
RS-Creep-17	53.40	54.20	107.70	671.0	2.14
RS-Creep-18	53.80	53.20	107.96	660.0	2.11
RS-Creep-19	54.70	52.76	107.50	665.5	2.14
RS-Creep-20	53.63	53.69	107.32	666.5	2.14
RS-Creep-21	53.45	53.97	108.03	663.5	2.11
RS-Creep-22	54.23	53.98	107.64	659.5	2.09
RS-Creep-23	54.35	55.35	107.05	668.0	2.10
RS-Creep-24	54.26	53.84	107.86	673.0	2.14
RS-Creep-25	53.26	53.68	107.36	653.0	2.13
RS-Creep-26	54.28	54.20	107.91	660.0	2.09
RS-Creep-27	53.85	54.25	107.76	652.0	2.08
RS-Creep-28	53.70	54.36	108.03	676.0	2.13
RS-Creep-29	54.15	53.36	107.87	657.0	2.11

Table 3.3 Potash specimens prepared for uniaxial creep tests.

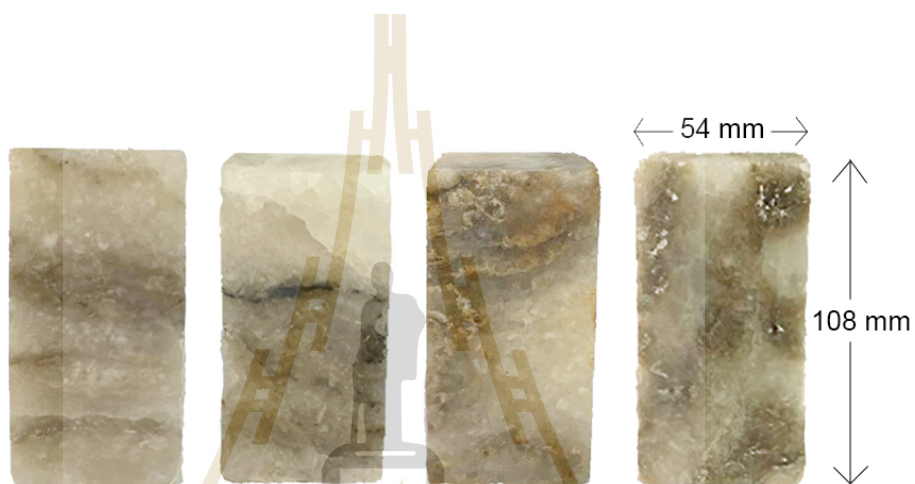
Specimen Number	Average Width (mm)	Average Length (mm)	Average Height (mm)	Weight (g)	Density (g/cc)	Carnallite content by weight (C%)
PT-Creep-01	53.20	53.60	106.80	542.2	1.76	71.43
PT-Creep-02	52.50	55.85	108.55	549.6	1.70	82.14
PT-Creep-03	55.85	57.05	111.79	583.0	1.63	94.64
PT-Creep-04	54.38	54.05	109.06	531.5	1.63	94.64
PT-Creep-05	56.35	56.55	110.45	546.4	1.61	98.93
PT-Creep-06	54.27	54.15	109.06	548.1	1.69	83.93
PT-Creep-07	54.18	55.10	109.65	531.0	1.63	94.64

Table 3.4 Specimens prepared for humidity tests.

Specimen Number	Average Width (mm)	Average Length (mm)	Average Height (mm)	Weight (g)	Density (g/cc)	Carnallite content by weight (C%)
PT-HM-01	50.14	50.25	95.12	488.10	2.04	22.03
PT-HM-02	45.13	45.15	90.15	481.00	2.05	19.12
PT-HM-03	44.81	44.97	89.73	390.60	2.16	00.00
PT-HM-04	45.04	44.62	89.80	301.00	1.67	87.81
PT-HM-05	43.91	45.53	86.75	328.50	1.89	47.40
PT-HM-06	44.12	43.81	87.56	295.00	1.74	74.39
PT-HM-07	44.31	44.03	87.73	294.50	1.72	78.41
PT-HM-08	47.36	45.33	90.05	319.10	1.65	90.95
PT-HM-09	43.73	45.40	90.46	317.20	1.77	70.30
PT-HM-10	43.73	43.14	85.81	268.80	1.66	89.18
PT-HM-11	44.34	45.30	92.21	361.15	1.95	37.42
PT-HM-12	50.93	51.74	96.60	523.70	1.98	32.28
PT-HM-13	42.68	42.27	84.21	261.80	1.72	77.92

Table 3.4 Specimens prepared for humidity tests (continued).

Specimen Number	Average Width (mm)	Average Length (mm)	Average Height (mm)	Weight (g)	Density (g/cc)	Carnallite content by weight (C%)
PT-HM-14	45.11	44.83	91.21	344.40	1.87	52.24
PT-HM-15	44.34	44.32	90.18	308.10	1.74	75.22

**Figure 3.1** Some salt specimens prepared for uniaxial creep tests with $L/D = 2.0$.**Figure 3.2** Some potash specimens prepared for uniaxial creep tests with $L/D = 2.0$.

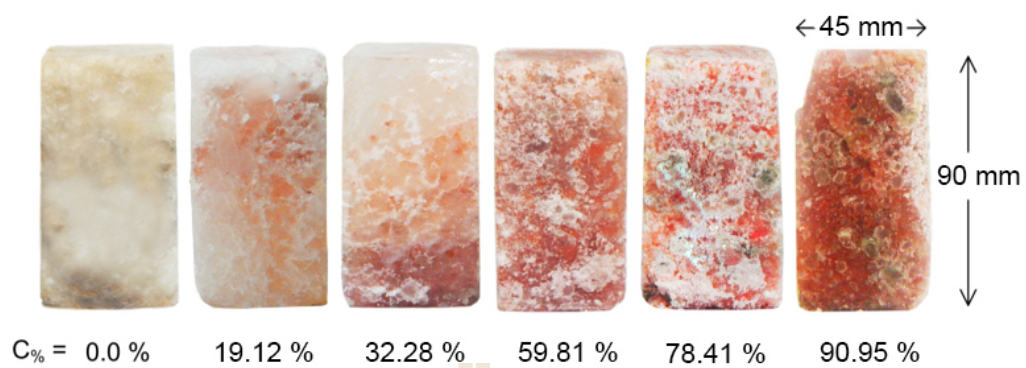
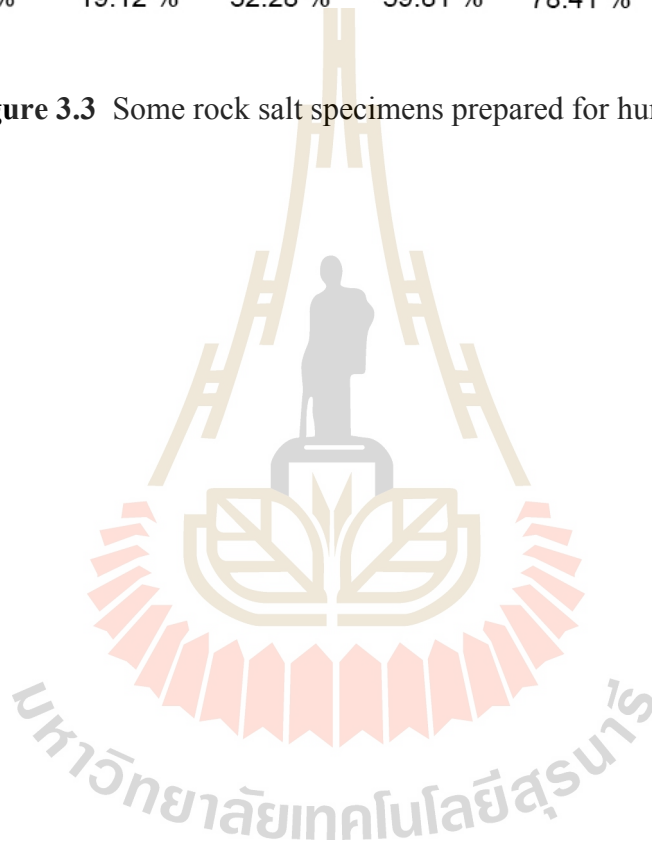


Figure 3.3 Some rock salt specimens prepared for humidity tests.



CHAPTER IV

LABORATORY TESTING METHODS AND RESULTS

4.1 Introduction

The objective of the laboratory testing is to determine the time-dependent properties of the Maha Sarakham rock salt under brine submersion and the effect of humidity on the dissolution of the specimens containing various percentages of halite and carnallite. This chapter describes the method, apparatus and results of the uniaxial creep test, humidity testing and weight loss testing.

4.2 Uniaxial creep test

A consolidation load frame (Jandakaew, 2007) has been used to apply constant axial stress for uniaxial creep test (Figure 4.1). It has been used in this study because the cantilever beam with pre-calibrated dead weight can apply a truly constant axial stress to specimens. Pre-calculated dead weight loading devices are used to apply constant axial loads to the specimens. Except the specimen shape the test procedure follows, as much as practical, the American Society for Testing and Materials (e.g. ASTM D7070-08). Neoprene sheets are placed at the interfaces between the loading platens and top and bottom specimen surfaces. Each specimen is tested up to 21 days. A total of 36 specimens have been tested. The axial deformation is monitored using displacement dial gages. They are used to calculate the axial strains of the specimen. The readings are made every one minute for the first hour. After that the reading interval are gradually increased to every hour. The specimens are tested under the axial

stresses of 2, 4, 6, 8, 10 and 12 MPa. Three types of saturated brine are used in this study: halite, carnallite and magnesium brines.

The halite brine is prepared by mixing distilled water with pure sodium chloride (NaCl). Halite is mixed with distilled water until no more salt can be dissolved. The solubility in fresh water under saturated condition of NaCl is 6.15 mole/L (Warren, 2016). The halite solution follows the reaction :



Pure carnallite ($\text{KMgCl}_3 \cdot 6\text{H}_2\text{O}$) obtained from a potash mine is used to prepare the carnallite brine. It is mixed with distilled water until no more carnallite can be dissolved. The solubility in fresh water under saturated condition of KCl is 4.78 mole/L (Warren, 2016). The carnallite solution follows the reaction :



Magnesium brine is prepared from pure magnesium chloride (MgCl_2) mixed with distilled water of 5.84 mole/L under saturated condition (Warren, 2016). The magnesium chloride solution follows the reaction :



The specimens are under loading for 7 days, they are separately submerged in three different saturated solutions. Then the solution is removed after 7 days by syringe and rubber tube (Figure 4.2). The specimens under three conditions (before, during and after solution submersion) are illustrated in Figure 4.3.

The cement slurry for the uniaxial creep testing is prepared in this study by mixing cement with sodium chloride (NaCl) saturated brine. The components of

cement slurry are commercial grade Portland cement mixed with chloride resistant agent, NaCl saturated brine, anti-form agent and a liquid additive for expansion. Table 4.1 gives the weight compositions of the mixtures which follows those of Pattani (2014).

Portland-pozzolan cement is selected due to its low brine demand, sulfate resistance and widely used in construction industry. A liquid additive contributes to expansiveness of the mixture. An anti-forming agent is used to decrease the air content of the cement slurry and to ease a control of cement slurry weight and volume. The tests are conducted under ambient temperature (25-28 Celsius). The specimens are under loading for 7 days, they are submerged in cement sealing material for 14 days.

Table 4.1 Weight compositions of cement.

Composition of slurry	(g)
Portland-pozzolan cement, type IP	1000
NaCl saturated brine	670
Intraplast Z _x	10
Plastocrete	10



Figure 4.1 Consolidation load frame used for creep testing of salt and potash specimens. Specimen is set in water-tight PVC cylinder for submerging solutions during loading.



Figure 4.2 The solution is removed by syringe and rubber tube.

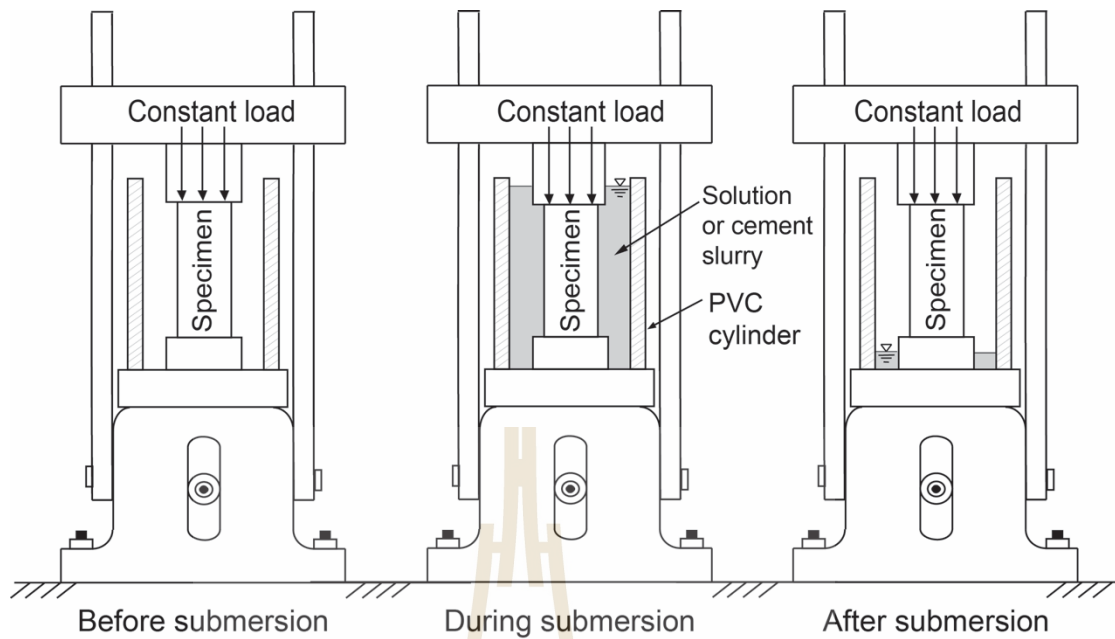


Figure 4.3 The specimens under three conditions before, during and after solution or cement submersion.

4.3 Humidity Testing

An attempt is made to assess the effect of humidity on the integrity of the specimens. The effect of humidity on the dissolution of the specimens containing various percentages of halite and carnallite is assessed by placing them in a humidity controlled chamber for 60 hours with R.H. = 95%. The weight of each specimens is measured every 6 hours to the nearest 0.1 g. Figure 4.4 shows the instrument using in humidity testing.



Figure 4.4 Humidity testing instrument.

4.4 Weight Loss Testing

An attempt is made here to further confirm the effects of carnallite contents on the creep deformation in the previous topic. It is postulated that the increase of strain rate during solution submersion of the specimens containing carnallite is primarily due to the dissolution of the creep specimen perimeter. This results in a decrease of the cross-section area of the specimens, and hence its axial stress is increased while under the same loading magnitude. To verify this postulation a series of weight loss testing has been performed. The specimens with carnallite contents ($C\%$) varying from 0 (pure halite) to 91% are separately submerged in the three different solutions for 7 days. Their weights are measured daily to the nearest 0.1 g. The weight loss is calculated by:

$$\text{Weight Loss} = [(W_o - W_i) / W_o] \times 100 (\%) \quad (4.1)$$

where W_o is the initial weight of specimen and W_i is the specimen weight during submersion each day.

4.5 Test results

4.5.1 Uniaxial creep test

Figures 4.5 to 4.7 give axial strain-time curves obtained from pure halite specimens under dry and submersion in halite brine, carnallite brine and magnesium brine, respectively. The creep rates of pure halite specimens are not affected by the three brine solutions. The curves show the instantaneous, transient and steady-state creep phases of the specimens. Figures 4.8 to 4.10 show examples of the axial strain-time curves for potash specimens. The potash (salt with carnallite contents) specimens are however highly sensitive to the solutions prepared from the saturated halite and carnallite brines. They fail almost immediately after submersion under halite and carnallite brines probably because the specimens can dissolve in these brines, and hence accelerates the creep rate and eventually reaches the tertiary creep phase (toward failure). Under saturated magnesium brine however the creep rates of the potash specimens do not vary with the conditions before, during and after solution submersion. Figures 4.11 and 4.12 show the axial strain as a function of time for salt tested specimens submerged in cement slurry and crosssection of some tested specimen after cement setting. The creep rates of specimens gradually decrease after adding the slurry and cement setting.

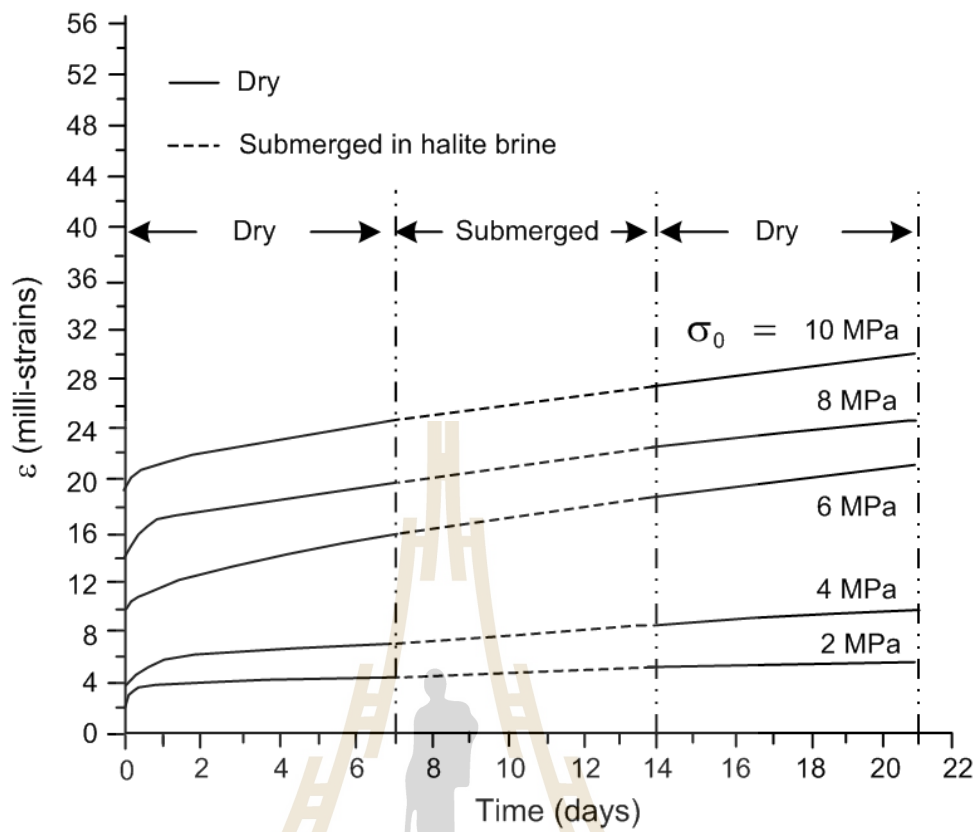


Figure 4.5 Strain-time curves obtained for creep testing of pure halite submerged in halite brine.

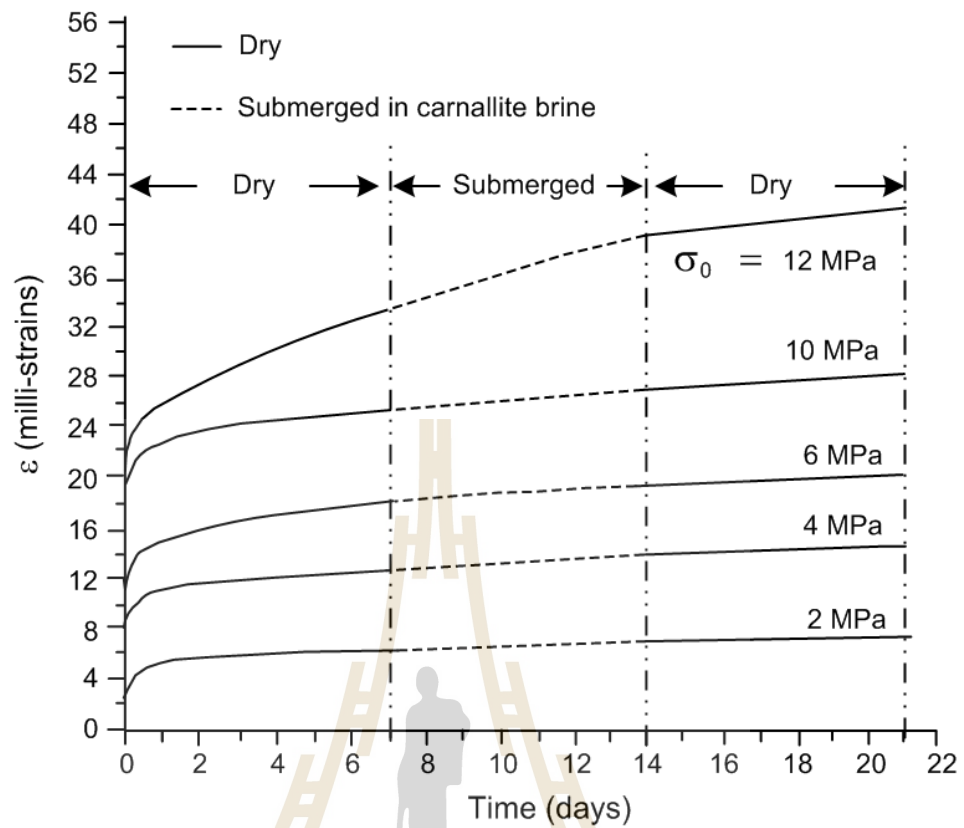


Figure 4.6 Strain-time curves obtained for creep testing of pure halite submerged in carnallite brine.

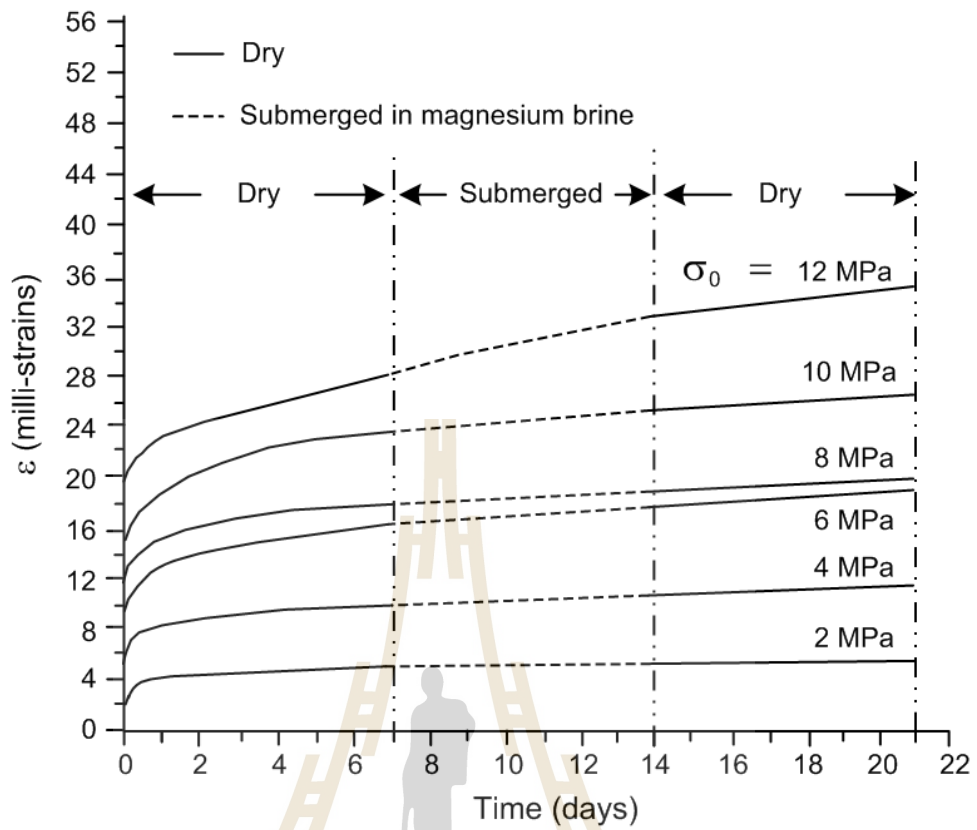


Figure 4.7 Strain-time curves obtained for creep testing of pure halite submerged in magnesium brine.

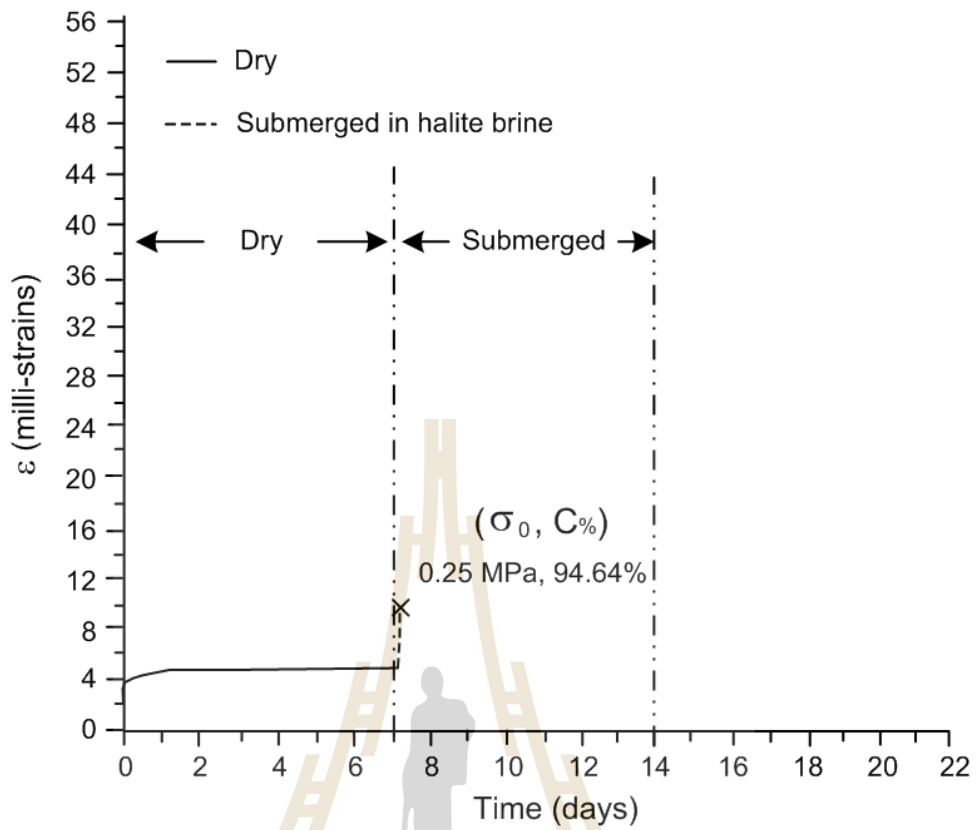


Figure 4.8 Strain-time curves obtained for creep testing of potash specimen submerged in halite brine.

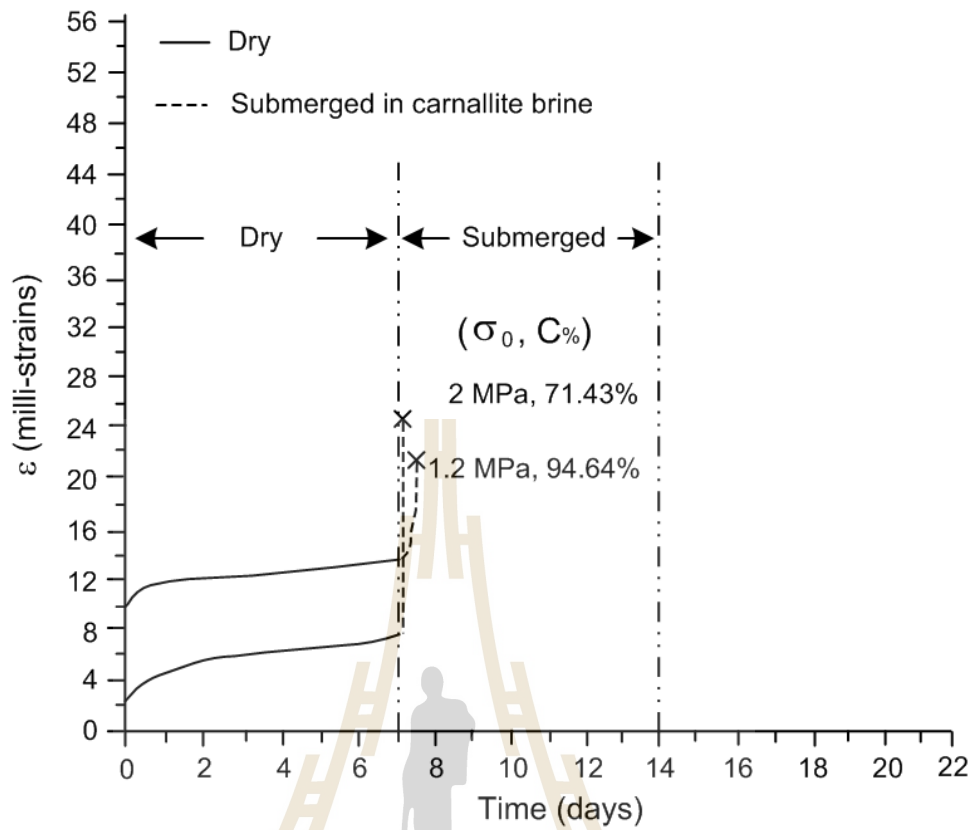


Figure 4.9 Strain-time curves obtained for creep testing of potash specimen submerged in carnallite brine.

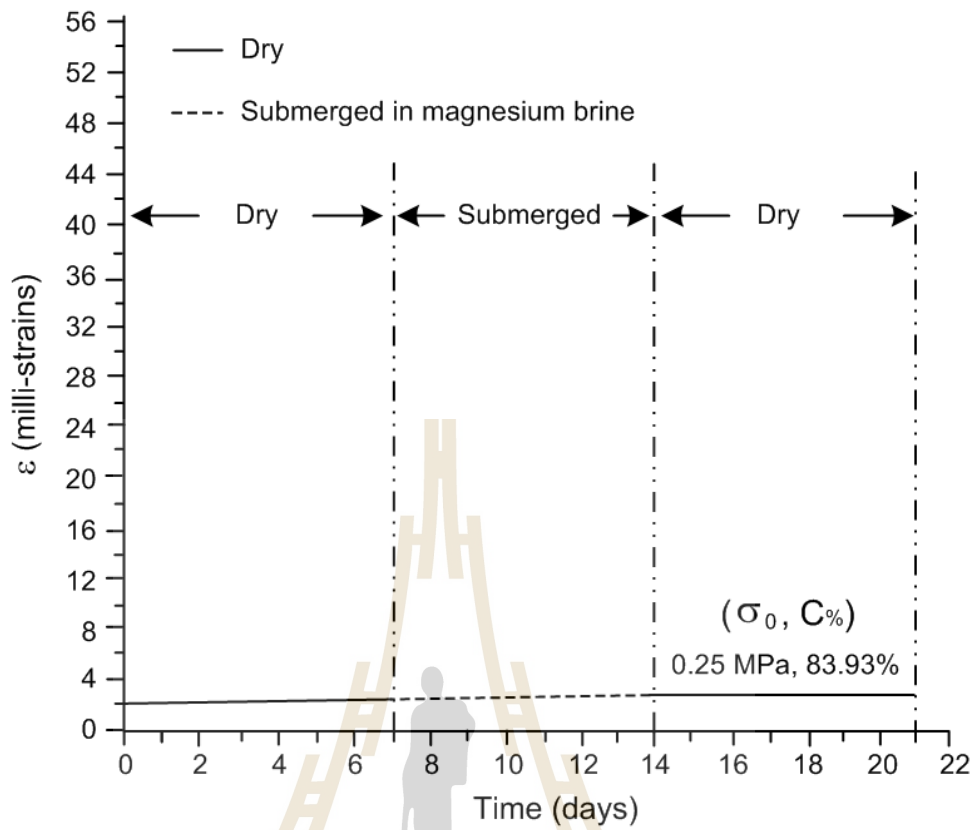


Figure 4.10 Strain-time curves obtained for creep testing of potash specimen submerged in magnesium brine.

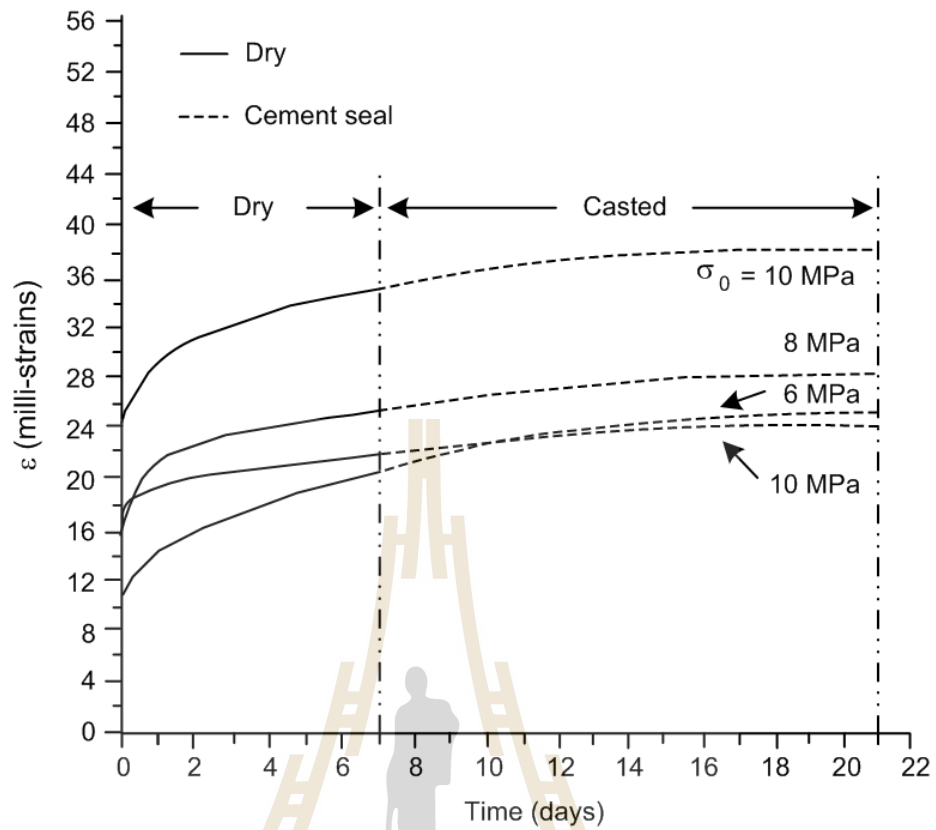


Figure 4.11 Strain-time curves obtained for creep testing of pure halite submerged in cement slurry.

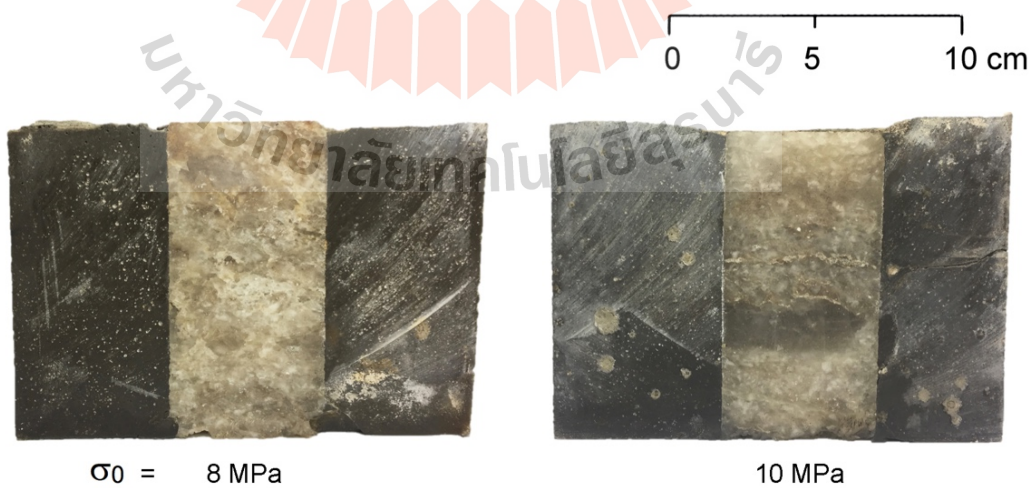


Figure 4.12 Cross-section of some tested specimens after cement setting.

4.5.2 Humidity test

Figure 4.13 plots the weight loss of the carnallite specimens as a function of time. The measured weight loss increases with time. Higher carnallite contents lead to greater weight loss. The findings can be used for the material selection and the performance assessment of the installed backfill in salt and potash mines.

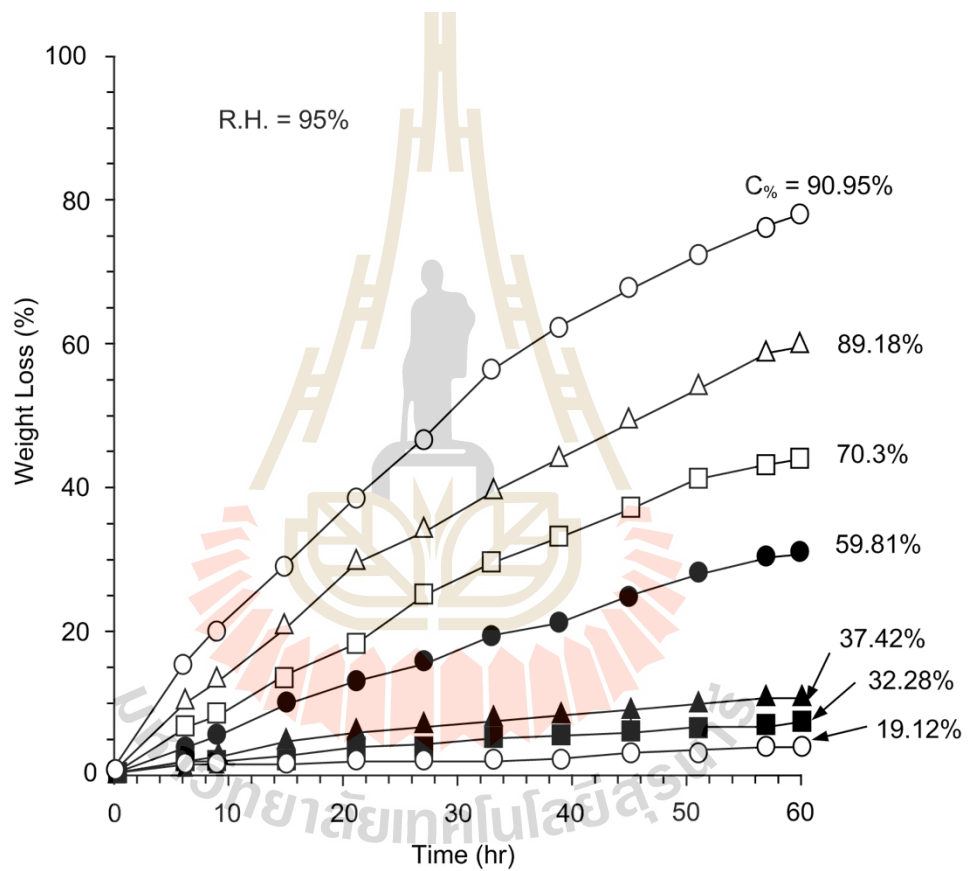


Figure 4.13 Weight loss (%) of the carnallite specimen as a function of time.

4.5.3 Weight loss testing

Tables 4.2 to 4.4 show the configurations of some specimens contained various carnallite contents submerged in different types of brine. The dissolution occurs with carnallite content remaining the halite content. The dark phase in carnallite specimen ($C_{\%} > 20\%$) represents the carnallite content and white phase represents the halite content. Figures 4.14 to 4.16 plot the weight loss as a function of time for each specimen under different submerging solutions. It is clear that pure halite specimens ($C_{\%} = 0$) is insensitive to the three solutions. The percentage of weight loss is largest when the potash specimens are subjected to halite solution (Figure 4.14). The saturated magnesium brine tends to have insignificant effect on the specimens even for those containing carnallite up to 96% (Figure 4.16). The solution prepared from carnallite can notably dissolve the specimens, and leads to the weight loss of up to 20% for specimen containing carnallite of 96%. Figures 4.17 to 4.19 show rate of dissolution of the carnallite specimens as a function of time under halite, carnallite and magnesium brine. The rate of the dissolution occurs higher at the first day of submersion compared with the last day for all cases.

Table 4.2 Comparison of some specimen configurations during submersion in halite brine each day.

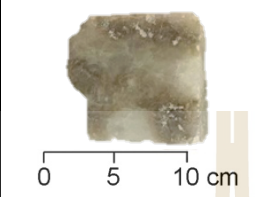
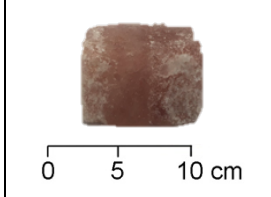
Submersible duration (days)	Carnallite content by weight (C%)		
	00.00%	30.68%	96.58%
0			
1			
2			
3			
4			
5			
6			
7			

Table 4.3 Comparison of some specimen configurations during submersion in carnallite brine each day.

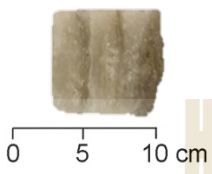
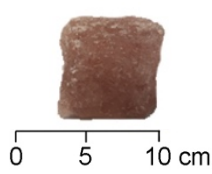
Submersible duration (days)	Carnallite content by weight (C%)		
	00.00%	42.39%	96.58%
0			
1			
2			
3			
4			
5			
6			
7			

Table 4.4 Comparison of some specimen configurations during submersion in magnesium brine each day.

Submersible duration (days)	Carnallite content by weight (C%)		
	00.00%	42.39%	96.58%
0	 0 5 10 cm	 0 5 10 cm	 0 5 10 cm
1			
2			
3			
4			
5			
6			
7			

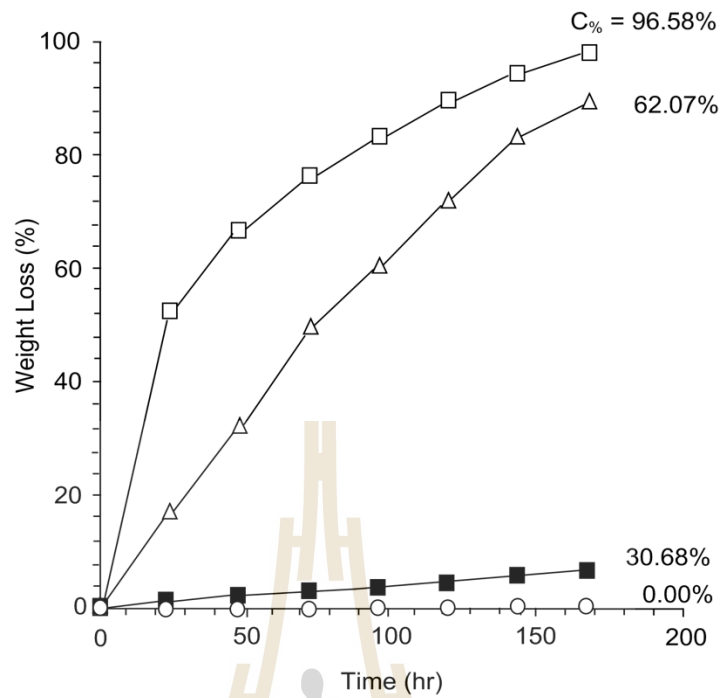


Figure 4.14 Weight loss (%) of the carnallite specimens as a function of time under halite brine.

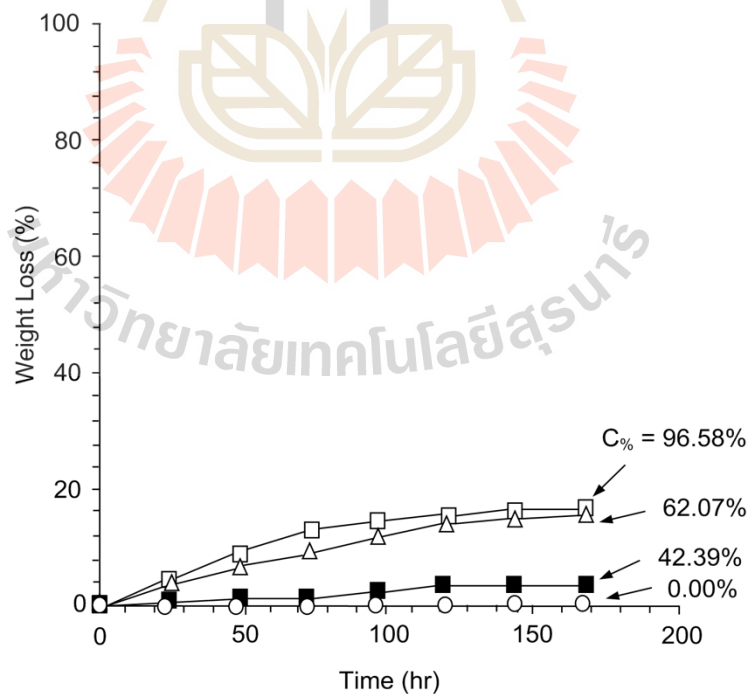


Figure 4.15 Weight loss (%) of the carnallite specimens as a function of time under carnallite brine.

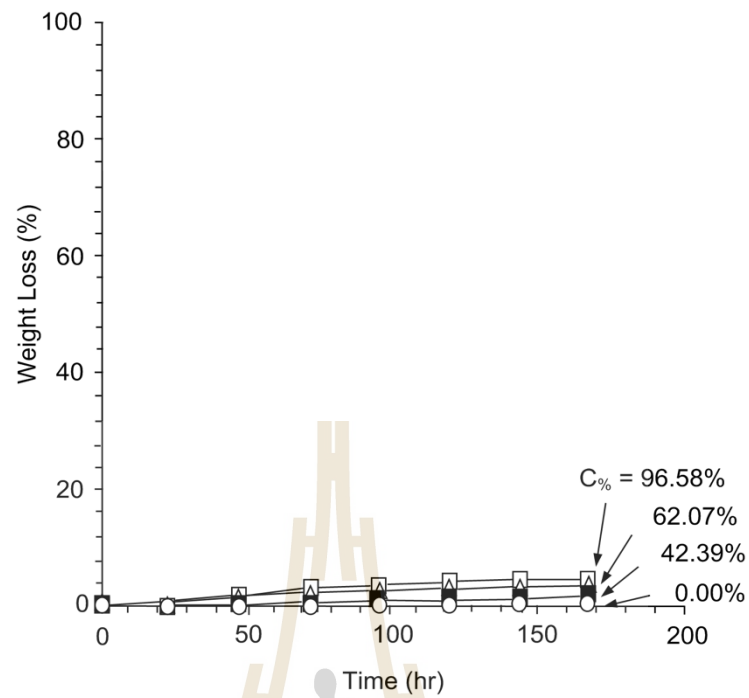


Figure 4.16 Weight loss (%) of the carnallite specimens as a function of time under magnesium brine.

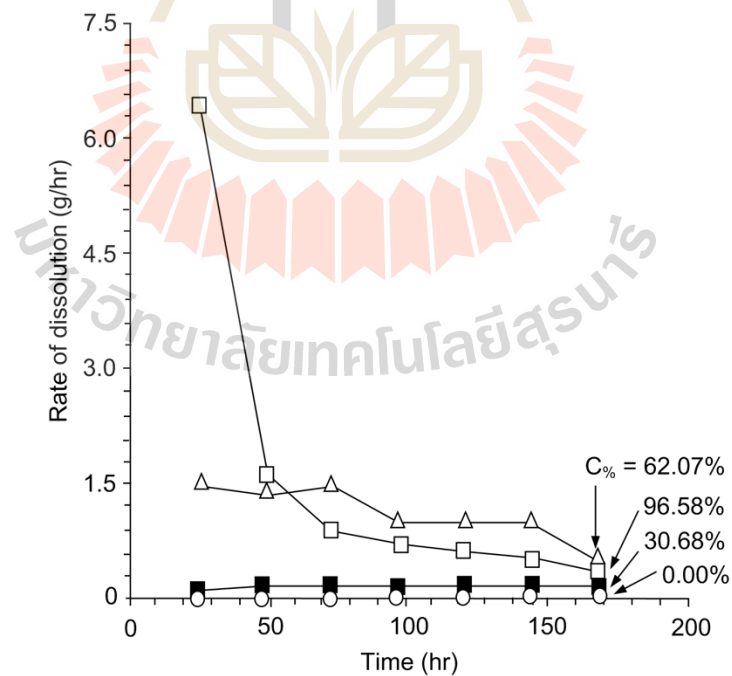


Figure 4.17 Rate of dissolution of the carnallite specimens as a function of time under halite brine.

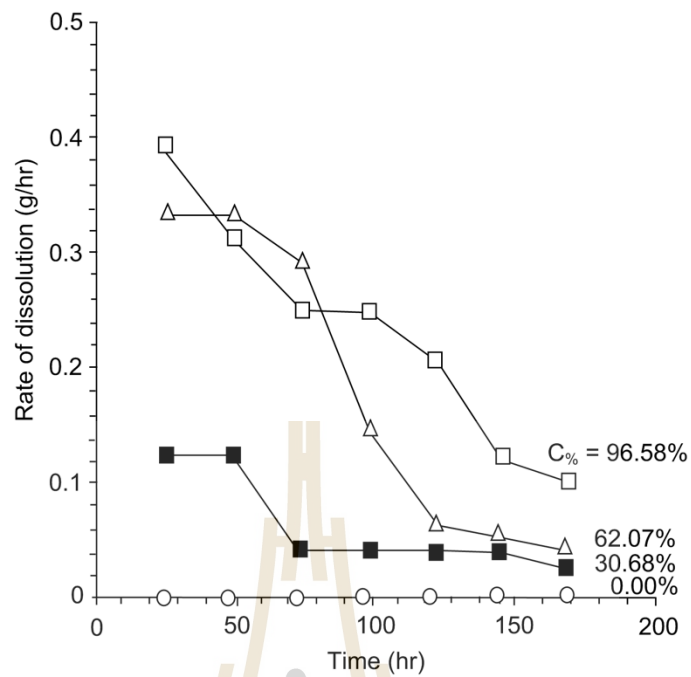


Figure 4.18 Rate of dissolution of the carnallite specimens as a function of time under carnallite brine.

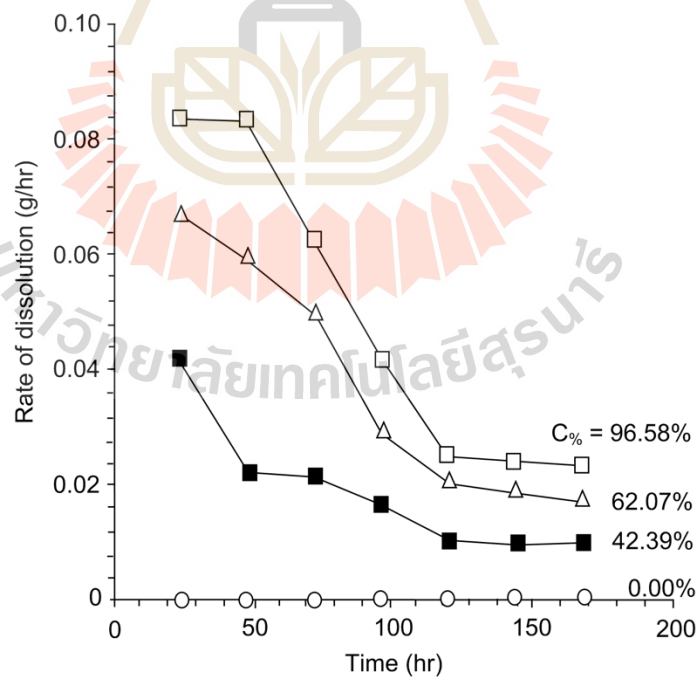


Figure 4.19 Rate of dissolution of the carnallite specimens as a function of time under magnesium brine.

CHAPTER V

CALIBRATION OF BURGERS PARAMETERS

5.1 Introduction

The purpose of this chapter is to calibrate the creep test results with the Burgers model. The objective is to help explain the visco-plastic coefficients measured before, during and after submersion in different solutions and casted in cement.

5.2 Burgers Model

The Burgers model (Richard, 1993) is used to describe the time-dependent deformation of the creep test specimens. It is recognized that numerous creep models or constitutive equations have been developed to represent the time-dependent behavior of rock salt (e.g., Gnirk and Johnson, 1964; Handin et al., 1984; Langer, 1984; Hardy and Sun, 1986; Senseny et al., 1992). The Burgers model is used because it is simple and capable of describing the elastic, visco-elastic and visco-plastic phases of deformation. The governing equation for uniaxial constant stress can present the visco-elastic strain as a function of time as follows (Fuenkajorn and Daemen, 1988):

$$\varepsilon(t) = \sigma_0 \left\{ \frac{1}{E_1} + \frac{t}{\eta_1} + \frac{1}{E_2} [1 - \exp(-E_2 t / \eta_2)] \right\} \quad (5.1)$$

where t is the testing time, E_1 is the elastic modulus, E_2 is the spring constant in visco-elastic phase, η_1 is the viscosity coefficient in steady-state phase, and η_2 is the viscosity

coefficient in transient phase. Regression analyses on the strain-time curves based on Equation (5.1) using the SPSS statistical software (Wendai, 2000) are performed to determine the Burgers parameters for each rock salt specimens before submersion. Figure 5.1 shows the physical components arranged in the Burgers model. Tables 5.1 and 5.2 summarize the calibration results.

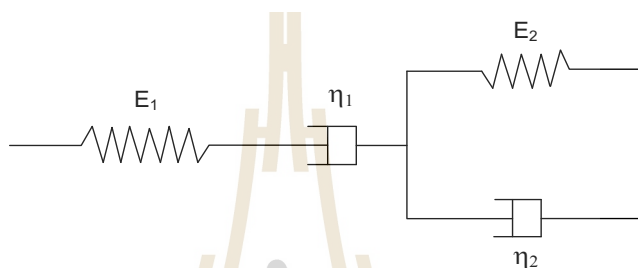


Figure 5.1 Modular components of Burgers model.

Table 5.1 Calibration of the Burgers parameters for salt specimens before submersion.

Sample No.	Stress (MPa)	Burgers parameter				R ²
		E ₁ (GPa)	E ₂ (GPa)	η ₁ (GPa.day)	η ₂ (GPa.day)	
RS-Creep-03	2	0.695	2.43	24.944	1.618	0.956
RS-Creep-13	2	0.655	1.43	20.944	1.818	0.976
RS-Creep-17	2	0.567	2.445	25.018	1.748	0.948
RS-Creep-02	4	1.31	1.515	19.69	0.747	0.929
RS-Creep-14	4	1.431	1.815	18.67	0.784	0.964
RS-Creep-19	4	0.685	1.105	28.16	0.344	0.986
RS-Creep-10	6	0.621	3.65	11.941	2.982	0.994
RS-Creep-15	6	0.621	2.985	12.865	2.973	0.997
RS-Creep-21	6	1.172	1.321	27.113	0.248	0.940

Table 5.1 Calibration of the Burgers parameters for salt specimens before submersion
(continued).

Sample No.	Stress (MPa)	Burgers parameter				R ²
		E ₁ (GPa)	E ₂ (GPa)	η ₁ (GPa.day)	η ₂ (GPa.day)	
RS-Creep-05	8	0.609	2.043	21.361	0.792	0.942
RS-Creep-24	8	0.557	2.745	25.008	1.549	0.959
RS-Creep-07	10	0.557	2.745	25.008	1.549	0.959
RS-Creep-11	10	0.785	1.004	18.16	0.444	0.976
RS-Creep-27	10	0.785	1.004	28.16	0.444	0.976
RS-Creep-12	12	1.022	1.161	19.113	0.248	0.940
RS-Creep-28	12	1.022	1.161	26.113	0.248	0.940
Mean ± SD		0.818 ± 0.284	1.910 ± 0.829	22.017 ± 5.036	1.159 ± 0.914	

Table 5.2 Calibration of the Burgers parameters for potash specimens before submersion.

Sample No.	Stress (MPa)	Burgers parameter				R ²
		E ₁ (GPa)	E ₂ (GPa)	η ₁ (GPa.day)	η ₂ (GPa.day)	
PT-Creep-04	0.25	0.279	1.781	5.980	0.250	0.966
PT-Creep-06	0.25	0.474	2.792	19.230	0.703	0.983
PT-Creep-03	1.2	0.317	1.220	5.218	0.320	0.953
PT-Creep-01	2	0.322	2.120	6.030	0.210	0.974
Mean ± SD		0.348 ± 0.086	1.978 ± 0.657	9.115 ± 6.754	0.365 ± 0.226	

In order to quantitatively determine the effects of the three different submerging solutions on the creep deformation of the specimen, the visco-plastic coefficients (η_1) during each phase of testing are calculated using :

$$\eta_1 = \sigma_0 / \dot{\varepsilon} \quad (5.2)$$

where σ_0 is the constant stress applied to each specimen (MPa) and $\dot{\varepsilon}$ is the strain rates within the steady-state creep phases before, during and after submersion. The visco-plastic coefficients will be used as an indicator of the effects of the solutions on the creep deformation of the specimens during loading. Tables 5.3 to 5.5 and Figures 5.2 to 5.4 show strain rate and visco-plastic coefficients of pure halite specimens measured before, during and after submersion in different solution. The visco-plastic coefficient decreases after adding halite brine but less sensitive with carnallite and magnesium chloride brine. Table 5.6 summarizes the results. Table 5.7 and Figure 5.5 show visco-plastic coefficients of pure halite specimens measured before and during casted in cement.

Table 5.3 Strain rate and visco-plastic coefficients measured before, during and after submersion in halite brine.

Stress (MPa)	Before Submersion		During Submersion		After Submersion	
	Strain rate ($\dot{\epsilon}$)	η_1 (GPa.day)	Strain rate ($\dot{\epsilon}$)	η_1 (GPa.day)	Strain rate ($\dot{\epsilon}$)	η_1 (GPa.day)
2	0.081	24.814	0.080	25.000	0.077	25.974
4	0.226	17.691	0.225	17.770	0.140	28.592
6	0.689	8.710	0.489	12.260	0.310	19.380
8	0.438	18.286	0.466	17.156	0.422	18.980
10	0.475	21.048	0.501	19.960	0.444	22.548
Mean \pm SD	0.382 \pm 0.235	18.110 \pm 5.961	0.352 \pm 0.190	18.429 \pm 4.627	0.278 \pm 0.165	23.095 \pm 4.170

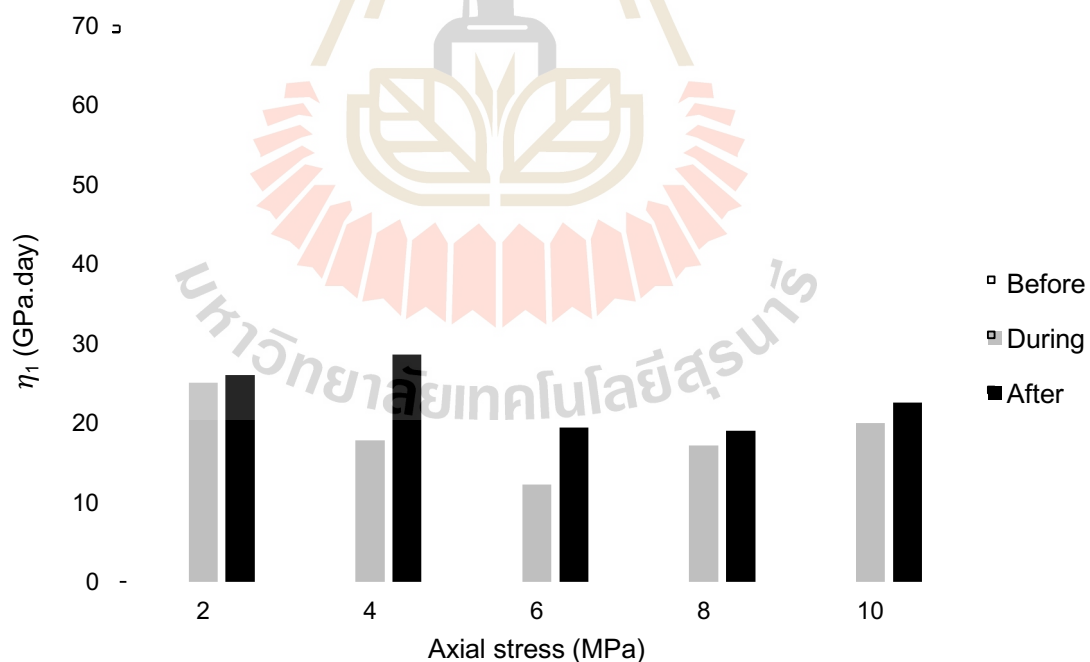


Figure 5.2 Visco-plastic coefficients of pure halite specimens measured before, during and after submersion in halite brine.

Table 5.4 Strain rate and visco-plastic coefficients measured before, during and after submersion in carnallite brine.

Stress (MPa)	Before Submersion		During Submersion		After Submersion	
	Strain rate ($\dot{\epsilon}$)	η_1 (GPa.day)	Strain rate ($\dot{\epsilon}$)	η_1 (GPa.day)	Strain rate ($\dot{\epsilon}$)	η_1 (GPa.day)
2	0.114	17.621	0.110	18.182	0.040	50.505
4	0.153	26.110	0.147	27.174	0.087	46.136
6	0.323	18.605	0.249	24.087	0.125	48.000
10	0.297	33.659	0.291	34.317	0.180	55.617
12	1.320	9.094	0.982	12.220	0.349	34.354
Mean \pm SD	0.441 \pm 0.499	21.018 \pm 9.291	0.356 \pm 0.358	23.196 \pm 8.454	0.156 \pm 0.120	46.923 \pm 7.877

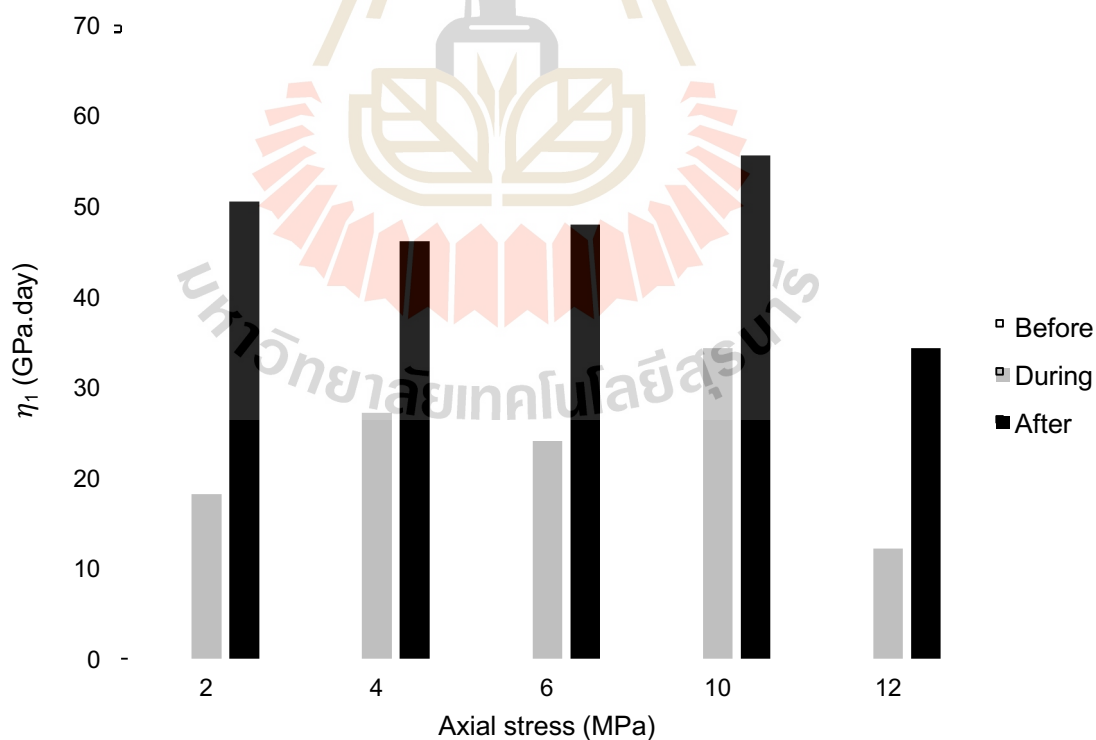


Figure 5.3 Visco-plastic coefficients of pure halite specimens measured before, during and after submersion in carnallite brine.

Table 5.5 Strain rate and visco-plastic coefficients measured before, during and after submersion in magnesium brine.

Stress (MPa)	Before Submersion		During Submersion		After Submersion	
	Strain rate ($\dot{\epsilon}$)	η_1 (GPa.day)	Strain rate ($\dot{\epsilon}$)	η_1 (GPa.day)	Strain rate ($\dot{\epsilon}$)	η_1 (GPa.day)
2	0.144	13.899	0.076	26.490	0.040	50.505
4	0.204	19.608	0.115	34.692	0.070	57.389
6	0.429	13.973	0.236	25.391	0.192	31.332
8	0.177	45.300	0.140	57.021	0.129	62.257
10	0.266	37.578	0.246	40.667	0.208	48.123
12	0.886	13.544	0.647	18.541	0.293	41.012
Mean \pm SD	0.351 \pm 0.281	23.984 \pm 13.923	0.243 \pm 0.209	33.800 \pm 13.741	0.155 \pm 0.094	48.436 \pm 11.164

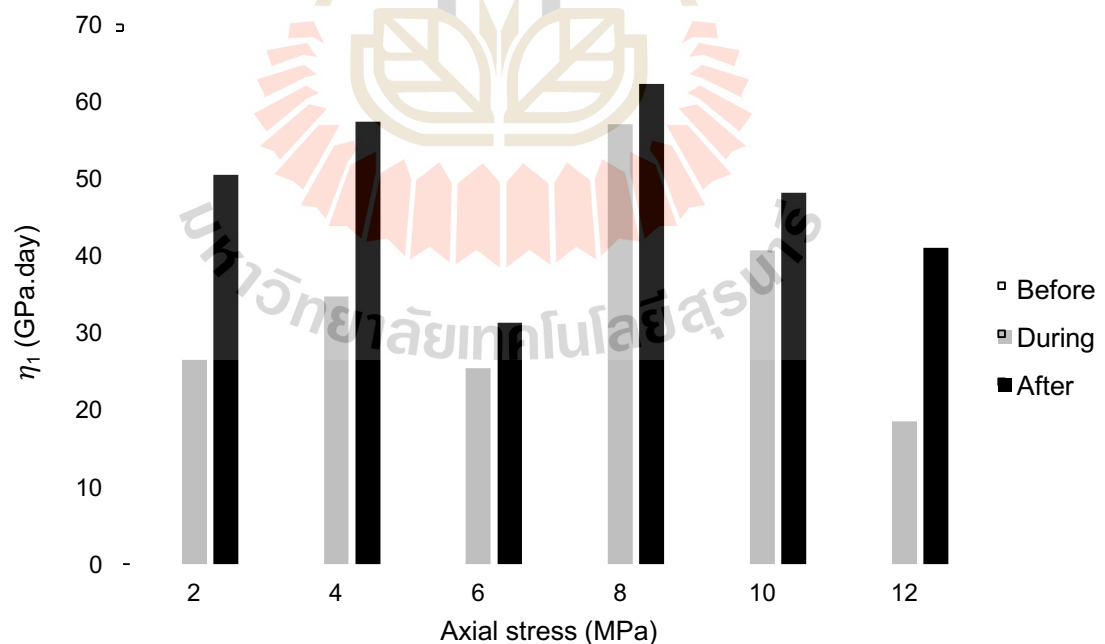


Figure 5.4 Visco-plastic coefficients of pure halite specimens measured before, during and after submersion in magnesium brine.

Table 5.6 Visco-plastic coefficients measured before, during and after submersion in different solutions.

Specimen Type	Type of Solutions	Visco-plastic Coefficient (η_1) (GPa.day)		
		Before Submersion	During Submersion	After Submersion
Salt	Halite Brine	18.11 \pm 5.96	18.43 \pm 4.63	23.09 \pm 4.17
	Carnallite Brine	21.02 \pm 9.29	23.19 \pm 8.45	46.92 \pm 7.88
	Magnesium Brine	23.98 \pm 13.92	33.80 \pm 13.74	48.44 \pm 11.16
Potash	Halite Brine	5.98	Fail	Fail
	Carnallite Brine	5.62 \pm 0.57	Fail	Fail
	Magnesium Brine	23.36	24.04	25.77

Table 5.7 Strain rate and visco-plastic coefficients measured before and during casted in cement.

Stress (MPa)	Before Submersion		During Submersion	
	Strain rate ($\dot{\epsilon}$)	η_1 (GPa.day)	Strain rate ($\dot{\epsilon}$)	η_1 (GPa.day)
6	0.774	7.749	0.077	78.227
8	0.526	15.224	0.164	48.721
10	0.377	26.511	0.126	79.428
10	0.785	12.737	0.181	55.188
Mean \pm SD	0.616 \pm 0.199	15.555 \pm 7.938	0.137 \pm 0.046	65.391 \pm 15.746

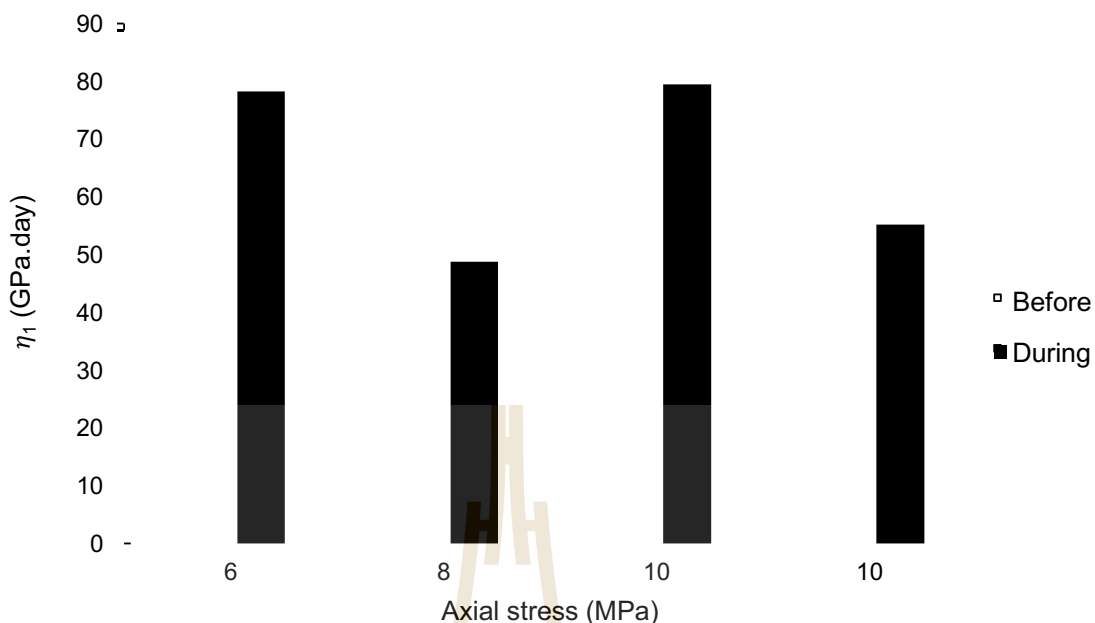


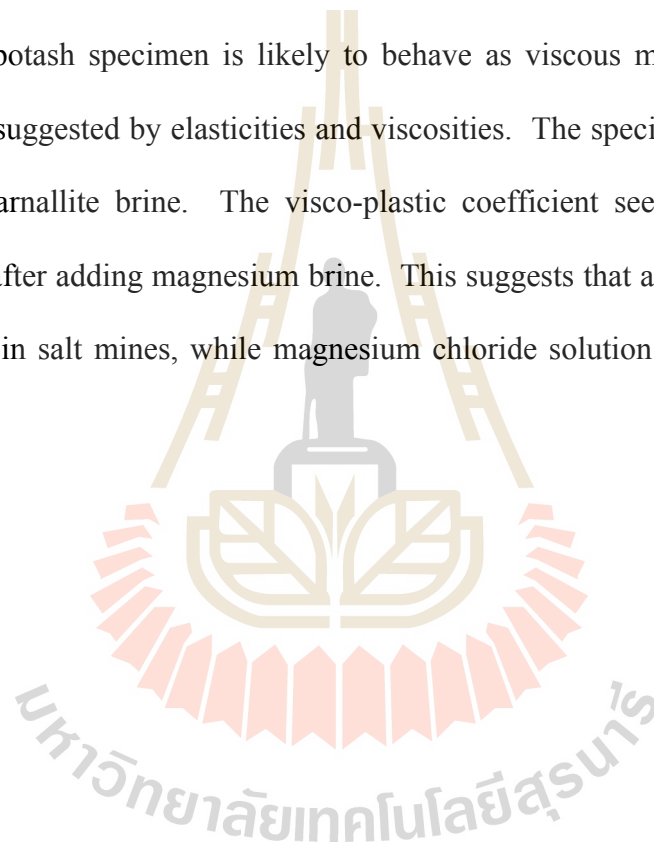
Figure 5.5 Visco-plastic coefficients of pure halite specimens measured before and during casting in cement.

5.3 Discussions

The test results fit fairly well to the Burgers model as suggested by the high values of the correlation coefficient (R^2). The first spring, E_1 the combination of E_2 and η_2 , and the first dashpot η_1 represent instantaneous response, transient behavior and steady state behavior, respectively. The variation of the instantaneous elastic modulus, E_1 is mainly due to the nonlinear relationship between stress and strain. For salt specimen before submersion, visco-plastic coefficient varies from 9.0 to 45.0 GPa.day. For the during submersion, visco-plastic coefficient varies from 12.0 to 57.0 GPa.day. For salt specimen after submersion, visco-plastic coefficient varies from 18.0 to 62.0 GPa.day. The visco-plastic coefficient of the specimens obviously decrease when the halite brine is added around the specimen comparing with carnallite and magnesium

chloride brine. When removing the solution, the values return to that before submersion. The salt specimens are sensitive with halite brine more than carnallite and magnesium chloride brine. The visco-plastic coefficient decreases when strain rate increasing. The visco-plastic coefficients measured of salt specimen before and after cement casted varies from 6 to 17 GPa.day and 23 to 36 GPa.day, respectively. The values seem high after cement casted.

The potash specimen is likely to behave as viscous material with very low elasticity as suggested by elasticities and viscosities. The specimens fail after adding halite and carnallite brine. The visco-plastic coefficient seems consistent before, during, and after adding magnesium brine. This suggests that all of the three solution can be used in salt mines, while magnesium chloride solution is suitable for potash mines.



CHAPTER VI

MODELLING OF BRINE STORAGE IN MINE

OPENINGS

6.1 Introduction

This chapter describes the results of finite difference analyses using FLAC (Itasca, 1992) to calculate the deformation of pillar, roof and surface subsidence before and after the brine has been stored in salt and potash mine openings. The time-dependent parameters calibrated from the uniaxial creep tests given in the previous chapter are used in the simulation. The objective is to assess the effect of halite, carnallite and magnesium brine storage on the mine deformations.

6.2 Numerical simulations

The finite difference code, FLAC is used in the simulations of the room and pillar under plane strain condition. The rock sequences at Bamnet Narong district, Chaiyaphum province are used in the simulations. The pillar heights are varied from 5, 10 to 15 m. The pillar width and room width are assumed constant at 15 m. The roof thickness is defined as 40% of the room width to comply with the local regulations. The opening depths are 175, 250 and 300 m. The overburden and underlying rocks are interbedded of the rock salt group : Phutok Formation, Upper Salt, Middle Clastic, Middle Salt, Lower Clastic and Lower Salt members. To cover the entire range of the mine opening dimensions, over 2,000 meshes have been constructed to obtain accurate

simulation results. The left and right boundaries are fixed in the x-axis, and the bottom boundary is fixed in the y-axis. The top boundary can move freely in both directions. The smallest element used around the opening is $0.5 \times 0.5 \text{ m}^2$ because the stress and strain gradients are high within this zone. The elements far from the opening are gradually larger. The simulations are made up to 20 years after excavations. The finite difference mesh for the simulation and model stratigraphic units are shown in Figures 6.1 to 6.3.

6.3 Property parameters used in numerical modelling

Table 6.1 shows the overburden parameters used for numerical modeling (Sriapai et al., 2012; Crosby, 2005 and Luangthip et al., 2016). The overburden formations are assumed to be elastic. The material property parameters of the Lower Salt member (salt and potash) are given in Table 6.2. The Lower Salt member is assumed to behave as the Burgers material. The Burgers parameters from the previous chapter are summarized in Table 6.3. The Burgers constitutive equation is a built-in subroutine in FLAC. The Poisson's ratio and tensile strength are obtained from Luangthip et al. (2016). The shear modulus and bulk modulus can be calculated as follow:

$$G = E / 2 \cdot (1 + \nu) \quad (6.1)$$

$$K = E / 3 \cdot (1 - 2\nu) \quad (6.2)$$

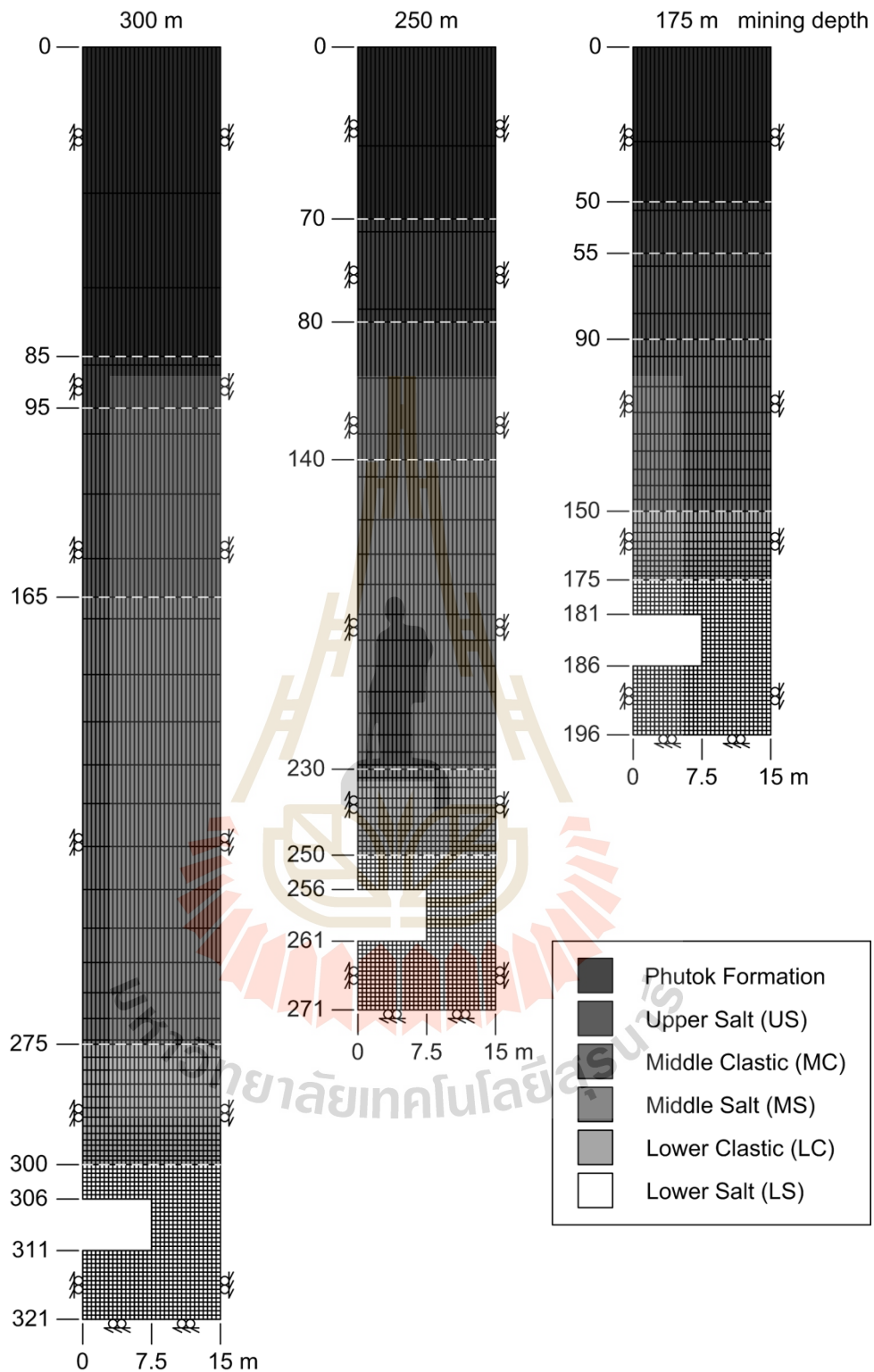


Figure 6.1 Finite difference mesh developed for FLAC simulation, mining depths are 175, 250 and 300 m and pillar height is 5 m.

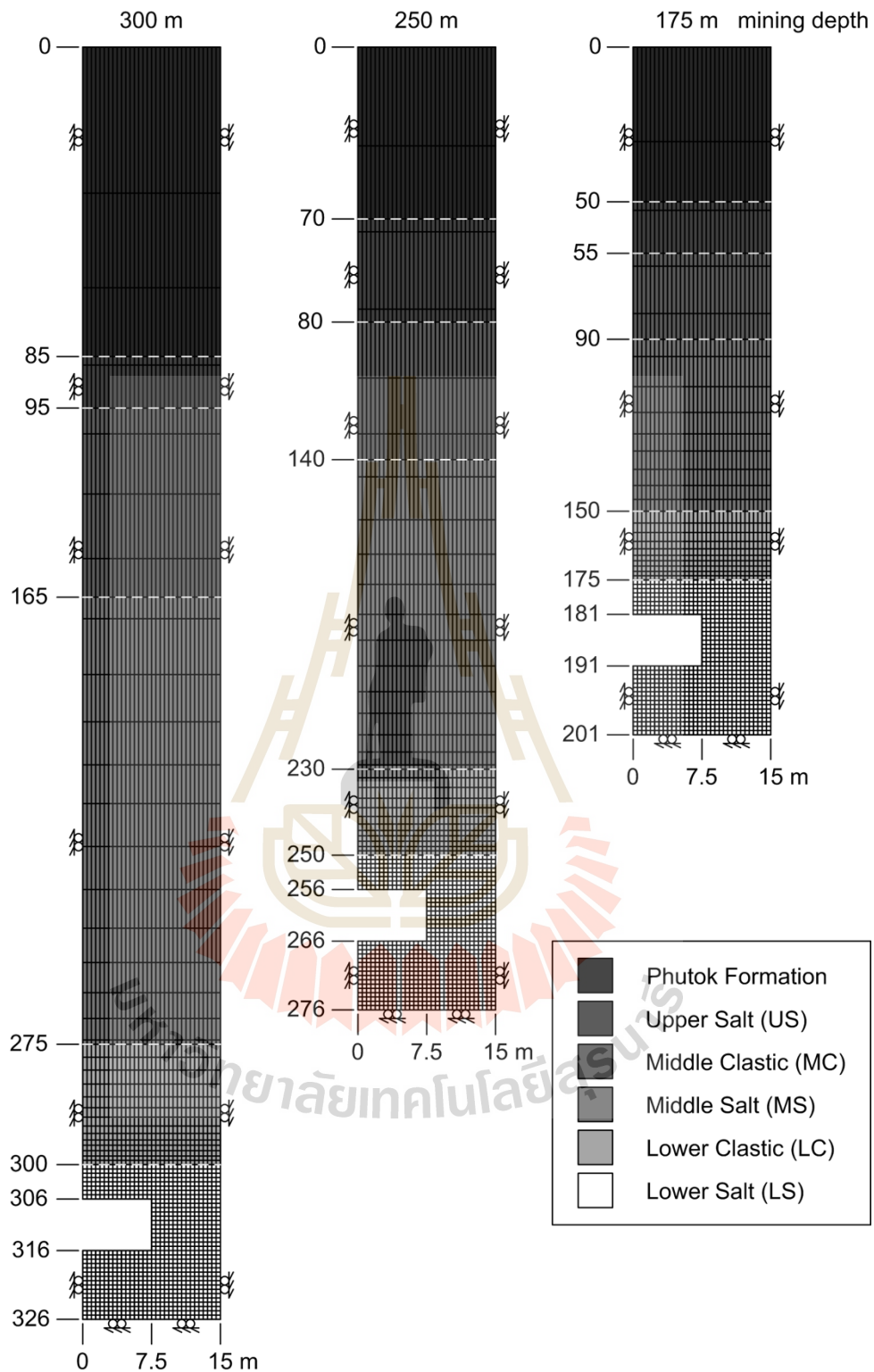


Figure 6.2 Finite difference mesh developed for FLAC simulation, mining depths are 175, 250 and 300 m and pillar height is 10 m.

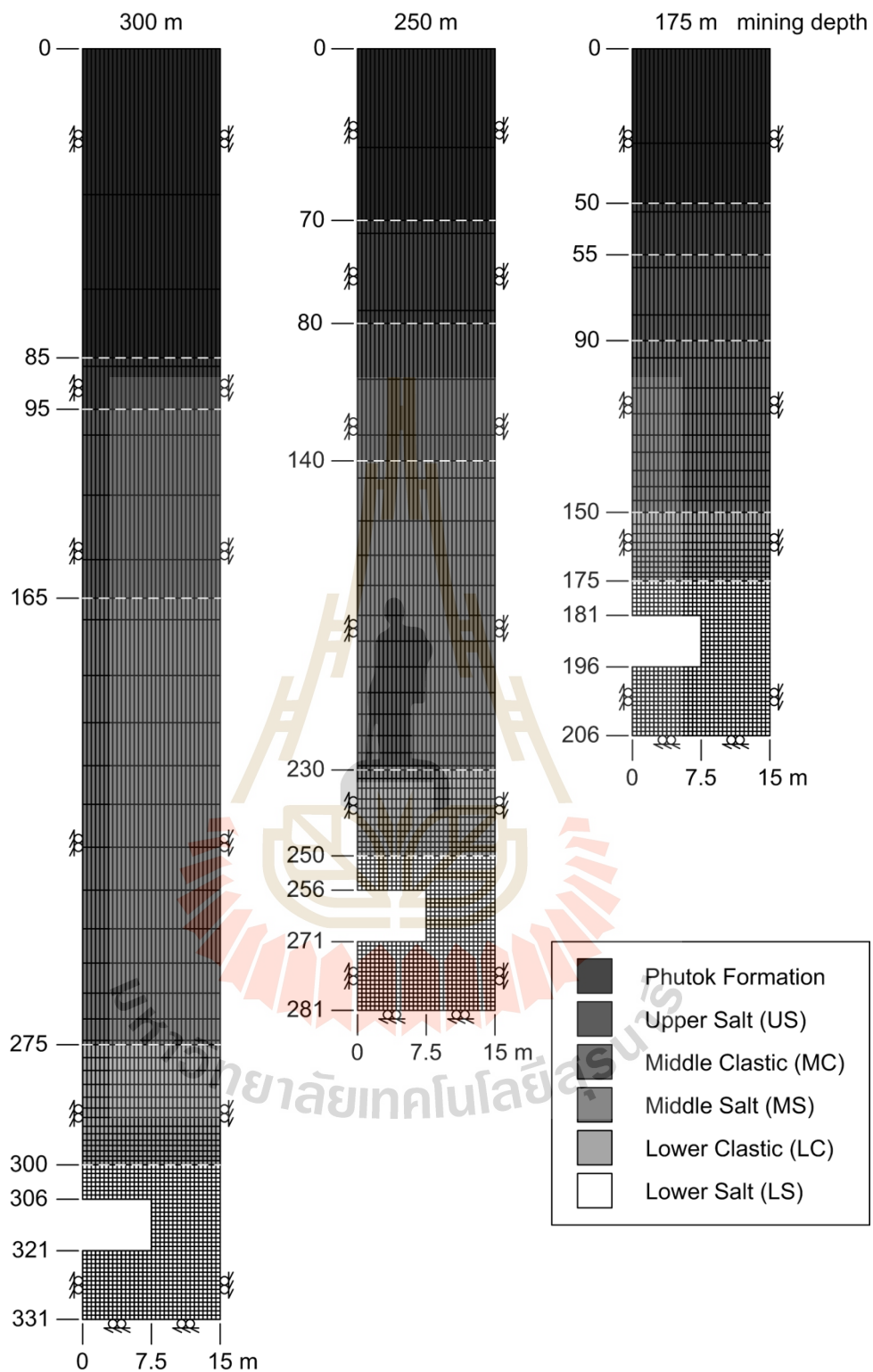


Figure 6.3 Finite difference mesh developed for FLAC simulation, mining depths are 175, 250 and 300 m and pillar height is 15 m.

Table 6.1 Overburden parameters used in numerical simulations (Sriapai et al., 2012; Crosby, 2005; Luangthip et al., 2016).

Rock unit	Bulk modulus, K (GPa)	Shear modulus, G (GPa)	Density, ρ (g/cm ³)	Cohesion, c (MPa)	Friction angle, ϕ (°)
Upper Clastic	3.52	1.44	2.49	3.50	25.00
Upper Salt	13.90	10.40	2.89	5.00	49.70
Middle Clastic	0.65	0.27	2.15	0.56	23.00
Middle salt	13.90	10.40	2.14	6.00	51.60
Lower Clastic	0.54	0.25	2.18	0.38	5.00

Table 6.2 Material property parameters of Lower Salt used in the FLAC (Luangthip et al., 2016).

Parameters	Lower Salt	
	Salt (C% < 20)	Potash (C% > 80)
Poisson's ratio (ν)	0.27	0.40
Shear modulus (G, GPa)	6.66	0.66
Bulk modulus (K, GPa)	12.00	3.00
Tensile strength (T, MPa)	1.88	0.23

Note : C% = Carnallite content by weight

Table 6.3 Burgers parameters of Lower Salt used in the FLAC.

Condition	Elastic modulus (E_1 , GPa)	Spring constant in visco-elastic phase (E_2 , GPa)	Visco-elastic coefficient in transient phase (η_2 , GPa.day)	Visco-plastic coefficient in steady-state phase, η_1 (GPa.day)	
				Before installed brine	After installed brine
Salt + Halite brine	0.82	1.91	1.16	18.11	18.43
Salt + Carnallite brine	0.82	1.91	1.16	21.02	23.19
Salt + Magnesium brine	0.82	1.91	1.16	23.98	33.80
Potash + Magnesium brine	0.35	1.98	0.36	23.36	24.04

6.4 Numerical results

6.4.1 Pillar and roof deformations

The pillar, roof, floor deformations and room closure after 20 years of excavation are determined from the simulations. The brine is installed in the mine opening after 2 years of excavation. Figures 6.4 and 6.5 show the pillar deformation in salt and potash mine openings. For example, at 300 m mining depth with 15 m pillar height, the halite brine storage can reduce the pillar deformation by up to 13.5% for the salt mine. The carnallite brine storage can reduce the pillar deformation by up to 18.2% for the salt mine. The magnesium brine storage can reduce the pillar deformation by up to 24.3% for the salt mine and 25% for the potash mine.

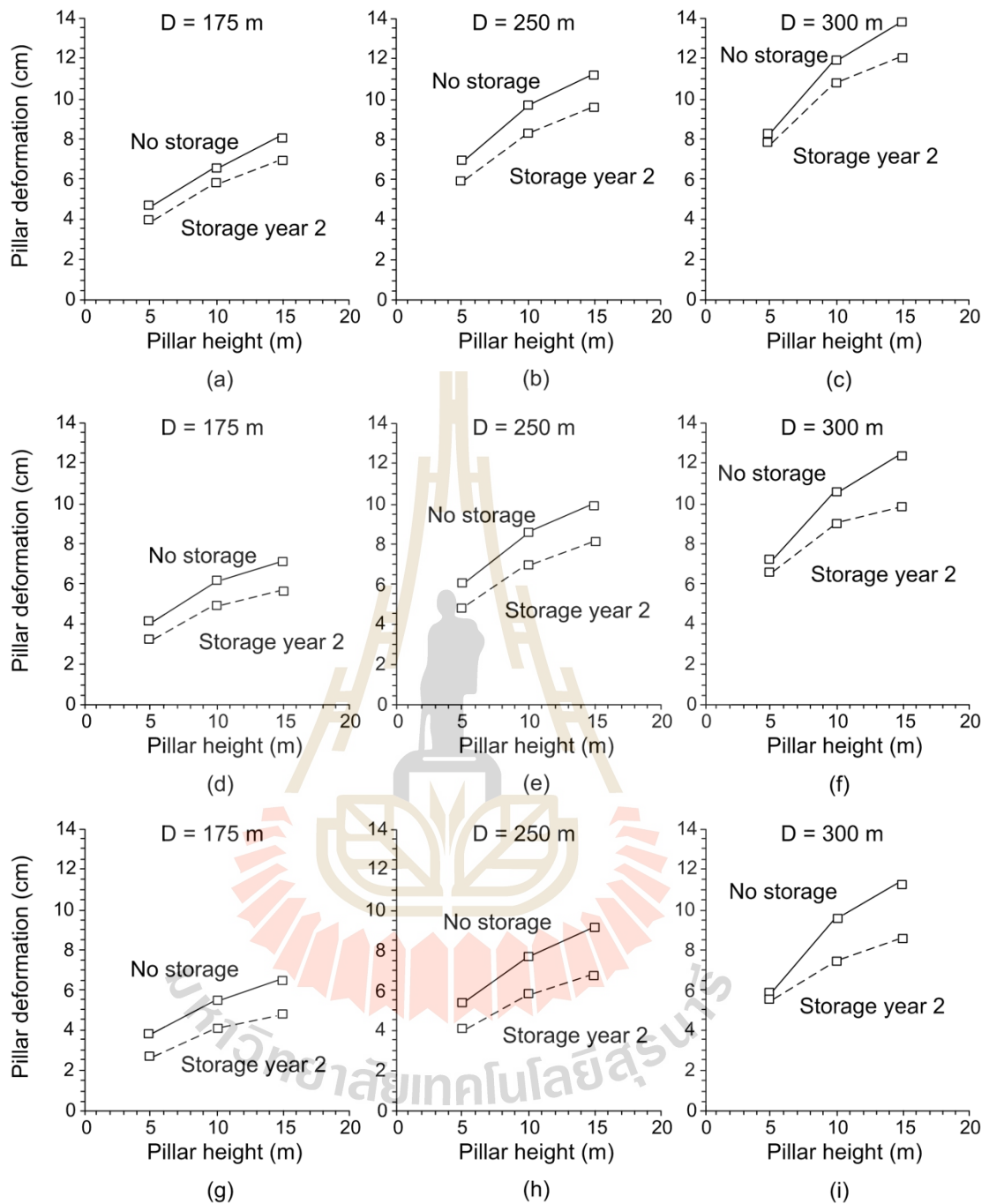


Figure 6.4 Pillar deformations after 20 years in salt openings storing with halite brine (a, b, c), carnallite brine (d, e, f) and magnesium brine (g, h, i) with different pillar heights and depths (D).

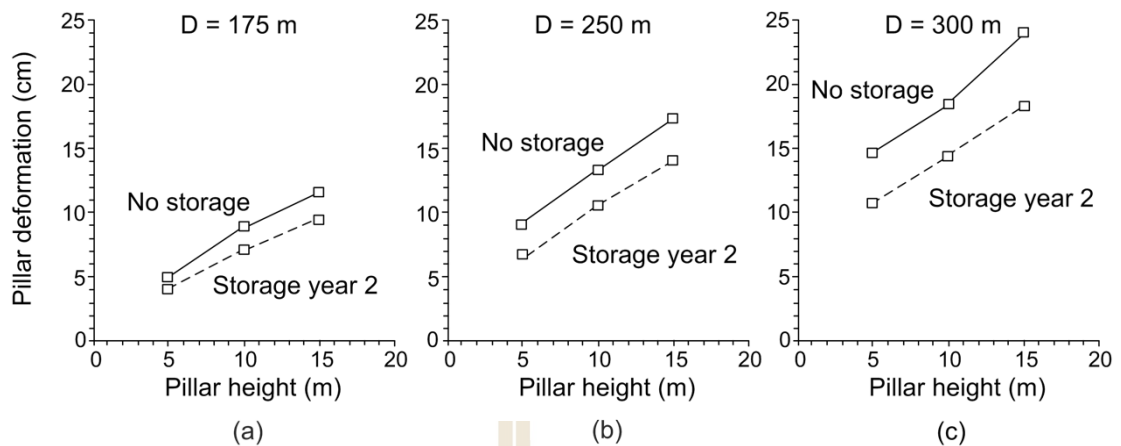


Figure 6.5 Pillar deformations after 20 years in potash openings storing with magnesium brine with different pillar heights and depths.

The results indicate that the performance of brine storage in the salt mine is as good as the potash mine. Greater opening depths and pillar heights show larger deformation of the pillar. At the same depth and pillar height, the magnesium brine storage provides the lowest deformation of pillar for all cases.

Figures 6.6 and 6.7 show the roof deformations after 20 years of excavation. The results indicate that the roof deformations increase with increasing room heights and mining depths. After the brine is installed in the salt opening, the roof deformation slightly decreases for all cases, compared those obtained from the potash mine.

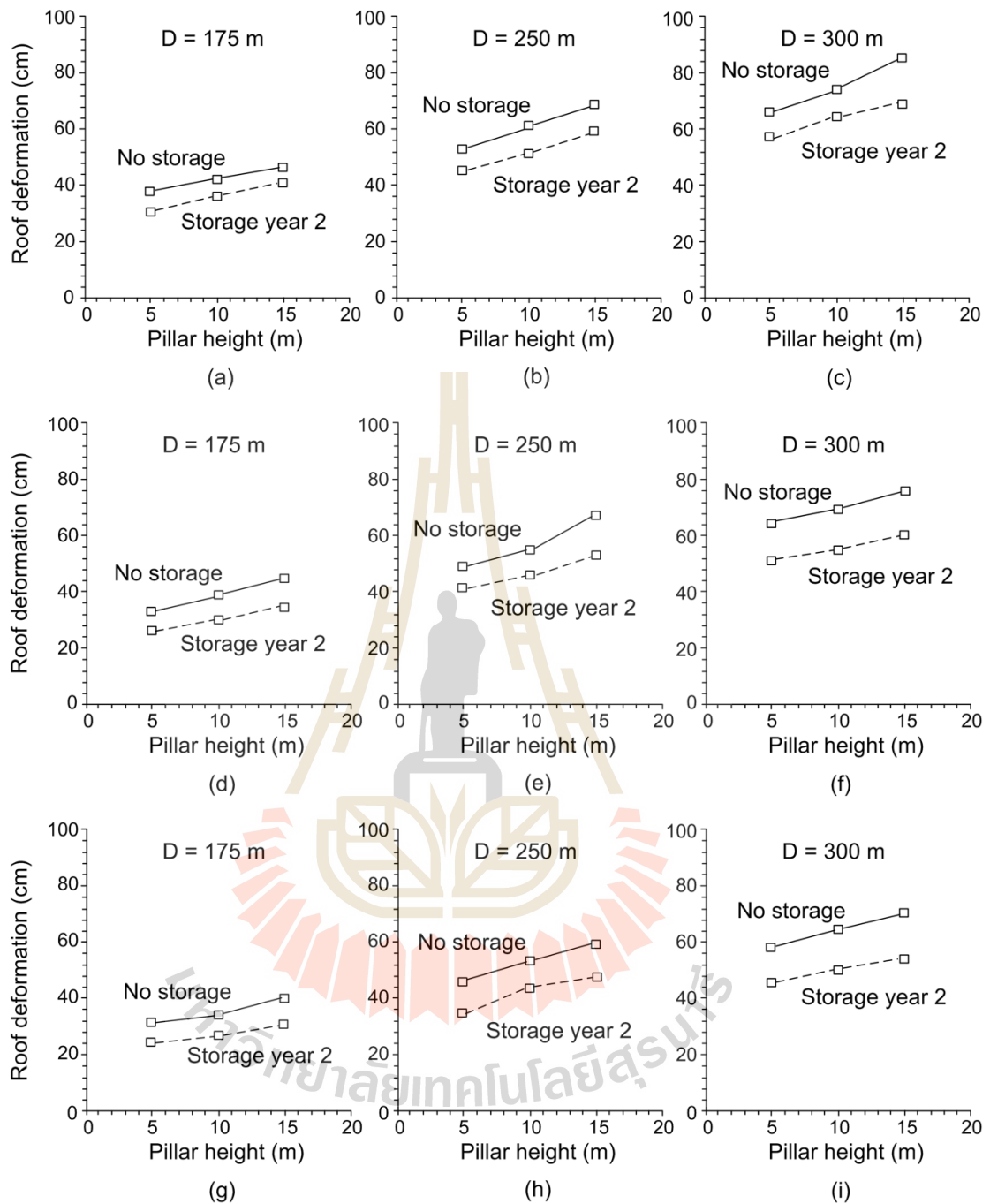


Figure 6.6 Roof deformations after 20 years in salt openings storing with halite brine (a, b, c), carnallite brine (d, e, f) and magnesium brine (g, h, i) with different pillar heights and depths.

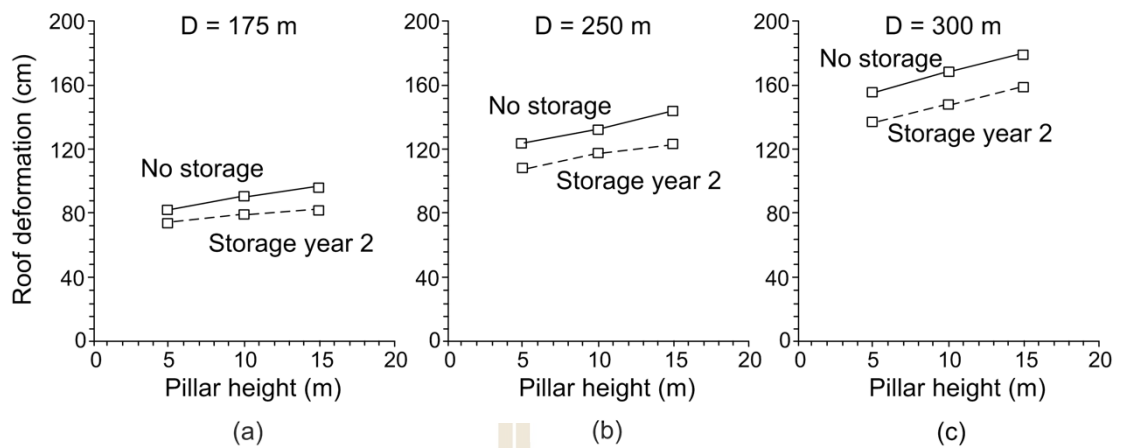


Figure 6.7 Roof deformations after 20 years in potash openings storing with magnesium brine with different pillar heights and depths.

Figures 6.8 and 6.9 show the floor deformation in salt and potash openings for various brine storages and pillar heights. For example, at 300 m mining depth and 15 m pillar height, the halite brine and carnallite brine storage can reduce the floor heave by up to 26.6% and 30.6% for the salt mine. The magnesium brine storage can reduce the floor heave by up to 34.4% for the salt mine and 10.5% for the potash mine. The results indicate that the floor heave slightly increases with increasing room heights and mining depths.

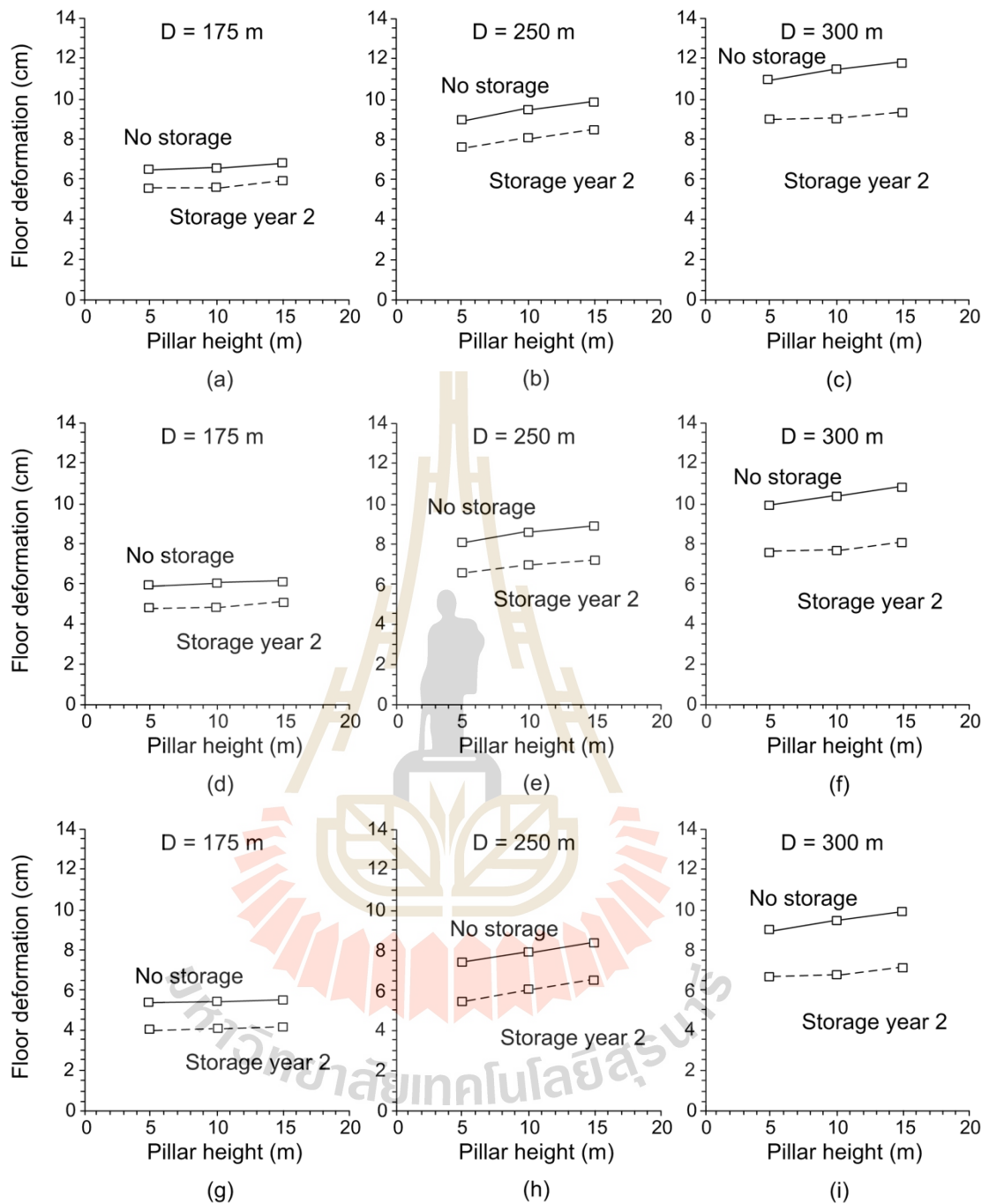


Figure 6.8 Floor deformations after 20 years in salt openings storing with halite brine (a, b, c), carnallite brine (d, e, f) and magnesium brine (g, h, i) with different pillar heights and depths.

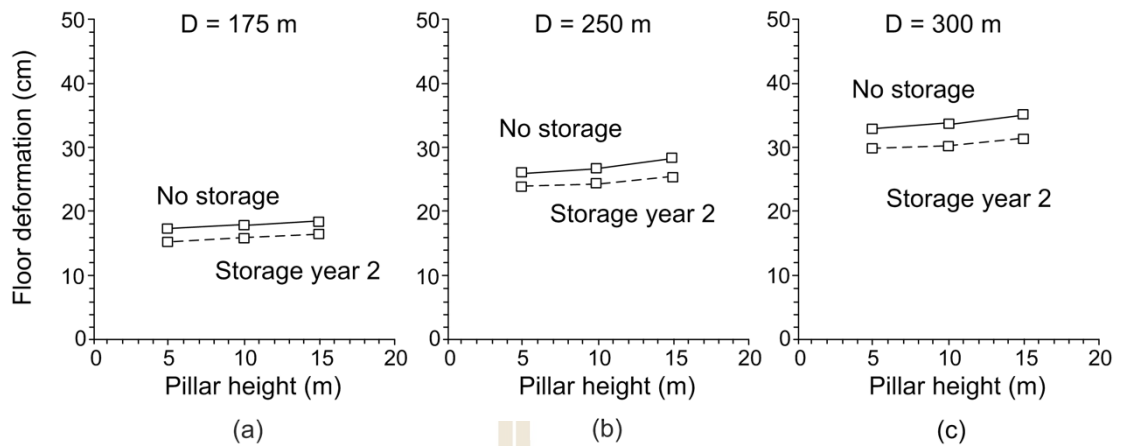


Figure 6.9 Floor deformations after 20 years in potash openings storing with magnesium brine with different pillar heights and depths.

The relationships between the vertical room closure with and without brine storage and mining depth and opening height are shown in Figures 6.10 and 6.11. The results indicate that the room vertical closure increases with increasing room heights and mining depths. After the brine is installed in the salt opening, the values slightly decrease for all cases including potash mine.

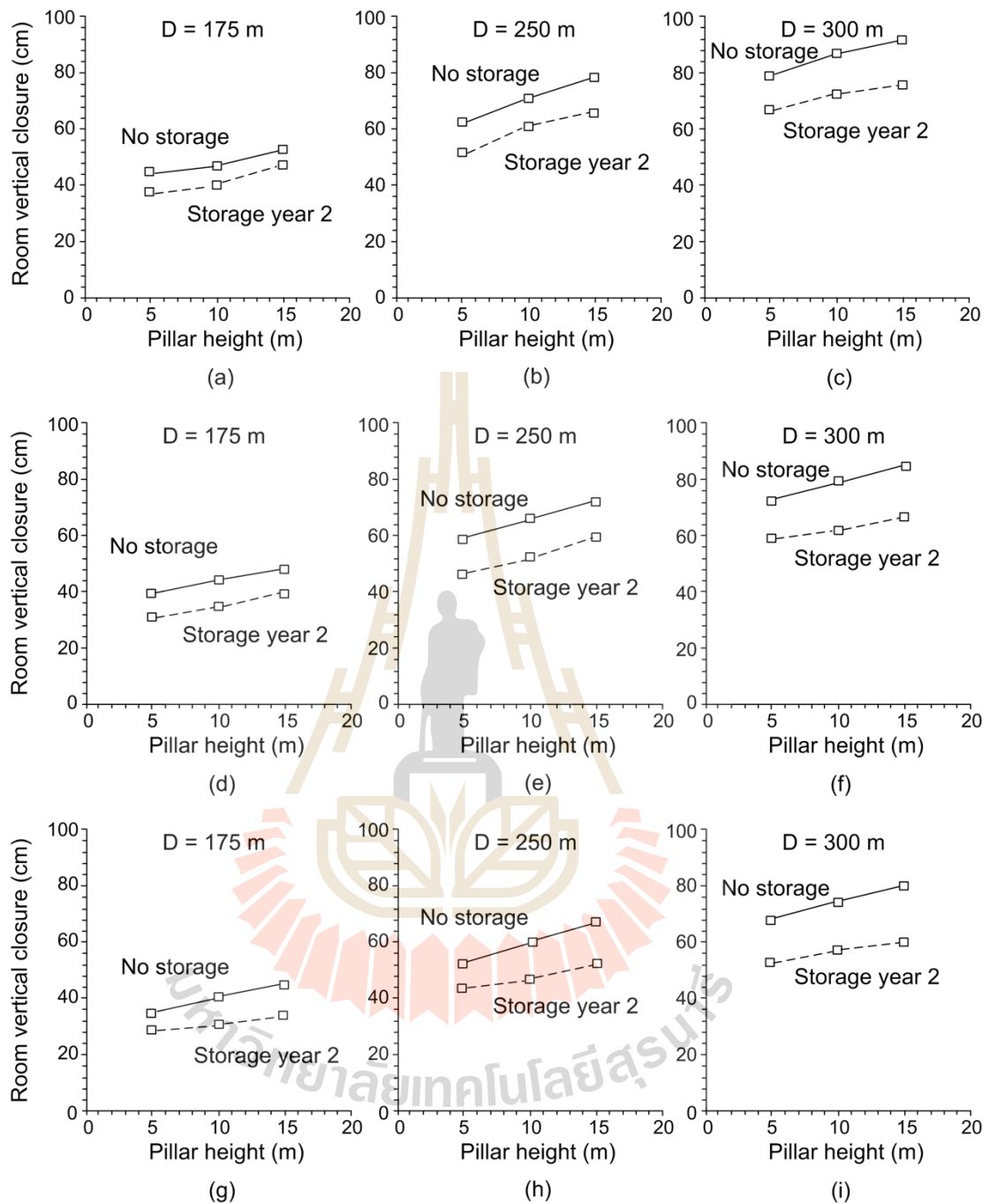


Figure 6.10 Room vertical closure after 20 years in salt openings storing with halite brine (a, b, c), carnallite brine (d, e, f) and magnesium brine (g, h, i) with different pillar heights and depths.

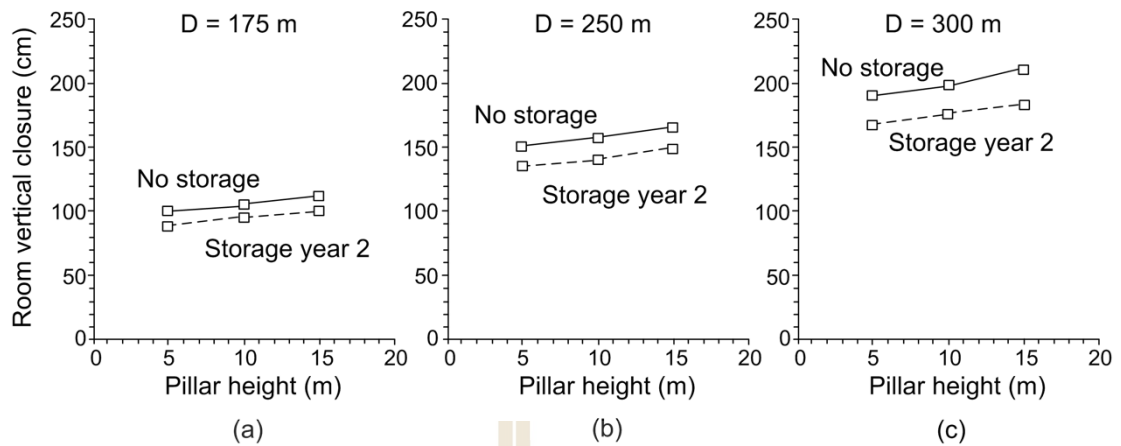


Figure 6.11 Room vertical closure after 20 years in potash openings storing with magnesium brine with different pillar heights and depths.

6.4.2 Surface subsidence

Figure 6.12 shows surface subsidence as a function of time after 20 years in salt openings storing with halite brine (H), carnallite brine (C) and magnesium brine (M) with different pillar heights and depths. The surface subsidence as a function of time after 20 years in potash openings storing with magnesium brine with different pillar heights and depths are shown in Figure 6.13. For example, the surface subsidence magnitude as affected by mining excavation at 300 m depth and 15 m pillar height. The brine is added in opening after 2 years of excavation. The results indicate that the brine storage reduces the surface subsidence by up to 9 cm for halite brine storage, 10 cm for carnallite brine storage and 11 cm for magnesium brine storage after 20 years in salt mine. The magnesium brine storage reduces the surface subsidence by up to 13 cm in potash mine.

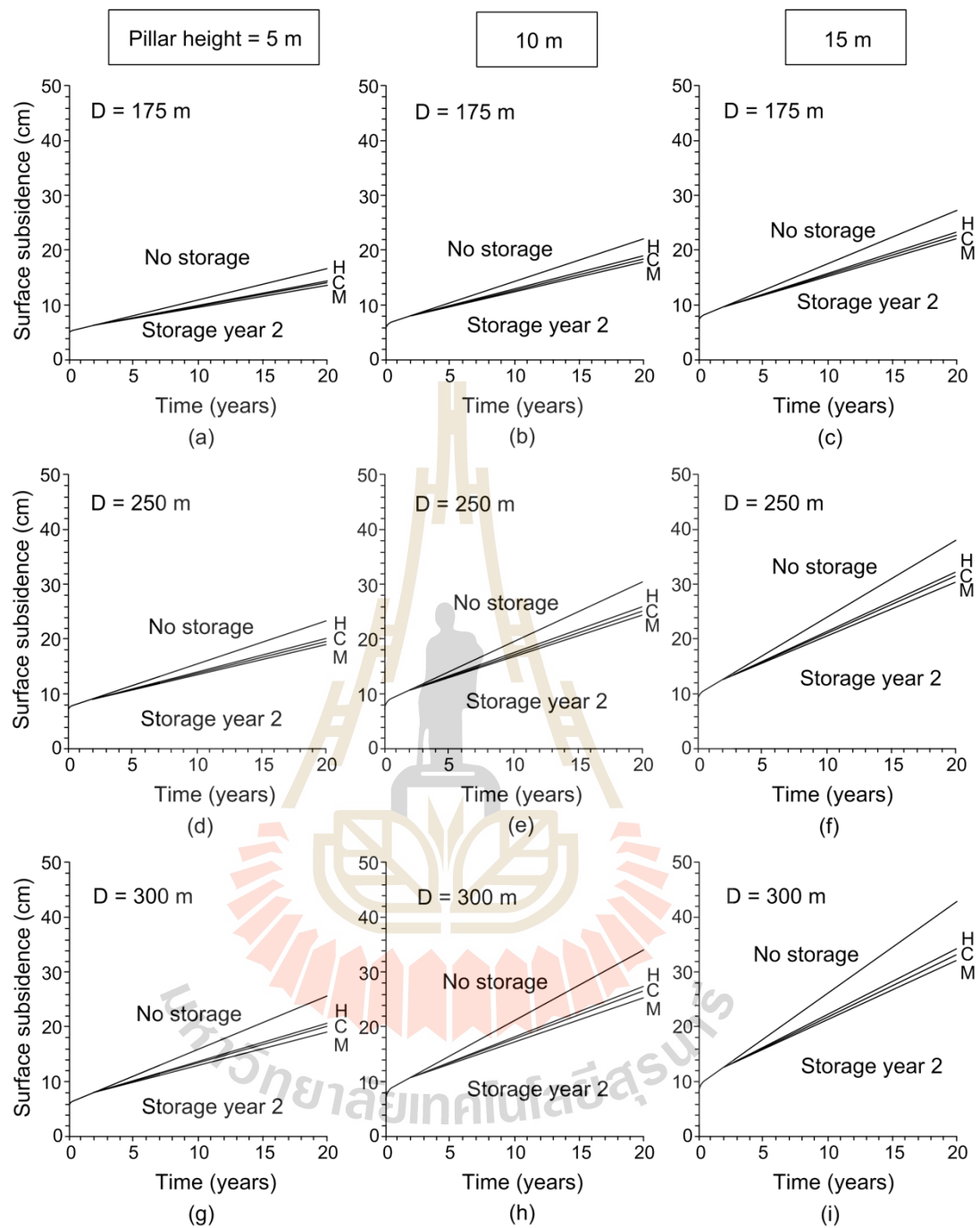


Figure 6.12 Surface subsidence as a function of time after 20 years in salt openings storing with halite brine (H), carnallite brine (C) and magnesium brine (M) with different pillar heights and depths.

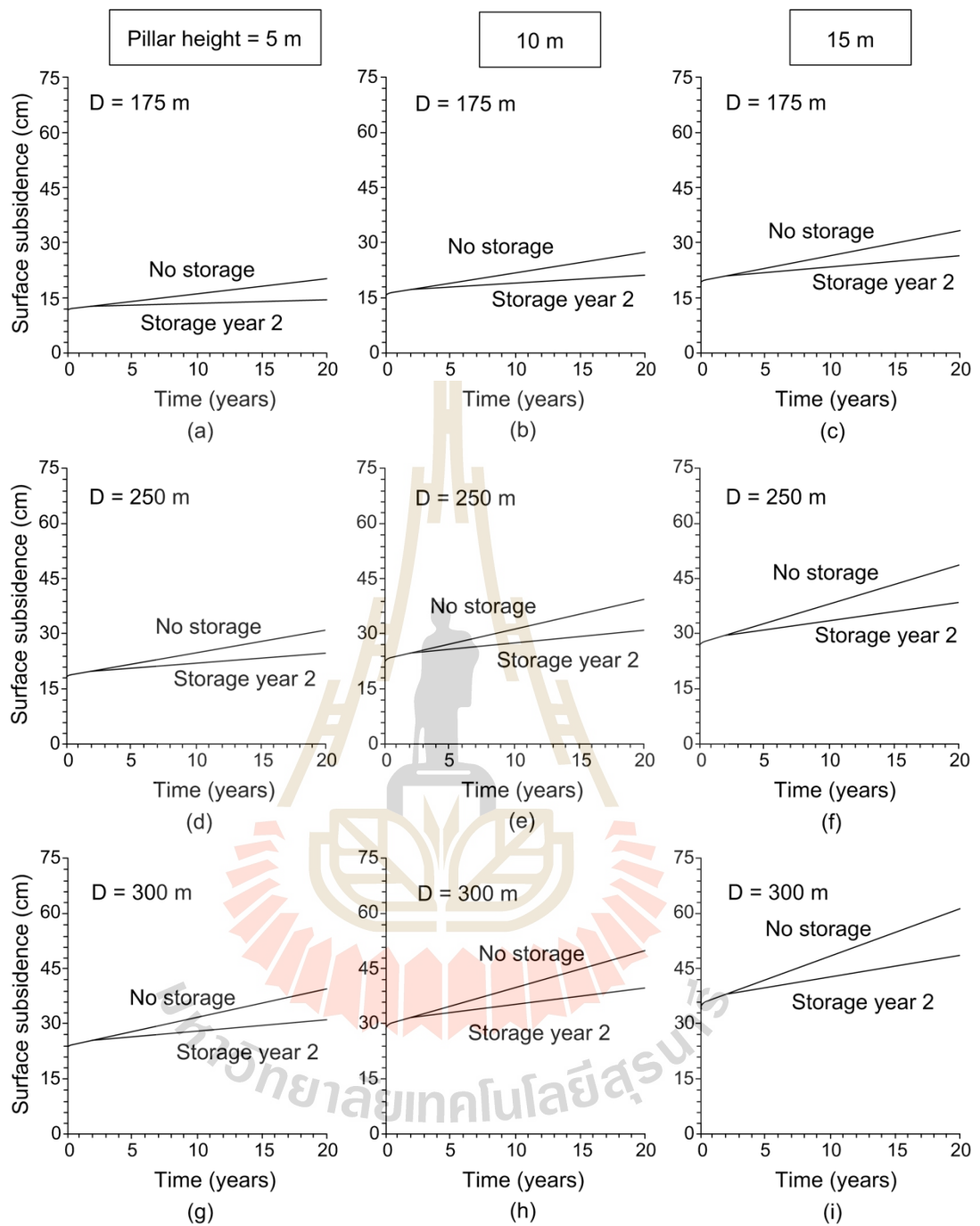
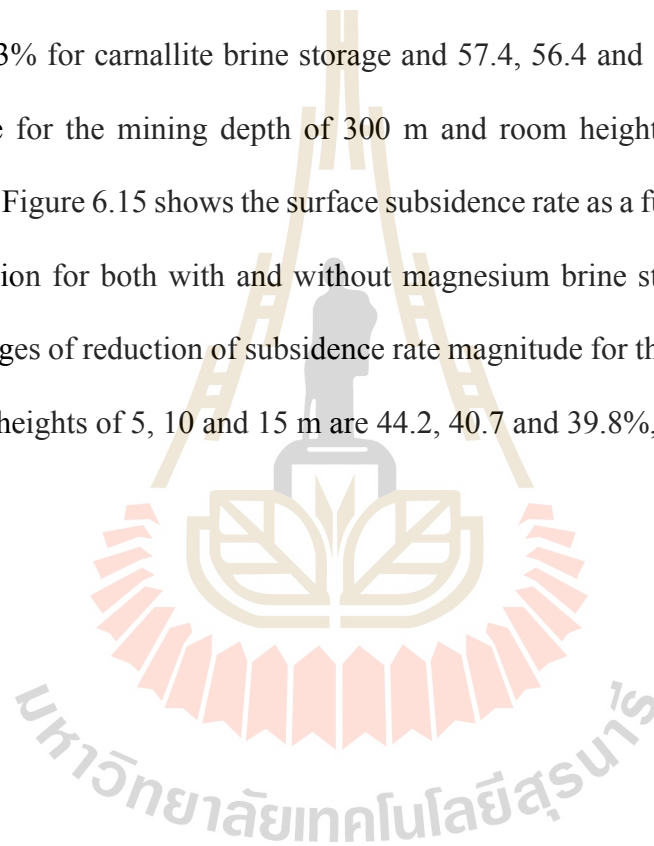


Figure 6.13 Surface subsidence as a function of time after 20 years in potash openings storing with magnesium brine with different pillar heights and depths.

Figure 6.14 shows the rate of surface subsidence after 20 years storage under various brine, mining depths and room heights. The results show that the rate of surface subsidence increase with the mining depth and room height. The magnesium brine tends to decrease much more subsidence rate with increasing of room height and mining depth than carnallite and halite brine. For example, the percentages of reduction of subsidence rate magnitude are 33.7, 32.7 and 33.1% for halite brine storage, 44.1, 43.0 and 43.3% for carnallite brine storage and 57.4, 56.4 and 56.7% for magnesium brine storage for the mining depth of 300 m and room heights of 5, 10 and 15 m, respectively. Figure 6.15 shows the surface subsidence rate as a function of pillar height after excavation for both with and without magnesium brine storing in potash mine. The percentages of reduction of subsidence rate magnitude for the mining depth of 300 m and room heights of 5, 10 and 15 m are 44.2, 40.7 and 39.8%, respectively.



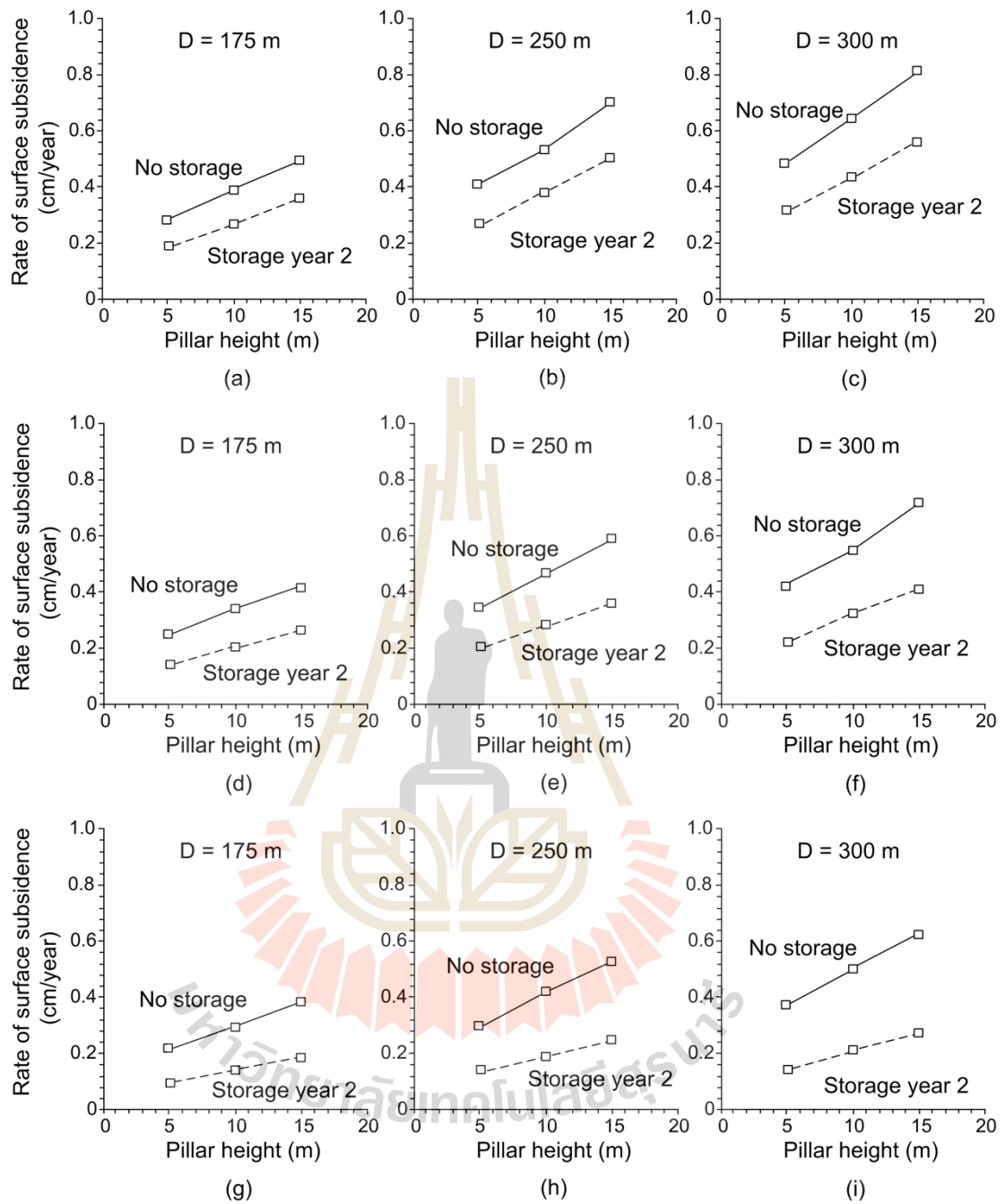


Figure 6.14 Rate of surface subsidence after 20 years in salt openings storing with halite brine (a, b, c), carnallite brine (d, e, f) and magnesium brine (g, h, i) with different pillar heights and depths.

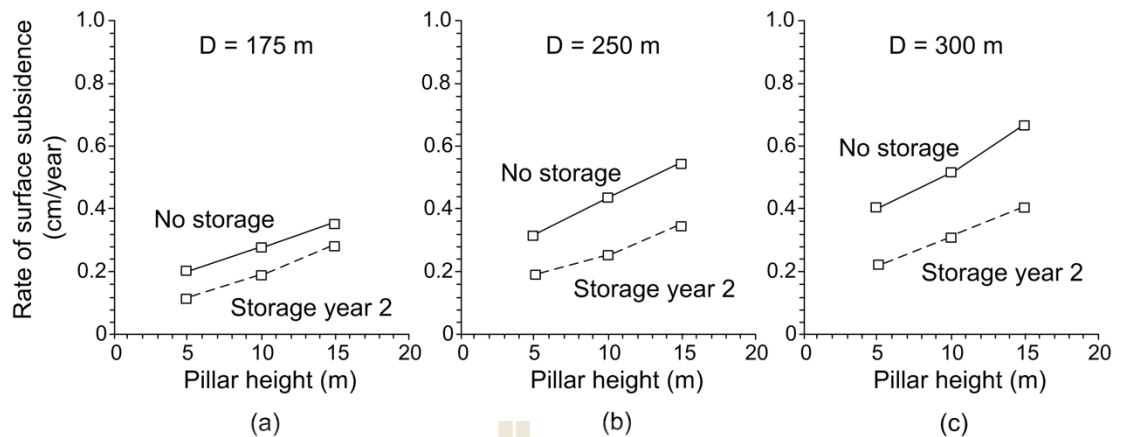


Figure 6.15 Rate of surface subsidence after 20 years in potash openings storing with magnesium brine with different pillar heights and depths.

The decrease of subsidence rate in salt and potash mine slightly reduces with increasing mining depth after magnesium brine and carnallite brine storage while the decrease of subsidence rate under halite storage seems constant. The brine is installed in the higher and deeper rooms show the higher rate of subsidence.

The distribution of the stresses in salt and potash mine are illustrated in Figures A.1 to A.18 in Appendix A. The results indicate that the distribution of stresses is concentrated in the rock close to the mine excavation, and the influence of the excavation reduces with increasing distance from room.

CHAPTER VII

DISCUSSIONS, CONCLUSIONS AND RECOMMENDATIONS FOR FUTURE STUDIES

7.1 Discussions

This section discusses the key issues relevant to the reliability of the test schemes and the adequacies of the test results. The objective of this research is to experimentally determine the effects of backfill or brine compositions on the mechanical stability of supported pillars in salt and potash mines. This thesis describes the detailed test methods, calibration of Burgers parameter and predicted deformations of pillar and surface subsidence of salt and potash mines.

A total of 36 salt and potash specimens have been prepared for creep test method for a period of 21 days. The results are reliable, as evidenced by the overlapping (repeating) of the measured axial strains under the same periods with different stresses.

The salt specimens under uniaxial creep test obtained from Lower Salt member may not contain 100% halite, as evidenced by the density of each specimen shown in Table 3.2 (density of pure halite is 2.16 g/cc). They could contain some carnallite or anhydrite. The density of the specimens contained some carnallite may be lower than 2.16 g/cc and the density of the specimens contained some anhydrite may be higher than 2.16 g/cc. Salt specimens are not affected by the three types of brine under low stress (Figures 4.5 to 4.7), but under increasing stresses, cracks are induced and allow brine infiltration into the cracks, and hence increasing the axial strain. This is because

the brine can decrease the resistance of creep deformation as suggested by the experiments performed by Urai et al. (1986), Brodsky and Munson (1991) and Lee and Souza (1998). The results from uniaxial creep test can be compared with the weight loss testing when the salt specimens are submerged in each brine without loading. The dissolution does not occur in salt specimens (Figures 4.14 to 4.16).

The potash specimens contain carnallite under uniaxial creep test are highly sensitive to halite and carnallite brine (Figures 4.8 and 4.9). The specimens fail after adding halite and carnallite brines. This is because the $\text{MgCl}_2 \cdot 6\text{H}_2\text{O}$ as carnallite content can be dissolved in NaCl and KCl, as shown in the reaction in chapter 4. When adding the magnesium brine around the specimen under loading, no failure occurs (Figure 4.10) probably because the saturated magnesium brine cannot dissolve the salt and carnallite.

The rate of the dissolution is higher during the first day of submersion as compared to the last day, as suggested by the non-linear curves in Figures 4.14 to 4.16 and the by dissolution rate of carnallite specimens in Figures 4.17 to 4.19. For example, the dissolution rate of specimen with $C\% = 97\%$ submerged in halite, carnallite and magnesium brine decrease from 6.50, 0.40 and 0.08 g/hr during the first day to 0.6, 0.1 and 0.02 g/hr at the last day. This is because the dissolution reduces the size and free surface of the specimen. When the free surface decreases, the dissolution rate decreases.

The dissolution rate depends on brine temperature and loading, as suggested by Shende (2003). After the specimen submerging in brine, the increase of brine temperature probably causes more dissolution and when temperature decreases, the brine recrystallizes. The temperature fluctuations range from 25 to 30 Celsius during the experiment.

The purity and the distribution of carnallite in the specimen may affect the dissolution. Under the same $C_{\%}$, uniform distribution of carnallite in the specimen may reduce its strain, as suggested by numerical analysis results performed by Wilalak (2016).

The Burgers model is used to describe the time-dependent deformations of the creep test specimens. It is recognized that numerous creep models or constitutive equations have been developed to represent the time-dependent behavior of rock salt (e.g., Gnirk and Johnson, 1964; Handin et al., 1984; Langer, 1984; Senseny, 1984; Hardy and Sun, 1986). The Burgers model is used because it is simple and capable of describing the elastic, visco-elastic and visco-plastic phases of deformation. Burgers model can adequately represent the creep behavior of the specimens. The calibration results seem adequate, as evidenced by the good correlation coefficients obtained from the calibration.

The objective of the modelling of brine storage is to demonstrate the effects of different types of brine on the pillar, roof, floor deformations and on the surface subsidence.

7.2 Conclusions

All objectives and requirements of this study have been met. The results of the laboratory testing and analyses can be concluded as follows:

1. The creep testing results indicate that the creep rate of salt specimen are not affected by the halite, carnallite and magnesium brine, no change in creep rate is detected before, during and after brine submersion. The potash specimens fail after submersion under halite and carnallite brine, probably because the specimen can

dissolve in these solutions, and hence accelerates the creep rate and eventually reaches the tertiary creep phase (toward failure). Under saturated magnesium brine, the creep rates of the potash specimens remain constant before, during and after brine submersion.

2. The pure rock salt ($C\% = 0$) is insensitive to the halite, carnallite and magnesium brines. The specimens containing carnallite of 30% to 90% by weight can dissolve in halite and carnallite brines, but tends to be insensitive to magnesium brine. The rate of dissolution of specimens with higher $C\%$ is higher than those with lower $C\%$. The magnesium brine provides the lowest rate of dissolution. The weight loss testing results agree well with those of the creep testing that the magnesium brine may be a suitable candidate to form backfill materials for the openings surrounded by carnallite.

3. From the calibration of the Burgers parameters, the visco-plastic coefficients are calculated for each phase of solution submersion. The visco-plastic coefficient of the salt specimens under high stress decreases when the halite brine is added around the specimen. When removing the solution, the values return to that before submersion. The potash specimens fail after adding halite and carnallite brine. Under magnesium brine however the visco-plastic coefficient of the potash specimens seems consistent before, during, and after submersion.

4. The numerical results obtained from the modelling of pillar and roof deformations and surface subsidence by brine storage in salt and potash mine openings indicate that the magnitudes of deformations and subsidence increase with the mining depth and room height. All types of brine storage or backfill decrease the underground deformations and subsidence. At the same depth and pillar height, the magnesium brine provides the lowest deformations of pillar and surface subsidence for all cases.

5. The brine installed in the taller and deeper rooms shows the higher rate of subsidence. The decrease of subsidence rate under halite brine storage however seems constant under the same pillar height and mining depth.

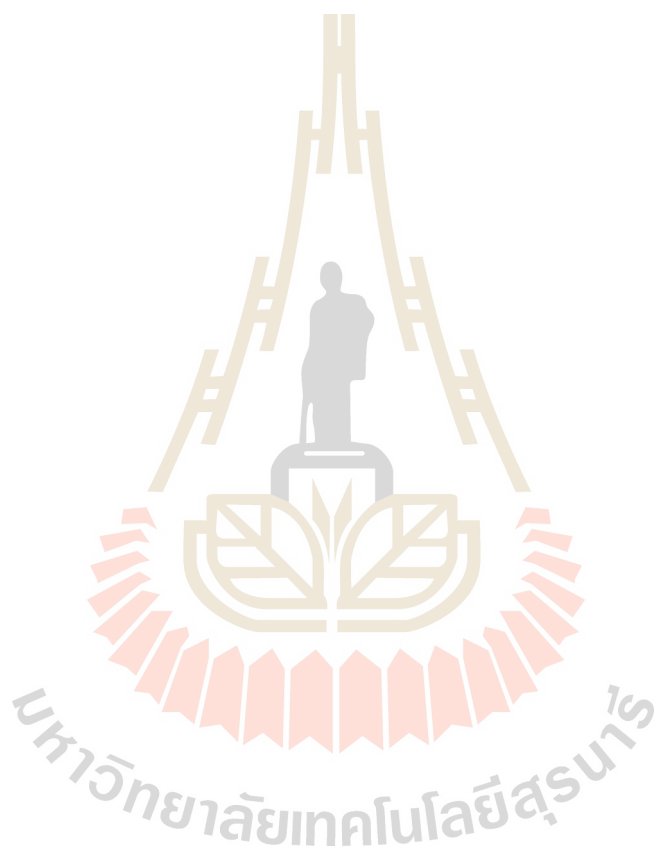
6. The halite and carnallite brines should be avoided for backfilling or storing in the potash mine openings. For the openings in pure rock salt all these solutions can be used as a mixing component for the backfill material or storage in the mine opening. This is because the salt is insensitive to these solutions as long as they are under saturated condition. For potash mine opening, the magnesium brine is suitable for mixing with backfilling material and storing in potash mine openings.

7.3 Recommendations for future studies

Recognizing that the numbers of the specimens and the test parameters used here are relatively limited. The uncertainties of the investigation and results discussed above lead to the recommendations for further studies as follows:

1. More testing is required on a variety of specimens with different carnallite contents.
2. Increasing the number of the specimens would statistically enhance the reliability of the test results.
3. The effect of rock salt inclusions (anhydrite, clay minerals, gypsum) under brine submersion should be verified for more precisely determination.
4. The effects of confining pressure under all types of brines submersion should be further investigated. In this study, no confining pressure is applied to the specimens.

5. The chemical analysis of the dissolution between rock salt specimen and brine should be performed to enhance the reliability of the test results.



REFERENCES

- Akgün, H. and Daemen, J.J.K. (1997). Analytical and experimental assessment of mechanical borehole sealing performance in rock. **Engineering Geology Journal**. 47(3): 233-241.
- American Petroleum Institute. (1986). Specifications for materials and testing for well cements. 3rd Edition, American Petroleum Institute, Production Department, Dallas, TX.
- Arioglu, E. (1983). Design of supports in mines, Wiley and Sons, New York, 248.
- ASTM D7070-08. (2008). Standard test methods for creep of rock core under constant stress and temperature. In **Annual Book of ASTM Standards** (Vol. 04.08). Philadelphia: American Society for Testing and Materials.
- Bachu, S. and Dusseault, M. B. (2005). Underground injection of carbon dioxide in salt beds. **Developments in Water Science**. 52: 637-648.
- Berest, P., Brouard, B. and Durup, J. G. (2000). Shut-in pressure test: Case studies. In **Proceedings Solution Mining Research Institute 2000 Fall Technical Meeting**, San Antonio, TX.
- Barret, J.R., Coulthard, M.A., and Dight, P.M. (1978). Determination of fill stability. **Mining with Backfill-12th Canadian Rock Mechanics Symposium** (vol. 19, pp. 85-91). Canadian Institute of Mining and Metallurgy, Quebec, Special.
- Billiotte, J., LeGuen, C., Deveughele, M., and Brulhet, J. (1996). On laboratory measurements of porosity and permeability of salt rocks (Bressa basis-France). In **Proceedings of the Third Conference on the Mechanical Behavior of Salt**

- (pp. 221-230). September 1993, Ecole Polytechnique, Palaiseau, France, Trans Tech Publications, Clausthal-Zellerfeld, Germany.
- Bonte, G. (1996). Mechanical aspects of the inhibition of a salt wall by brine initially contained in a cavity. In **Proceedings of the Third Conference on the Mechanical Behavior of Salt** (pp. 263-267). September, 1993, Ecole Polytechnique, Palaiseau, France, Trans Tech Publications, Clausthal-Zellerfeld, Germany.
- Brodsky, N.S. and Munson, D.E. (1991). The effect of brine on the creep of WIPP salt in laboratory tests. In **the 32nd U.S. Symposium on Rock Mechanics**. July, 1991, Norman, Oklahoma, American Rock Mechanics Association.
- Charpentier, J.P. (1984). Creep of rock salt elevated temperature. In **Proceedings of the Second Conference on the Mechanics Behavior of Salt** (pp. 131-136). Clausthal, Germany: Trans Tech Publications.
- Cristescu, N. and Hunsche, U. (1996). A comprehensive constitutive equation for rock salt determination and application. In **Proceedings of the Third Conference on the Mechanical Behavior of Salt** (pp. 191-205). Clausthal- Zellerfeld, Germany: Trans Tech Publications.
- Crosby, K.S. (2005). Overview of the geology and resources of the Udon Potash (sylvinite) deposits, Udon Thani province, Thailand. In **Proceedings of International Conference on Geology, Geotechnology and Mineral Resources of Indochina** (pp. 283-299). Khon Kaen, Thailand.
- Dusseault, M.B. and Fordham, C.J. (1993). Time-dependent behavior of rocks. **Comprehensive Rock Engineering Principles. Practice and Project: Rock Testing and Site Characterization**. London, Pergamon. 3: 119-149.

- Econoides, M.J., Watters, L.T. and Dunn-Norman, S. (1998). **Petroleum well construction**. Chichester: John Wiley & Sons.
- Eyermann, T.J., Van Sambeek, L.L., and Hansen, F.D. (1995). **Case studies of sealing methods and materials used in the salt and potash mining industries**. Sandia National Laboratories, United States of America.
- Fischle, W.R. and Stover, W.H. (1986). Construction of a bulkhead and measurement under brine pressure. presented at **the Solution Mining Research Institute**. September 21-24, Amsterdam.
- Franssen, R.C.M.W. and Spiers, C.J. (1990). Deformation of polycrystalline salt in compression and in shear at 250-350°C. **Deformation Mechanisms**. Rheology and Tectonics, Geological Society Special Publication No. 45. pp. 201-213.
- Fuenkajorn, K. and Daemen, J.J.K. (1987). Mechanical interaction between rock and multi-component shaft or borehole plugs. **Rock Mechanics: Proceedings of the 28th U.S. Symposium** (pp. 165-172). June 29-July 1, University of Arizona, Tucson.
- Fuenkajorn, K. and Daemen, J.J.K. (1988). Boreholes closure in salt. **Technical Report Prepared for the U.S. Nuclear Regulatory Commission**. Report No. NUREG/CR-5243 RW. University of Arizona.
- Gnirk, P.F. and Johnson, R.E. (1964). The deformational behavior of a circular mine shaft situated in a viscoelastic medium under hydrostatic stress. In **Proceedings of the 6th U.S. Symposium on Rock Mechanics** (pp. 233-259). University of Missouri, Rolla.

- Grice T. (1998). Underground Mining with Backfill. **The 2nd Annual Summit - Mine Tailings Disposal Systems** (pp. 14). November 24-25, 1998, Brisbane, Australia.
- Hamami, M., Tijani, S.M., and Vouille, G. (1996). A methodology for the identification of rock salt behavior using multi-step creep tests. In **Proceedings of the Third Conference on Mechanical Behavior of Salt** (pp. 53-66). Clausthal-Zellerfeld, Germany: Trans Tech Publications.
- Handin, J., Russell, J.E. and Carter, N.L. (1984). Transient Creep of Repository Rocks. Final Report: **Mechanistic Creep Laws for Rock Salts**, Texas A & M research Foundation, Office of Nuclear Waste Isolation, Battelle Memorial Institute, Report, BMI/ONWI-550.
- Hardy, H.R. and Sun, X. (1986). A nonlinear rheological model for time-dependent behavior of geologic materials. In **Proceedings of 27th U.S. Symposium on Rock Mechanics** (pp. 205-212). June 23-25, University of Alabama, Tuscaloosa, Howard L. Hartman ed., Ch.2.
- Hunsche, U.E. and Schulze, O. (1996). Effect of humidity and confining pressure on creep of rock salt. In **Proceedings of the Third Conference on the Mechanical Behavior of Salt** (pp. 237-248). September, 1993, Ecole Polytechnique, Palaiseau, France, Trans Tech Publications, Clausthal-Zellerfeld, Germany.
- Inada, Y., Kinoshita, N., Ebisawa, A., and Gomi, S. (1997). Strength and deformation characteristics of rocks after undergoing thermal hysteresis of high and low temperatures. **International Journal of Rock Mechanics and Mining Sciences**. 34(3-4): 688-702.

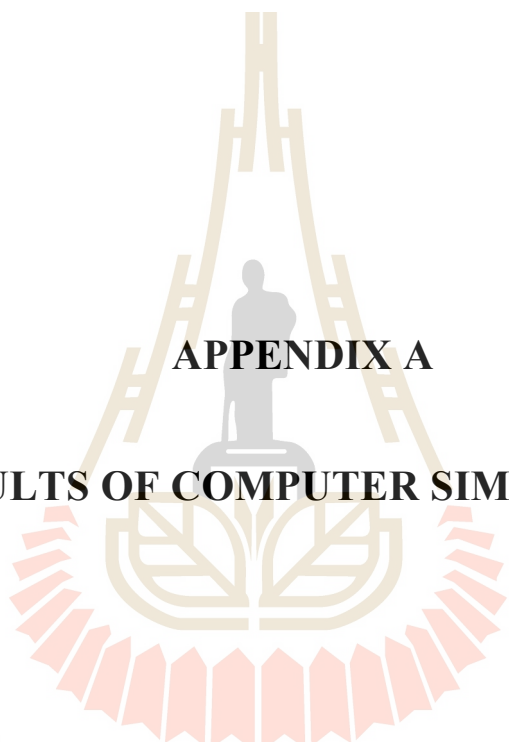
- Itasca. (1992). **FLAC-Fast Lagrangian Analysis of Continua, Version 4.0, User Manual**. Itasca Consulting Group Inc., Minneapolis, MN, USA.
- Jandakaew, M. (2007). Stress-path dependency of rock salt. In **Proc. of the First Thailand Symposium on Rock Mechanics** (pp. 171-188). September 13-14, Greenery Resort, Khao Yai, Nakhon Ratchasima, Suranaree University of Technology.
- Jeremic, M.L. (1994). **Rock mechanics in salt mining**. Rotherdam: A. A. Balkema. pp. 530.
- Kaew-iod, A. (2011). Application of backfill techniques in underground potash mine project. **Master's Thesis**. Department of Mining Engineering, Prince of Songkla University.
- Khalid, B. (2010). Effect of temperature and humidity on salt mine environment. **Pakistan Journal of Meteorology**. 7(13).
- Klein, C., Hurlbut, C.S. and Dana, J.D. (1998). **Manual of Mineralogy**. John Wiley & Sons Inc.
- Knowles, M.K., Borns, D., Fredrich, J., Holcomb, D., Price, R., and Zeuch, D. (1998). Testing the disturbed zone around a rigid inclusion in salt. In **Proceedings of the Fourth Conference on Mechanical Behavior of Salt** (pp. 175-188). Clausthal, Germany: Trans Tech Publications.
- Landriault, D.A., Verburg, R., Cincilla, W., and Welch, D. (1997). Paste technology for underground backfill and surface tailings disposal applications. **Short course notes, Canadian Institute of Mining and Metallurgy, Technical workshop**. April 27, 1997, Vancouver, British Columbia, Canada. pp. 120.

- Langer, M. (1984). The rheological behaviour of rock salt, mechanical behavior of salt
I. In **Proceedings of the First Conference on the Mechanical Behavior of Salt** (pp. 201-240). November 9-11, 1981, The Pennsylvania State University, Trans Tech Publications, ClausthalZellerfeld, Federal Republic of Germany.
- Lee, R. and Souza, E.D. (1998). The effect of brine on the creep behaviour and dissolution chemistry of evaporites. **Canadian Geotechnical Journal**. 35: 720-729.
- Liu, W.Y. and Sun, H.H. (1999). Solidifying tailings slurry with new binder at Meishan iron mine. In **Proceedings of the 99th International Symposium on Mining Science and Technology** (pp. 571-574). Beijing, China.
- Luangthip, A., Khamrat, S. and Fuenkajorn, K. (2016). Effects of Carnallite Contents on Stability and Extraction Ratio of Potash Mine. In **9th Asian Rock Mechanics Symposium**. October 18-20, Bali, Indonesia.
- Mostafa, B., Fall, M., and Belem, T. (2004). A contribution to understanding the hardening process of cemented pastefill. **Minerals Engineering**. 17: 141–152.
- Oladapo, S.A. and Ekanem, E.B. (2014). Effect of sodium chloride (NaCl) on concrete compressive strength. **International Journal of Engineering Research & Technology**. 3(3): 2395-2397.
- Pattani, S. (2014). Time-dependent bond strength of cement sealing in rock salt. **Master's Thesis**. Geotechnology, Engineering, Suranaree University of Technology.
- Pattani, S. and Tepnarong, P. (2015). Experimental assessment of mechanical and hydraulic performance of cement sealing in rock salt. **Vietrock2015 an ISRM Specialized Conference**. March 12-13, 2015, Hanoi, Vietnam.

- Pudewills, A., Muller-Hoeppe, N., and Papp, R. (1995). Thermal and thermomechanical analyses for disposal in drifts of a repository in rock salt. **Nuclear Technology**. 1: 79-88.
- Raj, S.V. and Pharr, G.M. (1992). Effect of temperature on the formation of creep substructure in sodium chloride single crystal. **American Ceramic Society**. 75(2): 347-352.
- Richard, J. (1993). Plasticity and creep. Theory, Example, and Problems, English Edition Editor, **Rochester Institute of Technology**, Rochester, New York.
- Ruhaak, W., Luo, J., and Diersch, H.J.G. (2009). 3D Modelling of brine flow - A case study for a flooded salt mine. **The International Mine Water Conference** (pp. 688-693). October 19-23, 2009, Berlin, Germany.
- Senseny, P.E. (1984). Specimen size and history effects on creep of salt. In **Proceedings of the First Conference on the Mechanics Behavior of Salt** (pp. 369-379). Clausthal-Zellerfeld: Trans Tech Publications.
- Senseny, P.E., Hansen, F.D., Russell, J.E., Carter, N.L., and Handin, J.W. (1992). Mechanical behaviour of rock salt: phenomenology and micromechanisms. **International Journal of Rock Mechanics and Mining Sciences**. 29(4): 363-378.
- Shende, F.P. (2003). Cause, effect and control of potash dissolution by brine. **Doctoral dissertation**. Department of Mining Engineering, Queen's University, Kingston, Ontario, Canada.
- Spencer, R.J. and Lowenstein, T.K. (1990). **Evaporites**. In: Mcllreath, I.A., Morrow, D.W. (Eds.), Diagenesis II, Geoscience Canada Reprint Series 4. pp. 141-164.

- Sriapai, T., Walsri, C., and Fuenkajorn, K. (2012). Effect of temperature on compressive and tensile strength of salt. **ScienceAsia**. 38: 166-174.
- Stanton, R.L. and Gorman, H. (1968). A phenomenological study of grain boundary migration in some common sulfides. **Economic Geology**. 63: 907-923.
- Tepnarong, P. (2012). Bond strength of cement sealing in Maha Sarakham salt. **Proc. of 7th Asian Rock Mechanics Symposium** (pp. 584-593). October 15-19, 2012, Seoul, Korea.
- Urai, J.L., Spiers, C.J., Zwart, H.J., and Lister, G.S. (1986). Weakening of rock salt by water during long-term creep. **Nature**. 324: 554-557.
- Varo, L. and Passaris, E.K.S. (1977). The role of water in the creep properties of halite. **Proc. Conference on Rock Engineering** (pp. 85-100). Univ. of Newcastle-upon-Tyne.
- Warren, J.K. (1999). **Evaporites: Their evolution and economics**. Blackwell Science, Oxford. pp. 438.
- Warren, J.K. (2010). **Evaporites through time-tectonic, climatic, and eustatic controls in marine and nonmarine deposits: Earth-Science Reviews**. February, 2010, 98(3-4): 217-268.
- Warren, J.K. (2016). **Evaporites: A Geological Compendium**. Springer. pp. 613-614.
- Wayment, W.R. (1978). Backfilling with Tailings - A New Approach. **Mining with Backfill - 12th Canadian Rock Mechanics Symposium** (pp. 111-116). Canadian Institute of Mining and Metallurgy, Quebec.

- Wendai, L. (2000). **Regression analysis, linear regression and probit regression**, in 13 chapters, SPSS for Windows: statistical analysis: Publishing House of Electronics Industry, Beijing.
- Wittrup, M.B., Kyser, T.K., and Danyluk, T. (2010). The use of stable isotopes to determine the source of brines in Saskatchewan potash mines. **Saskatchewan Geological Society, 2010 - Economic Minerals of Saskatchewan**. pp. 159-164.
- Wilalak, N. (2016). Time-dependent behavior of Maha Sarakham salt as affected by carnallite content. **Master's Thesis**. Geotechnology, Engineering, Suranaree University of Technology.
- Yang, C. and Daemen, J.J.K. (1997). Temperature effects on creep of tuff and its time-dependent damage analysis. **International Journal of Rock Mechanics and Mining Sciences**. 34 (3-4): 383-395.
- Yang, C., Daemena, J.J.K., and Yin, J. (1999). Experimental investigation of creep behavior of salt rock. **International Journal of Rock Mechanics and Mining Sciences**. 36: 233-242.

The logo of Sakon Nakhon Rajabhat University is a large, stylized emblem. It features a central figure of a person standing on a platform, surrounded by a circular arrangement of red and orange segments. Above the figure is a large, golden, stylized letter 'H' or similar symbol. The entire logo is centered on the page.

APPENDIX A
RESULTS OF COMPUTER SIMULATION

มหาวิทยาลัยเทคโนโลยีสุรนารี

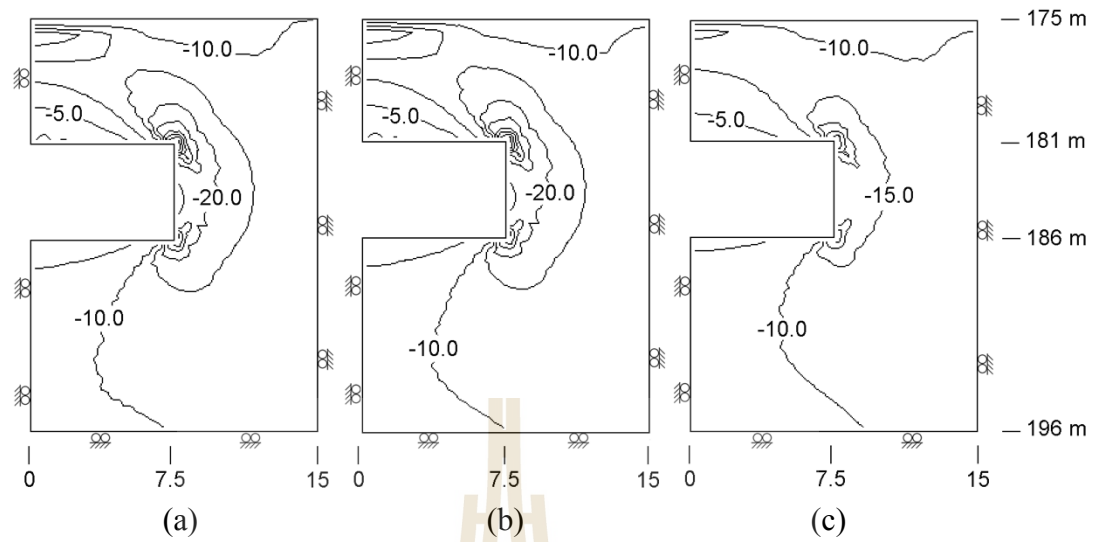


Figure A.1 Stress distribution in salt mine opening for depth 175 m with 5 pillar height after halite (a), carnallite (b) and magnesium brine (c) storage.

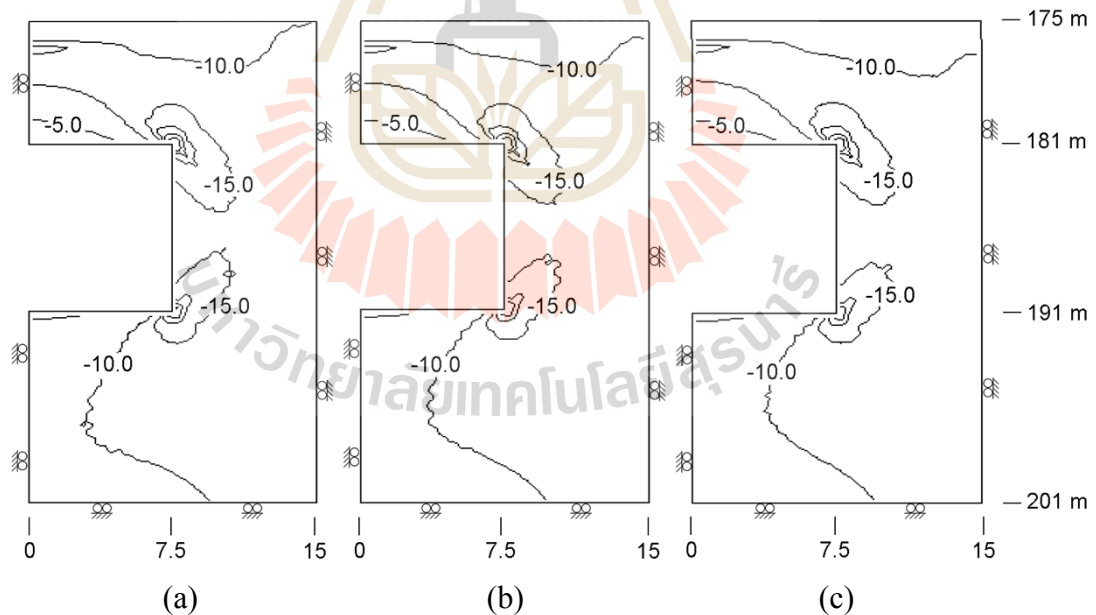


Figure A.2 Stress distribution in salt mine opening for depth 175 m with 10 pillar height after halite (a), carnallite (b) and magnesium brine (c) storage.

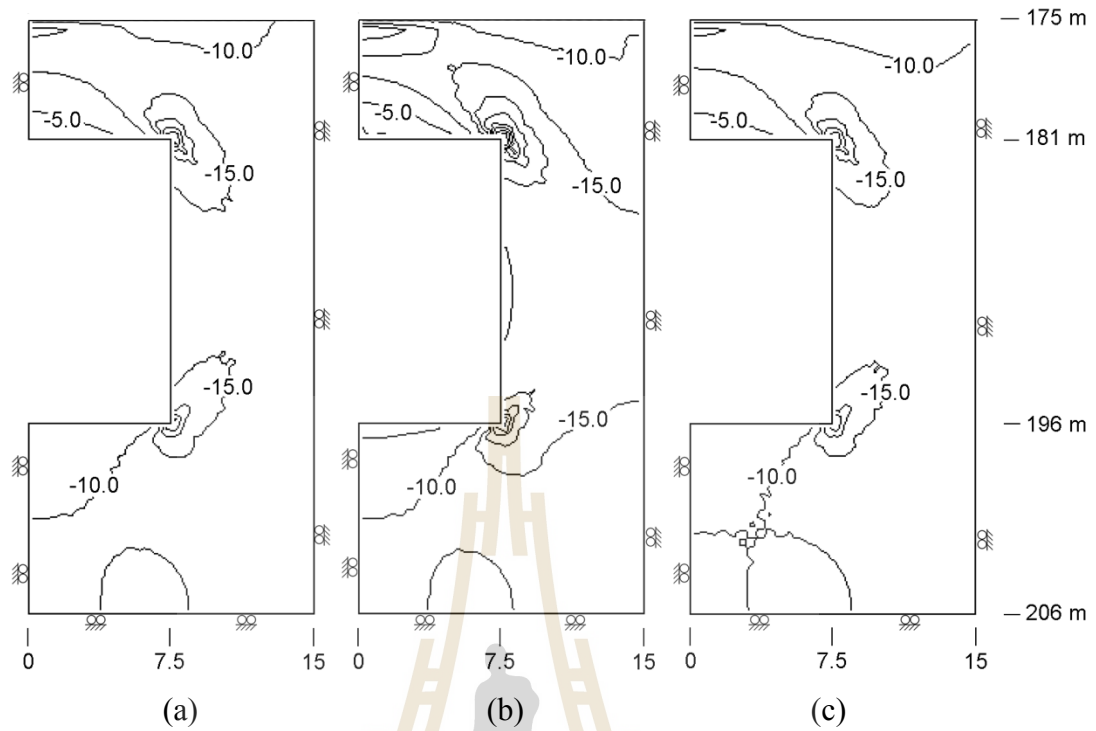


Figure A.3 Stress distribution in salt mine opening for depth 175 m with 15 pillar height after halite (a), carnallite (b) and magnesium brine (c) storage.

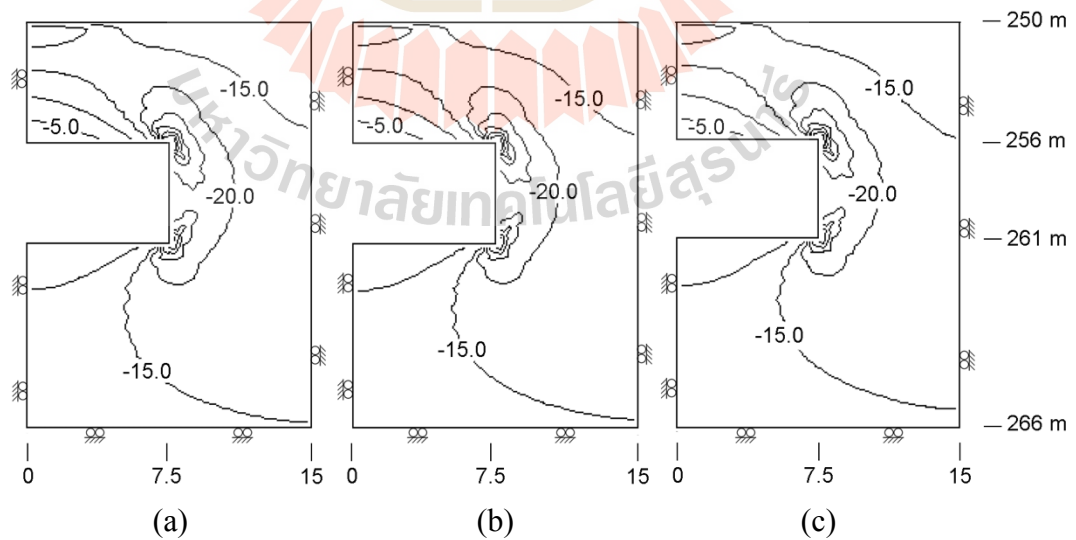


Figure A.4 Stress distribution in salt mine opening for depth 250 m with 5 pillar height after halite (a), carnallite (b) and magnesium brine (c) storage.

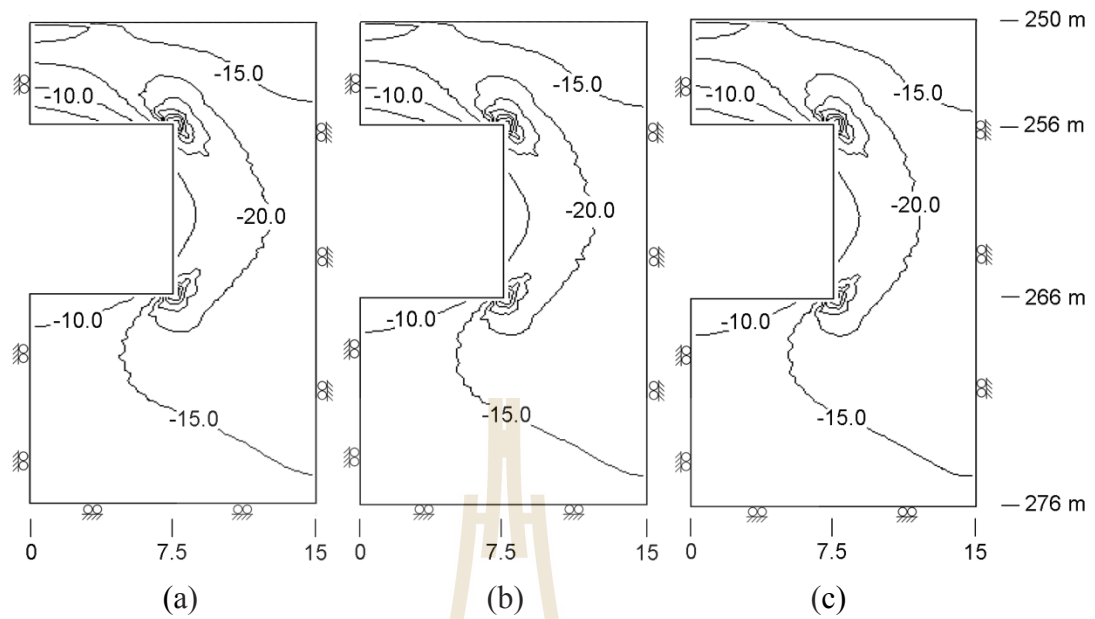


Figure A.5 Stress distribution in salt mine opening for depth 250 m with 10 pillar height after halite (a), carnallite (b) and magnesium brine (c) storage.

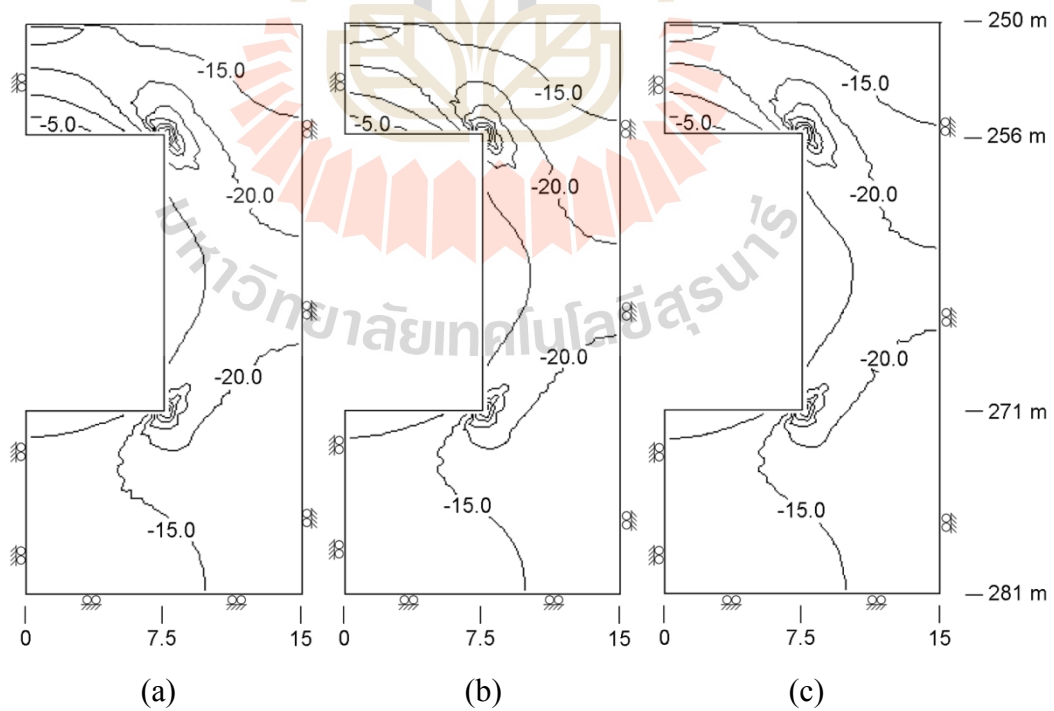


Figure A.6 Stress distribution in salt mine opening for depth 250 m with 15 pillar height after halite (a), carnallite (b) and magnesium brine (c) storage.

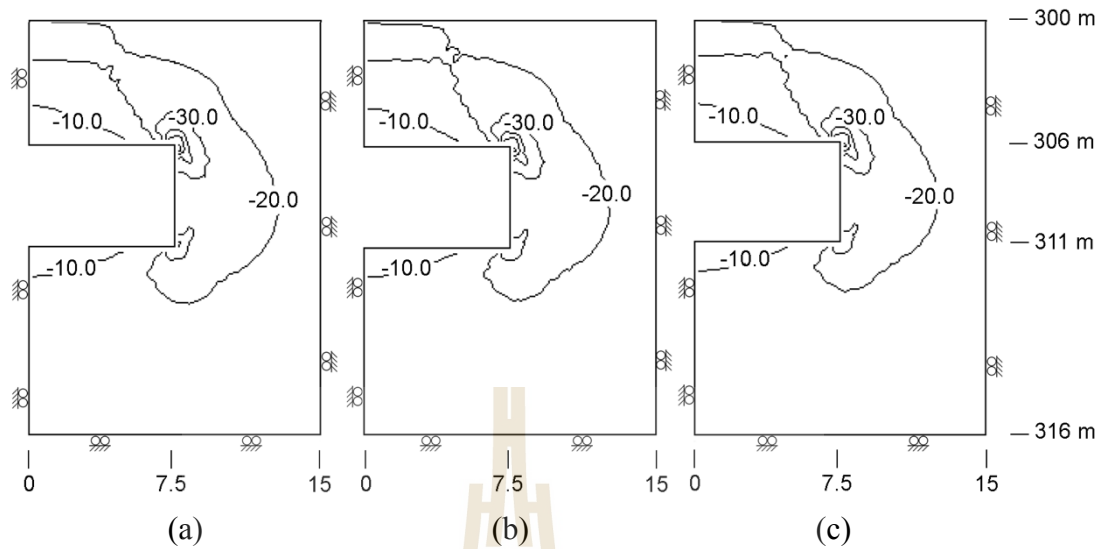


Figure A.7 Stress distribution in salt mine opening for depth 300 m with 5 pillar height after halite (a), carnallite (b) and magnesium brine (c) storage.

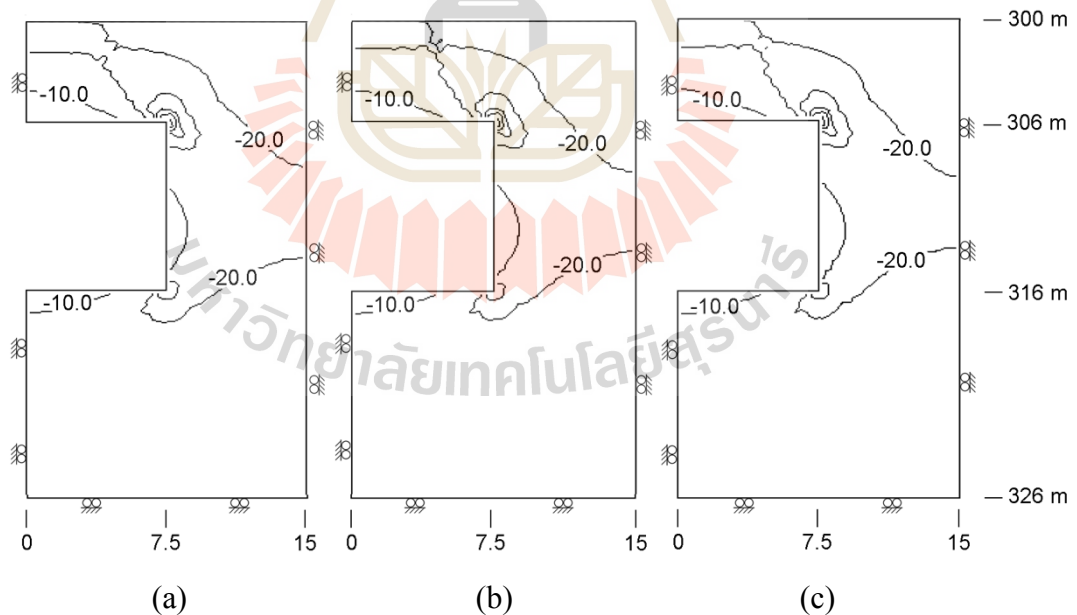


Figure A.8 Stress distribution in salt mine opening for depth 300 m with 10 pillar height after halite (a), carnallite (b) and magnesium brine (c) storage.

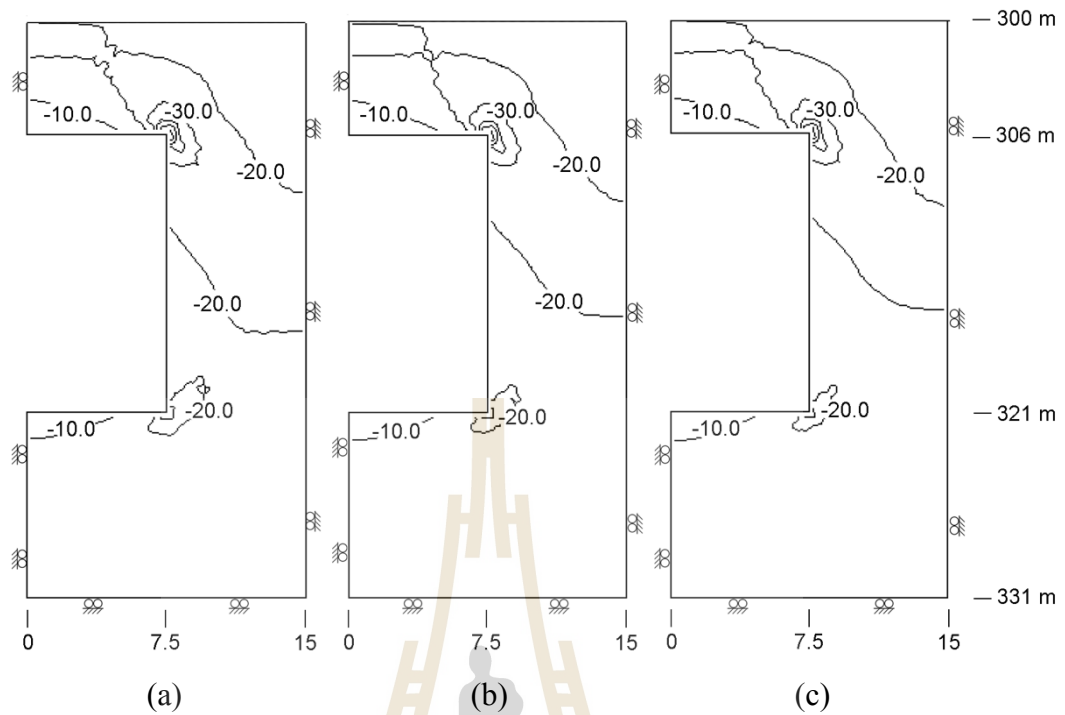


Figure A.9 Stress distribution in salt mine opening for depth 300 m with 15 pillar height after halite (a), carnallite (b) and magnesium brine (c) storage.

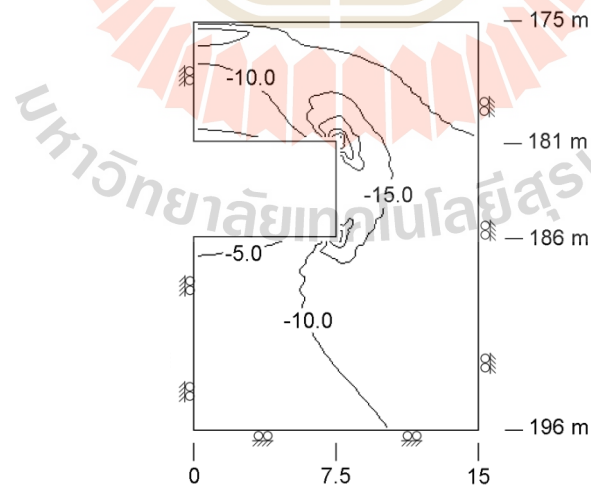


Figure A.10 Stress distribution in potash mine opening for depth 175 m with 5 pillar height after magnesium brine storage.

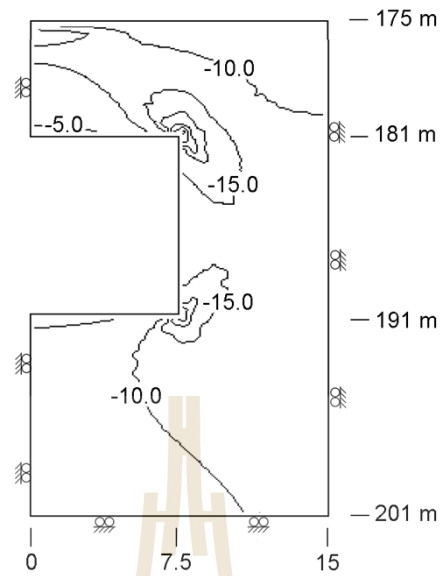


Figure A.11 Stress distribution in potash mine opening for depth 175 m with 10 pillar height after magnesium brine storage.

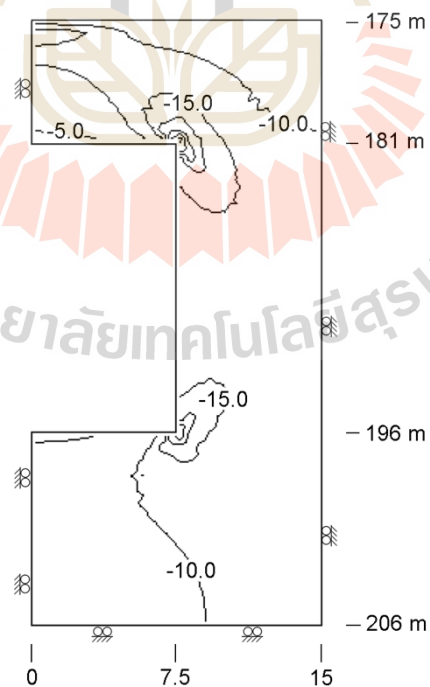


Figure A.12 Stress distribution in potash mine opening for depth 175 m with 15 pillar height after magnesium brine storage.

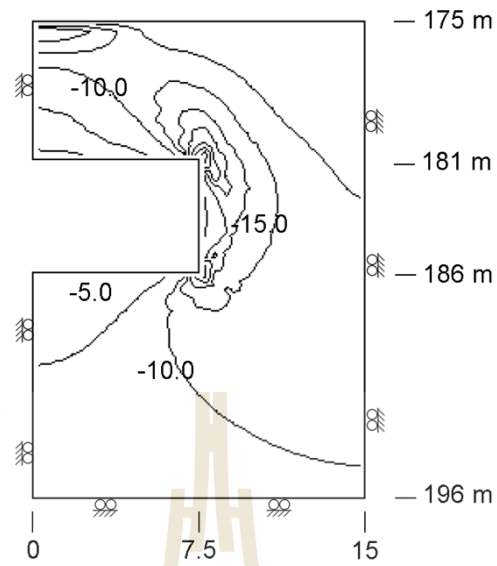


Figure A.13 Stress distribution in potash mine opening for depth 250 m with 5 pillar height after magnesium brine storage.

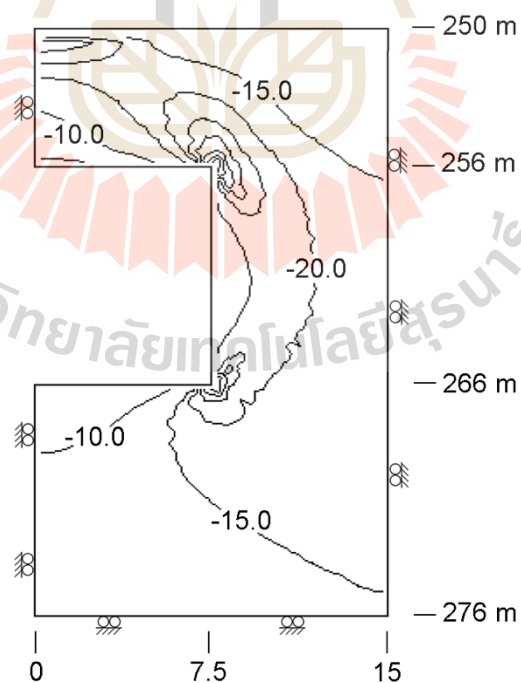


Figure A.14 Stress distribution in potash mine opening for depth 250 m with 10 pillar height after magnesium brine storage.

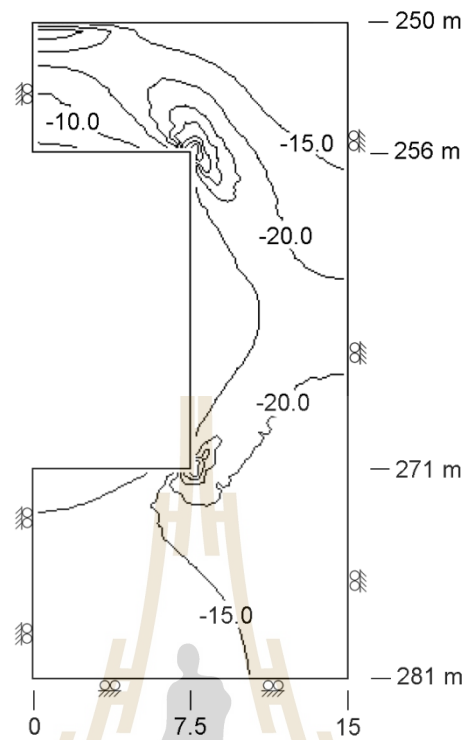


Figure A.15 Stress distribution in potash mine opening for depth 250 m with 15 pillar height after magnesium brine storage.

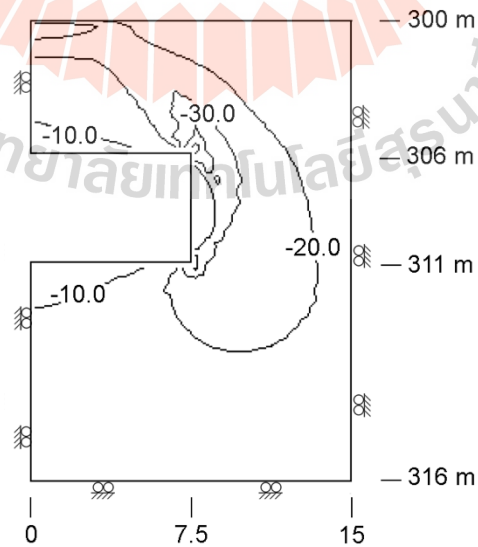


Figure A.16 Stress distribution in potash mine opening for depth 300 m with 5 pillar height after magnesium brine storage.

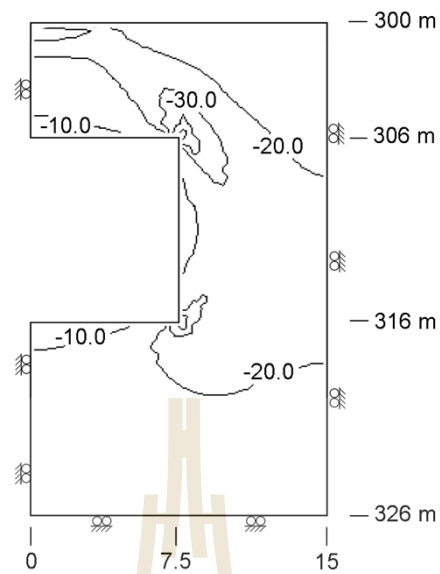


Figure A.17 Stress distribution in potash mine opening for depth 300 m with 10 pillar height after magnesium brine storage.

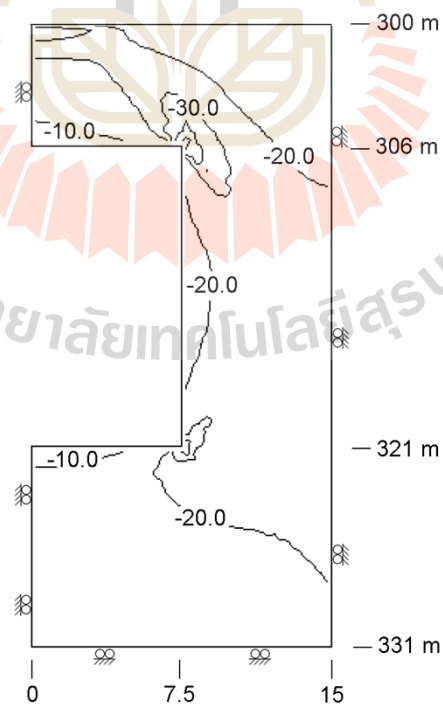
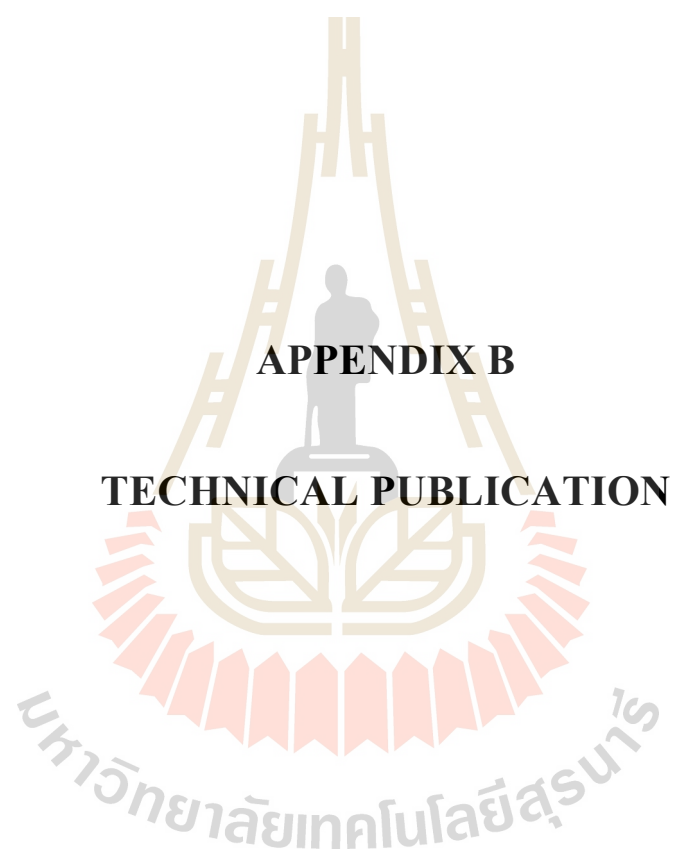


Figure A.18 Stress distribution in potash mine opening for depth 300 m with 15 pillar height after magnesium brine storage.



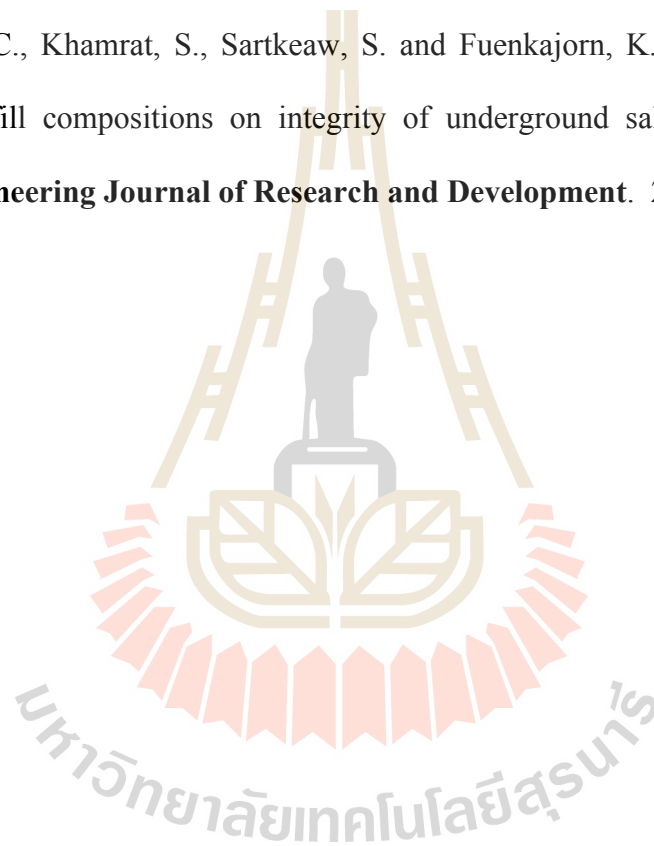
APPENDIX B

TECHNICAL PUBLICATION

Technical Publication

Theerapun, C., Chitnarin, A., Artkhonghan, K. and Fuenkajorn, K. (2017). Effect of mine tailing backfill on pillar stability in salt and potash mines. In **11th South East ASEAN Technical University Consortium Symposium (SEATUC2017)**. March 13-14, Ho Chi Minh City, Vietnam.

Theerapun, C., Khamrat, S., Sartkeaw, S. and Fuenkajorn, K. (2017). Effects of backfill compositions on integrity of underground salt and potash mines. **Engineering Journal of Research and Development**. 28(2): 15-22.



BIOGRAPHY

Miss Chatchita Theerapun was born on September 23, 1993 in Pathum thani, Thailand. She received her Bachelor's Degree in Engineering (Geotechnology) from Suranaree University of Technology in 2016. For her post-graduate, she continued to study with a Master's degree in the Geological Engineering Program, Institute of Engineering, Suranaree university of Technology. During graduation, 2016-2018, she was a part time worker in position of research assistant at the Geomechanics Research Unit, Institute of Engineering, Suranaree University of Technology.

